A Search for H_3 Molecules in the Planetary Nebula NGC 7027

by
Grant Trevor Gussie
B.Sc., University of Manitoba, 1985

A Thesis Submitted In Partial Fulfillment
Of The Requirements For The Degree Of

Master of Science

In the Department
of
Physics

We accept this thesis as conforming
to the required standard

[redacted]
Supervisor: Dr.C.J.Pritchet

[redacted]
Departmental Member: Dr.J.B.Tatum

[redacted]
Outside Member: Dr.T.W.Dingle

[redacted]
External Examiner: Dr.J.D.Poll

University of Victoria
August, 1987

Supervisor: Dr. Christopher J. Pritchet

ABSTRACT

Spectrophotometric observations near $\lambda = 7100$ Å have been made of the young planetary nebula NGC 7027. The spectra were obtained with the 1.83 m telescope at the Dominion Astrophysical Observatory. The observations were made in an attempt to confirm the tentative identification by Pritchet and Grillmair (1984) of a weak emission line at $\lambda = 5624$ Å as triatomic hydrogen emission.

None of the newly discovered spectral features have the structure expected of H_3 molecular emission. The previous identification of the 5624 Å feature is therefore challenged.

Theoretical chemical models are discussed, with emphasis on the production of H_3 in the planetary nebula's transition zone and the surrounding molecular envelope. It is found that H_3 is produced very inefficiently in these regions.

The theory of H_3 molecular spectroscopy is reviewed. Those spectral features that may be observed optically are emphasized.

Also reviewed are procedures for the computer reduction of digitally recorded spectral observations. More specifically, the use of the spectrophotometric reduction package RETICENT is discussed.

Examiners:

[redacted]

Supervisor: Dr.C.J.Pritchet

[redacted]

Departmental Member: Dr.J.B.Tatum

[redacted]

Outside Member: Dr.T.W.Dingle

[redacted]

External Examiner: Dr.J.D.Poll

TABLE OF CONTENTS

LIST OF TABLES

LIST OF FIGURES

ACKNOWLEDGEMENTS

I would like to thank my supervisor Dr.Chris Pritchet for suggesting this project and providing me with a major portion of the observational data on which this thesis is based. I would also like to thank him for instruction and guidance during the reduction of the data.

I am also very grateful to Dr.Jeremy Tatum for his invaluable and occasionally humorous instruction in both the science and the art of spectroscopy, as well as for introducing me to such esoterica as the "Product of Prime Factors Notation".

I would like to thank David Gibney, Les Saddlemeyer and Douglas Bond for their patient instruction and help in the use of the DAO's 1.83 m telescope and its ancillary apparatus.

Finally, I would like to make a very special mention of my gratitude toward Dr.Gerhard Herzberg and Dr.James Watson, as this project would have been impossible without their theoretical and laboratory studies of H_3. They also offered valuable and sagacious advice that allowed me to overcome the hurdles encountered in the completion of this thesis.

FOOD FOR THOUGHT

Space is big. Really big. You just won't believe how vastly hugely mindbogglingly big it is. I mean you may think it's a long way down the road to the chemist, but that's just peanuts to space.

Douglas Adams,
The Hitch Hiker's Guide to the Galaxy,
Pan Books,London,1979.

CHAPTER 1

INTRODUCTION

The apparently ageless stars must grow old and die, just as we all must do. Most dying stars will enshroud their remains in the delicate clouds of fluorescence that we call planetary nebulae. A planetary nebula is an evanescent thing, and the shroud will last for merely a few tens of thousands of years before dissipating into the interstellar medium. The planetary nebulae therefore make the stars somehow seem less timeless and unworldly.

A planetary nebula (PN) forms from matter lost near the end of a moderately massive star's life. PN formation is not a sudden event, as all stars possess significant stellar winds for their entire red giant lifetimes. It follows that gas liberated by a post-main-sequence stellar wind might still surround a fully formed planetary nebula. This gas would be expected to contain both dust grains and molecules as well as free atoms, just as the red giant's atmosphere did before it was blown into space. One would also expect the wind-liberated material to encase the PN in a roughly spherical molecular envelope. This envelope would then be progressively eaten away as the nebula's ionized region grows at its expense.

What could be said of the chemistry of such a molecular envelope? The chemical reactions in the envelope would not be

those with which we are most familiar. The properties of the interstellar medium are such that molecules which are readily oxidized in the Earth's dense atmosphere can exist freely in space. In fact, the most common molecules in a PN's envelope are two gases that can hardly be found at all on Earth; diatomic hydrogen and carbon monoxide.

In the relatively hot transition zone between the PN's ionized (or H II) region and the molecular shroud, some H_2 will be present in an ionizing radiation field (see Black 1978, 1983). The radiation would create the H_2^+ ion, which in turn could result in the formation of H_3^+. This is significant because H_3^+ is an important ion in interstellar chemistry. Its creation is followed by numerous subsequent reactions that synthesize progressively larger molecules. H_3^+ will also recombine rapidly with free electrons to create the elusive and short lived H_3 molecule. H_3 radiates strongly at visible wavelengths and so it may be detectable in the PN optical spectrum.

H_3 emission is therefore a potentially powerful tracer of molecular reactions in planetary nebulae. It is unfortunate that H_3 has not been positively identified in a single PN up to this time. But PN are as individual as fingerprints, and so it is not surprising that there exists a nebula seemingly tailor-made to the search for triatomic hydrogen. This PN is

named NGC 7027 and lies in the constellation Cygnus, high in the summer Milky Way.

NGC 7027 looks tiny in a telescope since it is only 11 arc seconds across, but an instrument of sufficient aperture shows it to be a distinctly gaseous object with a beautiful emerald green colour. NGC 7027 does however lack the characteristic circular shape that earned planetary nebulae their name, since it is cleft by a prominent dark lane that obscures its central star.

The dark lane is composed of dust, and is a visual indication of the nebula's massive molecular envelope. The molecular envelope is in turn an indication of the nebula's extreme youth. In such a young PN, one might expect the nebula's ionization front to expand into the molecular cloud, and perhaps to create an H_3 formation region.

NGC 7027 is also a relatively bright nebula and this combined with its convenient location and interesting spectrum makes it the most intensely studied of all the planetary nebulae. One of the many spectrophotometric studies of this nebula was conducted by Dr.Christopher Pritchet and Carl Grillmair in 1984, who discovered a weak (but relatively broad) spectral emission line at $\lambda = 5624$ Å. They tentatively identified this feature as H_3 emission after laboratory and theoretical work by Dr.Gerhard Herzberg *et al.* revealed a relatively intense H_3 emission feature near that wavelength.

The purpose of this thesis is to continue the work of Pritchet and Grillmair in an attempt to verify their tentative identification of H_3. Herzberg predicted that even more intense emission features of H_3 would lie near 7100 Å, and so spectral observations were subsequently made to find them. In this way, it was hoped that another small part of the Universe would be revealed.

CHAPTER 2

THE PLANETARY NEBULA NGC 7027

The planetary nebula NGC 7027 is in many ways the most suitable of the planetary nebulae for an H_3 search. Not only is it easily observable from mid-northern latitudes, it also possesses unique structural and spectral properties that make it a very promising target for a study of interstellar molecules. The structure and history of the nebula will be discussed in this chapter, with particular emphasis on observations of the nebula's massive molecular envelope.

2.1 VISUAL APPEARANCE AND GROSS SPECTRAL PROPERTIES

NGC 7027 has a higher surface brightness than any other resolvable planetary nebula. The integrated photographic magnitude of the nebula is 9.6, while its angular dimensions are only 11"x18". This gives an average surface brightness measure of 15 stellar magnitudes per square arc second [15 $m_\star/(\text{arc sec})^2$], which can be compared with 18 $m_\star/(\text{arc sec})^2$ for the more famous Ring Nebula (M57).

An alternative measure of surface brightness of an extended astronomical object is the so called *relative exposure index* as defined by Curtis in 1917. This parameter is simply defined as the time required to obtain a photograph of

the brightest part of the nebula. The time unit that is used is the interval required to record an equally dense image of several standard regions in the Orion Nebula (M42). With this definition, the relative exposure of NGC 7027 is 0.1, while M57 has a relative exposure of 1.6. The nebulae NGC 6778 and NGC 3587 have relative exposures of 250 and 300 respectively. The Curtis relative exposure index is admittedly rather archaic, but it provides the casual observer with a greater intuitive feel for the observability of an extended object than does "stellar magnitudes per square arc second".

The Curtis relative exposure index also shows that NGC 7027's high surface brightness makes for short spectrographic exposure times. This in turn reduces the problem of spectral sky contamination, which is very important when trying to raise very faint emission features above the continuum radiation of the nebula and the sky. When searching for hitherto undetected nebular emission lines it is desirable that the target nebula have a high surface brightness, a preference admirably met by NGC 7027.

The most obvious visible feature of NGC 7027 is its brilliant green colour. Its colour is quite startling when viewed through a large telescope, and is sufficient cause for comment for the most jaded observer. The clarity of the nebula's colour is at least partly due to its high surface brightness and the improvement of human colour perception

with light intensity, but the nebula's unique spectral properties contribute as well.

The spectrum of NGC 7027 is dominated by emission lines, as is the spectrum of all planetary nebulae. The spectrum of NGC 7027 is astoundingly rich, and displays lines with ionization levels from N I to Fe VII. The brightest of the visual emission lines are the so-called nebulium lines at 5007 Å and 4959 Å. Rather than being produced by an element called "nebulium", these lines are actually two thirds of a forbidden triplet of O III which happens to be coloured green.

The green [O III] lines are unusually dominant in the spectrum of NGC 7027 and saturate the nebula with green light to a far greater degree than in most planetary nebulae. This was shown by Liller and Aller in 1954, who determined the ratio of the sum of the intensities of the two nebulium lines (N_1+N_2) and the intensity of the Hβ line for a sample of 11 bright PN (see Table 1). The $I_{N1+N2}/I_{H\beta}$ ratio for NGC 7027 is 20.2, which is substantially greater than the average value of this ratio of 13:1 for the other high surface brightness PN in their sample.

TABLE 1 (1)

THE RATIO $I_{N1+N2} / I_{H\beta}$ FOR SEVERAL PLANETARY NEBULAE

Nebula	$I_{N1+N2} / I_{H\beta}$	Nebula	$I_{N1+N2} / I_{H\beta}$
IC 418	1.78	NGC 1535	15.4
NGC 2149	5.40	NGC 6572	15.6
NGC 6543	8.86	NGC 7009	16.1
NGC 6826	9.32	NGC 7662	18.2
NGC 6818	11.6		
NGC 6210	15.1	**NGC 7027**	**20.2**

The relative intensity of the spectral lines should be kept in mind when the data collected for this thesis are inspected. The data frames recorded show the nebula's spectrum near $\lambda = 7100$ Å, and so do not contain either the bright nebulium lines or any of the lines of the Balmer series. All the lines displayed on the data frames are relatively minor.

The brightest line on the frames taken of the 7100 Å region is the 7136 Å feature of [Ar III]. This line is quite weak compared with the visually dominant 5007 Å [O III] line, having less than one twentieth the latter's intensity. Be that as it may, many of the other features are pitifully insignificant in comparison to the 7136 Å line. The lesser lines barely rise above the continuum when plotted on scales that show the 7136 Å peak. The sought-after emission lines of

---

[1] Adapted from Gurzadyan,G.A. (1969) *Planetary Nebulae (English Edition)* p. 10, Gordon and Breach.

H_3 would be much weaker still, making them several orders of magnitude weaker than the nebula's most intense features.

It is helpful to know the wavelengths of the major lines beforehand in order to determine precisely the wavelengths of any newly detected spectral features. The major spectral lines of NGC 7027 were identified by Aller, Bowen and Minkowski (1955), and by Kaler *et al.* (1976). The more recent paper by Kaler *et al.* includes both photographic and photoelectric data, and served as an important reference for line identification. Those lines identified by Kaler that are on the 7100 Å frames are listed in Table 2.

The infrared spectrum of NGC 7027 is noteworthy as well. Kaler *et al.* have identified emissions lines from the visual band to hydrogen's Pfund 10 line at 9014.9 Å, while Condal *et al.* extended this list to 9850 Å.

Among the strongest emission features detectable from 1 μm to 10 μm are the higher order hydrogen and helium recombination lines. Near 2 μm, the emission lines of H_2 are visible as well. These lines were first detected in 1976 by Treffers *et al.*, and were the first diatomic hydrogen lines observed in any planetary nebula. Another molecular transition easily visible in NGC 7027 is CO at millimeter wavelengths.

TABLE 2 [1]

MAJOR SPECTRAL FEATURES OF NGC 7027 NEAR 7100 Å

WAVELENGTH (Å)	ION	MULTIPLET	TRANSITION	INTENSITY
7065.31	He I	10	$2p\,^2P \leftarrow 3s\,^3S$	23.5
7135.78	[Ar III]	1F	$3p^4\,^2P \leftarrow 3p^4\,^1D$	77.9
7170.62	[Ar IV]	2F	$3p^3\,^2D_{3/2} \leftarrow 3p^3\,^2P_{3/2}$	2.2
7177.77	He II	11	$5g\,^2G \leftarrow 11h\,^2H$	2.0
7237.26	[Ar IV]	2F	$3p^3\,^2D_{5/2} \leftarrow 3p^3\,^2P_{3/2}$	2.47
7262.77	[Ar IV]	2F	$3p^3\,^2D_{3/2} \leftarrow 3p^3\,^2P_{1/2}$	1.39
7281.32	He I	45	$3s\,^1S \leftarrow 2p\,^1P$	2.25
7319.92	[O II]	2F	$3p^3\,^2D_{5/2} \leftarrow 3p^3\,^2P$	55.8
7330.19	[O II]	2F	$3p^3\,^2D_{3/2} \leftarrow 3p^3\,^2P$	47.5

The entries listed in the **MULTIPLET** column refer to the line's multiplet number from the *Revised Multiplet Table* by C.E.Moore (1945). The **INTENSITY** column shows the line's relative intensity (as determined by Kaler) as a percentage of the intensity of Hβ. The required intensity measurement of Hβ was obtained photoelectrically by Kaler, but was unfortunately (although necessarily) contaminated by the Pickering 8 line of He II. The scale is therefore set to I(Hβ + He II Pi 8) = 100. An approximate correction that changes the intensities to I(Hβ) = 100 would be to multiply each by 1.02.

[1] Adapted from Kaler, J.B., Allen, L.H., Czyzak, S.J., Epps, H.W. (1976) *Ap.J.Suppl.* **31**, 163.

The presence of readily observable molecules is an obviously good omen for the observer searching for H_3. H_2 in a dilute ultraviolet radiation field should result in the formation of H_2^+ and H_3^+, the precursors of H_3.

2.2 Distance and Luminosity

The distance to NGC 7027 was discussed by Pottasch *et al.* (1982) who describes several methods of distance determination. They find a lower limit of 1 kpc based on the velocity of 21 cm interstellar absorption lines under an assumed Schmidt Galactic rotation model. An upper limit of 1.5 kpc was also determined from comparison of the number density of electrons (as derived by the ratios of forbidden line intensities) to measurements of the Hβ irradiance.

The Hβ irradiance from the nebula was originally determined by Collins, Daub, and O'Dell (1961) from measurements of Capriotti and Daub (1960) and from Liller (1955). They arrived at a value of $E(H\beta) = 7.59 \times 10^{-14}$ W/m^2. This estimate was subsequently revised downward by nearly 20% by Miller and Mathews in 1979. A final determination of this number was subsequently made by Shaw and Kaler (1982), who arrived at a higher Hβ irradiance of $E(H\beta) = (7.64 \pm 0.18) \times 10^{-14}$ W/m^2.

Since the nebula distance determination by Pottasch relied on the earlier determination of the Hβ irradiance by

Miller and Mathews, their upper limit to the distance of NGC 7027 should be revised slightly upward in light of the latter work by Shaw and Kaler. The uncertainty in the distance to NGC 7027 is therefore greater than fifty percent.

Although the planetary's distance modulus has not been accurately determined, NGC 7027 is known to be intrinsically very luminous. A distance near the lower bound would indicate (after correction for extinction) a luminosity as great as the brightest extragalactic PN observed in M32, M31, the LMC, the SMC, NGC 6822 and the Fornax dwarf system. A distance of 1.5 kpc would mean that NGC 7027 is twice as luminous as any other known PN. Incidentally, the intrinsic luminosity of the nebula assuming a distance of 1.5 to 2.0 kpc ($\approx 3 \times 10^4 L_\odot$) is in close agreement with that predicted by Iben (1981) for a young planetary nebula with a $3 M_\odot$ progenitor star.

2.3 Central Star

The remnant of the original star is not readily visible either visually or photographically. Atherton *et al.* attempted to locate this star in 1979 by using bandpass filters to suppress the nebula's brighter emission lines. They succeeded in detecting an enhancement in the continuum at a position just north of the center of the dark lane. The size of the enhanced region was 1.1 arc seconds (FWHM), which was comparable with the seeing at Kitt Peak that night ($\approx 1"$).

They therefore tentatively identify this feature as the nebula's central star, and determine its apparent visual magnitude as $m_v = 19.4 \pm 1.0$.

Atherton also determined the star's effective temperature as $T_{star} > 200\,000\,K$ on the basis of the ratio of the Hβ irradiance of the star and the nebula (assuming a nebula optically thick beyond the Lyman limit). Shaw and Kaler lowered this estimate to 180000 K in their 1982 recalibration of the Hβ irradiance. Even at the lower temperature estimate, the central star would be one of the hottest stars known. Such an extremely high stellar temperature is strongly indicative of a very young and actively evolving nebula.

2.4 The Ionized Nebula

The structure of NGC 7027 is revealed by clues provided by detailed study of the nebula's spectrum. It is found that NGC 7027 has a dynamic and complex structure that creates a bewildering array of spectral features.

Some of these spectral features have already been discussed. As previously mentioned, NGC 7027 has an unusually strong forbidden line spectrum. The forbidden lines are so strong that the third line of the "nebulium series" (resulting from the $^3P_0 \leftarrow {}^1D_2$ transition of O III) is visible

despite having a theoretical intensity less than one ten thousandth that of the $^3P_2 \leftarrow {}^1D_2$ line at 5007 Å.

Forbidden lines are observable only if sufficient numbers of atoms accumulate in metastable levels. This can occur only if the densities of free particles and photons are low enough that the metastable atoms are not physically disturbed before undergoing spontaneous transitions. Therefore the values of n_e and T_e could hypothetically be determined by a study of forbidden line intensities, but this proves difficult in practice. The emission lines from the various ions in NGC 7027 gives such disparate results that no homogeneous or simple gradient model will fit the determined values of these parameters.

This fact gives important information on the structure of NGC 7027 which may significantly affect the possibility of detecting H_3 gas in the nebula. The wide range of ionization levels and electron densities derived for NGC 7027 has been explained by Kaler *et al.* (1976) as due to filamentary structures throughout the nebula. In this model, the number densities of electrons would range over a factor of twenty at a given radius within the nebula, creating pockets of low ionization. The ions are undoubtedly stratified, with lower ionization levels at larger radii, dropping to zero ionization near the periphery. It is entirely likely that the filaments are dense enough near the H II region's edge to allow

partially shielded molecular reactions. Stated another way, it is thought probable that the knotty structure of NGC 7027 would create a larger H_3 formation region than would a more homogeneous structure.

2.5 EXPANSION

The physical structure of NGC 7027 must continually change since NGC 7027 undergoes differential expansion. The outer regions of all planetary nebula expand at a higher rate than the inner regions. An early study of planetary nebular expansion was conducted by Wilson (1950), who determined the Doppler broadening velocity (which corresponds to twice the radial expansion velocity) of several spectral lines in NGC 7027 as well as some other bright nebulae. His relevant results are tabulated in Table 3.

TABLE 3 [1]

TWICE THE EXPANSION VELOCITY OF NGC 7027 FROM SEVERAL EMISSION LINES

ION AND IONIZATION POTENTIALS (IN eV)		TWICE EXPANSION VELOCITY (IN KM/S)
H	13.6	42.4
[O II]	13.6	47.2
[O III]	35.0	40.9
[Ne III]	40.9	44.7
He II	54.2	39.6
[Ne V]	96.0	38.2

[1] Adapted from Wilson, O.C. (1950) *Ap.J.* **111**, 163.

There is a statistically significant inverse correlation between the line ionization potentials and the derived expansion velocities (90% confidence of significance). This may be understood only if one assumes that the expansion velocity increases from the high ionization region near the nebula's center to the low ionization region of the periphery.

A twice expansion velocity of 42.4 km/s corresponds to a Doppler broadening of only $\Delta\lambda \approx 1$ Å at $\lambda = 7100$ Å. As we shall see, the natural widths of the sought-after H_3 emission lines are ≈ 8 Å, so the H_3 lines would be far broader than (and readily distinguishable from) the atomic emission features. We should be easily able to identify molecular emission lines by their width even if the molecular gas does not partake in the expansion of the nebula.

However, the molecular gas *does* expand, as revealed by Doppler broadening measurements of the radio emission lines of CO. Observations by Thronson (1983) show a Doppler velocity of 32 km/s for the bulk of the CO gas, indicating an expansion velocity of 16 km/s. The ionized gas is therefore expanding into the molecular cloud with a velocity of some 6 km/s.

2.6 H_2 Molecular Emission

The velocity of the ionized gas relative to the molecular cloud may be responsible for the rotational-vibrational emission lines of H_2 observable near $\lambda = 2\,\mu m$. Beckwith *et al.* (1980) measured the relative intensity of various H_2 lines, and found the intensity ratios of the $v = 1 \rightarrow 0$ and $v = 2 \rightarrow 1$ emission bands to be inconsistent with an ultraviolet excitation model. Beckwith therefore proposes that the H_2 gas is shock heated by an expanding ion cloud. In Beckwith's model, the shock front precedes the ionization front, creating a compressed region of neutral gas at $T \geq 1000\,K$. A shock velocity of 13 km/s is assumed in Beckwith's calculations. An upper limit to the vibrational excitation temperature of $T_{vib} \leq 3200\,K$ is observed by Beckwith, which indicates an H_2 density of $4 \times 10^4\,cm^{-3}$ for the unshocked gas. On this basis they propose a total molecular mass of 1 to $3\,M_\odot$, assuming that gas density in the molecular cloud falls off at the rate of r^{-3} (based on photometric observations of the extended reflection nebula cospatial with the molecular envelope).

Beckwith *et al.* could detect H_2 over a slightly greater angular extent than they could ionized hydrogen (observed as the Brackett γ line). The molecular transition lines were easily visible with the aperture placed 8" from the nebula's center, even though Bγ had dropped far below its central intensity at this position. Furthermore, the H_2 data seem

better represented by a shell distribution model than by a homogeneously filled sphere, although this could not be ascertained as a precise H_2 distribution map was not produced. It was proposed that the H_2 emission region is a spherical shell just outside the ionization region.

Observations by Smith, Larson and Fink (1981) support the findings of Beckwith's group. The signal-to-noise ratio of Smith's data were an improvement over Beckwith's, but the velocity resolution was only ≈ 75 km/s. The expansion velocity of the excited H_2 could only be very roughly determined, but it appeared to be equal to the hydrogen recombination lines to within ± 17 km/s.

Smith, Larson and Fink also reject an ultraviolet pumping model for the H_2 emission on the basis of the $v = 1 \rightarrow 0$ and $v = 2 \rightarrow 1$ intensity ratios. In Smith *et al.*'s model a shock of velocity 22 km/s excites the H_2. Their velocity estimate is based on measurements of the expansion velocity of the H II region (see Table 2).

This is very curious since this velocity refers to the expansion of the ionized gas relative to the central star and not relative to the molecular gas. Since CO observations show that the molecular cloud is itself expanding at some 16 km/s, the velocity of the H II region relative to the H_2 region is at most 6 km/s, and not 22 km/s.

Even at this lower velocity, the H II region would be expanding at a highly supersonic velocity into the surrounding molecular envelope, since the sound speed of the preshock gas is only ≈340 m/s.

A supersonically expanding H II region is expected to produce a "D-type" ionization front, with the density ahead of it being greater than that behind it (Spitzer,1978). The development of a high density neutral region preceding the ionization region would create a shock, analogous to the bow shock that develops in front of a solid body travelling at supersonic velocities.

If one assumes that the gas pressure behind the ionization front is much greater than the pressure in front of it, one finds that the velocities of the shock front and the ionization front are equal. This means that the shock front cannot leave the ionization front behind. The two fronts are stationary with respect to each other, just as a supersonic jet is stationary with respect to its bow shock. In the case of our expanding H II region, the maximum possible shock velocity is consequently the velocity of the ionization front with respect to the surrounding neutral gas, which is 6 km/s. This is less than one half the velocity assumed by Beckwith *et al.* and less than one third the velocity assumed by Smith *et al.*.

It is apparent that the shock velocities assumed by both Beckwith *et al.* and by Smith, Larson and Fink are too high, and so one wonders if the observed H_2 irradiance could be produced by a more realistic shock velocity estimate. A "back-of-the-envelope" calculation can easily be made following the treatment by Masson *et al.* (1985).

First, we assume that the particles in the H II region consist solely of electrons, H^+ ions, and neutral helium, and also that the number density of helium nuclei is 0.1 times the total number density of hydrogen nuclei. The total number density of all particles is then 2.1 times the number density of electrons. By the ideal gas law, we find that

$$P = 2.1 n_e k T.$$

The value of electron density of the outer ionization region of NGC 7027 is $n_e = 5.7 \times 10^{10} (1.77/d)^{1/2} m^{-3}$, where d is the nebula's distance in kpc (Atherton *et al.*, 1979). The temperature is taken to be T = 14000 K (Masson *et al.*, 1985). We then find that the gas pressure in the H II region is

$$P = 3.0 \times 10^{-8} d^{-1/2} \text{ Pa}.$$

We can now relate the pressure of a gas to the properties of a shock propagating through it. The law of conservation of momentum stipulates that

$$P_1 + \rho_1 v_1^2 = P_2 + \rho_2 v_2^2$$

where P_1, P_2, and ρ_1, ρ_2 respectively denote the gas pressure and gas density following and preceding the shock. The v_i

parameters are the gas velocities in a reference frame where the shock is stationary (Spitzer, 1978; Clutton-Brock, 1984).

We now include the law of mass conservation, which in our context is written as

$$\rho_1 v_1 = \rho_2 v_2$$

where the same notation is used as in the previous equation. With a little algebraic manipulation we find that

$$\rho_1 v_1^2 = \rho_2 v_2^2 \frac{v_1}{v_2} .$$

Substitution into the momentum equation then yields the result

$$P_1 + \rho_2 v_2^2 \frac{v_1}{v_2} = P_2 + \rho_2 v_2^2 .$$

High resolution CO observations by Masson *et al.* (to be discussed below) have shown that the expansion velocity of the molecular gas in the postshock region is $\approx$22 km/s. The velocity of the expanding H II region is also $\approx$22 km/s, and so the velocity of the postshock gas relative to the shock front is close to zero. The value of v_1 is therefore negligibly small compared to v_2, and the second term in the left hand side of the previous equation can be neglected.

We substitute v_2 with the observed quantity u, where u is the difference between the expansion velocity of H II region and the molecular envelope (6 km/s). Now assume that the gas pressure of the cold preshock gas (P_2) is negligibly small

compared to the gas pressure of the hot HII region (P_1). We can then write that

$$\rho_2 = \frac{P_1}{u^2}$$

Finally, by accepting our derived value for P_1 and setting $u = 6$ km/s we find that the number density of H_2 in the preshock gas is

$$n(H_2) = 2.5 \times 10^{11} d^{-1/2} m^{-3}.$$

We now compare this value with the value predicted by considering the nebula's brightness in H_2 light. The irradiance from NGC 7027 in the $v = 1 \rightarrow 0$ S(1) H_2 line is $(3.7 \pm 1) \times 10^{-15}$ W m^{-2} as measured by Smith, Larson and Fink (1981). The size of the H_2 shell is $\approx 6 \times 10^{-9}$ sr according to maps produced by Atherton *et al.* (1979), and so we find that the average surface brightness of the $v=1 \rightarrow 0$ S(1) line is $\approx 6 \times 10^{-7}$ W m^{-2} sr^{-1}. However, direct low resolution observations of the H_2 gas by Beckwith *et al.* and Smith *et al.* have shown some evidence that the H_2 gas is highly confined. The adopted value of the surface brightness is consequently accepted only as a lower limit since it is derived by assuming the largest plausible value of the H_2 emission region size.

We now inspect Figure 2 of Kwan (1977), where the theoretical surface brightness of a shocked H_2 region in the $v = 1 \rightarrow 0$ S(1) line is plotted in $[u, n_o]$ space. The u in Kwan's diagram is shock velocity, while n_o is the total number density of the preshock gas. It is found that a shock velocity of

6 km/s can produce the derived lower limit to the surface brightness only if $n_o \geq 5 \times 10^{12} m^{-3}$. This is more than an order of magnitude greater than the value of $n(H_2)$ that we would derive from shock propagation considerations if we assume a reasonable value of the nebula's distance.

It is therefore found that a simplified shock propagation model can *not* easily explain the observed H_2 surface brightness. This result is in contradiction to the conclusions of Beckwith *et al.*, Smith *et al.*, as well as Masson *et al.*, and so defies conventional wisdom.

The discrepancy between the predicted and observed H_2 emission line radiance might eventually be removed by models which incorporate a more realistic, clumpy distribution of gas. Inspection of Kwan's Figure 2 shows quite clearly that H_2 emission increases very rapidly with gas density for shock velocities near 6 km/s.

To illustrate, let us now compare the average surface brightness of a gas cell with a smooth distribution of matter to one with a clumpy distribution when excited by 6 km/s shocks. Assume that the inhomogeneously distributed gas cell has 10% of its volume at a density of $10^7 cm^{-3}$ and 90% of its volume at a density of $10^6 cm^{-3}$. According to Kwan's diagram this cell would have an average surface brightness 1.4 times greater than a homogeneous gas cell of the same mass.

Thus it is found that clumpy H_2 gas could result in the observed emission line radiance in NGC 7027. Unfortunately, spatial observations of sufficient resolution to map the H_2 gas have yet to be made. It remains unproven that the H_2 emission can be explained by shock excitation alone.

The shock excitation scenario was challenged by Black (1979), who modelled the formation of molecules at the edge of the ionized nebula. In Black's model, H_2 gas coexists with atomic and ionized hydrogen at a relatively high temperature (ranging from $T=10^3 K$ to $T=10^4 K$). H_2 is excited by both UV and electron collisions, as well as by the residual energy of gas-phase formation reactions.

Most probably, elements of both the shock excitation model and Black's model are in play in the real nebula. It appears that most of the observed H_2 emission arises from shocked excitation of the neutral molecular envelope, but this certainly does not preclude the existence of H_2 at the outer edge of the ionization zone. It is to be assumed in this thesis that neither model can adequately account for the observed H_2 emission alone, and that H_2 emission is produced both in the molecular envelope and the edge of the H II region. We shall also accept the density and abundance calculations of Black for the transition zone, and by Mitchell, Ginsburg and Fink (1978) or Herbst and Klemperer (1973) for the molecular envelope. It is nevertheless acknowledged that

both approaches are less than satisfactory, and that a comprehensive and realistic model of H_2 emission in NGC 7027 has yet to be made.

Since we accept both models as being fundamentally correct, we must consider two separate molecular formation regions. The first is the molecular envelope proper (ME), where the gas is shielded from the ionizing radiation from the central star. The second region is the very much hotter nebula transition zone (TZ), where molecules are continuously (and rapidly) being synthesized and subsequently destroyed by ultraviolet light from the PN nucleus.

2.7 Emission From Other Molecules

The first observations of polyatomic molecules in planetary nebulae were announced by Zuckerman (1983) who detected weak $J = 1 \rightarrow 0$ HCN emission in NGC 7027. Zuckerman contends that the detection indicates that the molecular envelope is carbon rich, with the carbon/oxygen number ratio given by $C/O \geq 1$.

This view is supported by the non-detection of SiO emission by Thronson and Lada (1981). They find that the $J = 2 \rightarrow 1$ SiO transitions are unobservable to a limiting antenna temperature of $T_a \leq 0.01$ K, and think it is unlikely that this is due to a lack of SiO excitation because of the nebula's density and infrared luminosity. They feel that the

missing SiO must be locked in dust grains, but as we shall see, this view is not held by those who study the nebula's dust. This indicates that oxygen is truly underabundant.

The high carbon abundance implies that the atmosphere of nebula's ancestral star must have undergone substantial chemical evolution. A similar conclusion was reached by Thronson (1983), who used CO observations to determine a lower limit of the abundance ratio of ^{12}CO to ^{13}CO as 36 ± 6. Under the assumption that this ratio accurately reflects the carbon isotope ratio of the precursor star's atmosphere, Thronson suggests that the precursor star was an evolved post-asymptotic branch object of mass $3\ M_{\odot}$.

Thronson's mass estimate is of course highly uncertain, as he relies heavily on suspect assumptions of interstellar chemistry and on questionably accurate computer evolutionary models. One possible difficulty with Thronson's analysis was mentioned by Duley and Williams (1984). They suggest that the $^{12}CO / ^{13}CO$ ratio may be decreased in regions of shocked or otherwise partially ionized gas by the reaction

$$^{13}C^{+} + {}^{12}CO \leftrightarrow {}^{12}C^{+} + {}^{13}CO$$

which occurs preferentially in the forward direction. Thus the $^{12}CO / ^{13}CO$ ratio might not accurately measure the $^{12}C/^{13}C$ ratio. Nevertheless, if one assumes a mass of a few solar masses for the molecular envelope, Thronson's work is a strong indication that a substantial fraction of the progeni-

tor star's original mass ($\geq 30\%$) now resides in the molecular envelope.

Carbon monoxide is detectable in NGC 7027 as emission from the $J = 1 \rightarrow 0$ and $J = 2 \rightarrow 1$ transitions. Detection of CO is possible over an even larger area than is H_2, probably because the detected CO is thermally excited and not dependent on shock excitation. Mufson *et al.* (1975) have detected $J = 1 \rightarrow 0$ CO emission over 40"x 60", as compared to the 11"x 18" size of the ionized nebula. The $J = 2 \rightarrow 1$ bands have been detected over a similar area by Knapp *et al.* (1982), who measured a half-power size of 38"x 50". The expansion velocity of the CO gas is 16.5 km/s. Presumably, the CO map is a far better indicator of the properties of the molecular cloud as a whole than is the previously mentioned H_2 data.

Knapp's group also tried to estimate the mass of the molecular envelope from CO observations, and arrived at a value of $M_{envelope} > 5 M_{\odot}$. They determined the cloud's size as $R > 10^{16}$ m (assuming a distance of 1090 kpc) and an age of $\tau > 13\,100$ years. The age estimate was found from the derived average mass loss rate of $4 \times 10^{-4} M_{\odot}$ year^{-1}, which is far greater than the maximum mass loss rate that can be obtained by radiation pressure: $\frac{dm}{dt} \leq \frac{P}{c\,v}$; where P is the nebula's radiant power output in Watts; v is the expansion velocity of the gas; and c is the speed of light. They believe that it is unlikely that the observed excessively high mass loss can be

explained by a recent substantial drop in the central star's luminosity since the available time scale is simply too short [1]. They therefore suggest that NGC 7027 has ejected mass via some unmentioned exotic process. Knapp's group also found that the carbon stars tend to have highest mass loss rates of all the evolved giant stars, and therefore suggest that the stellar precursor of NGC 7027 was a carbon star of mass $M_{star} \geq 6.4\,M_{\odot}$. This view is supported by Zuckerman's discovery that NGC 7027 is carbon rich.

The CO emission was mapped in high resolution by C.R.Masson with the help of eleven of his colleagues at the Owens Valley Radio Observatory (1985). Their high velocity resolution allowed them to detect a component of CO gas expanding at 22.5 km/s. This gas is expanding 6 km/s faster than the bulk of the CO cloud, and is located close to the nebula's H II region. Masson *et al.* propose that the CO emission is produced behind the shock responsible for H_2 emission, where the temperature has fallen to $T_{vib} \leq 100\,K$.

Masson's group finds no evidence of a low velocity component to the CO emission, as the observed Doppler profile is

---

[1] However, Knapp *et al.*'s conclusions are strongly challenged by Jura (1984), who finds no reason to assume that dM/dt was greater than LV/c at the time of the molecular envelope ejection. He instead proposes that both the mass loss rate and the luminosity of the central star have decreased dramatically over the last 1000 years.

easily modelled by the convolution of a 16 km/s and a 22 km/s Gaussian profile. We therefore find no evidence that the innermost preshock molecular gas is expanding more slowly than the bulk of the CO envelope. This argues against the high H II expansion velocities that were assumed by Beckwith *et al.* and by Smith, Larson and Fink.

Masson's group arrives at a value of $\approx 2\,d^{5/2}\,M_{\odot}$ (where d is the distance in kpc) for the mass of the molecular shroud. This is lower than Knapp's mass estimate, and so it is interesting to note that Masson's estimate of the *mass loss rate* is significantly *higher* than Knapp's, at $1.1 \times 10^{-2}\,d^{-3/2}$ $M_{\odot}$/year. The discrepancy may be because Masson's determination relies on an estimate of the number density of H_2 in the inner preshock regions, while Knapp's estimate is based on the integrated emission of the entire envelope. Masson's derivation would find the mass loss rate immediately prior to the ionization of the innermost nebula, while Knapp's value is a time average over the molecular envelope's formation period. The calculations of Masson and Knapp would have agreed only if the star's mass loss rate was roughly constant throughout the envelope ejection period, A stellar mass loss rate that increases with time will result in the inner envelope having the unexpectedly high density derived by Masson. The two estimates do in fact agree quite closely if one assumes that the molecular gas density drops off as r^{-3}, and not r^{-2} as a steady mass loss rate would imply.

2.8 Dust Component

Unlike most bright planetary nebulae, NGC 7027 lacks the classical planetary ring-like or oval shape, but instead has a decidedly asymmetrical, bilobate appearance. There is a prominent dark lane across the nebula's face that is visible at optical frequencies, but is very much less apparent at longer wavelengths. In fact the entire structure of the nebula is much more regular and symmetrical in the infrared and radio bands than it is in the optical, indicating that the apparent irregularity of the nebula is due to differential extinction by dust.

The dust component of NGC 7027's molecular envelope can be studied by observations of extinction across the face of the nebula. One such investigation was conducted by Condal *et al.* (1981), who made two 2-dimensional, monochromatic intensity maps of the nebula. The images were made through two band-pass filters centered on the nebulium [O III] lines and on the Hα line. The filters had a band width of 100 Å (FWHM), so the Hα image was heavily contaminated by the 6548 Å/6584 Å doublet of [N II]. It was assumed that the intrinsic emission ratios of Hα/[O III] and [N II]/Hα are constant throughout the ionized nebula and that variations in the observed ratio of (Hα+[N II])/[O III] are due solely to reddening by dust. It was found that the correlation between the nebula's optical image and a map made of the observed line intensity ratios is

excellent, with the visually brightest regions showing the least reddening. The PN's central dark lane corresponds to a local maximum of reddening, indicating a dusty composition.

Atherton *et al.* (1979) employed a completely different technique to study the dust of NGC 7027's ionization region. A scanning Fabry-Perot interferometer was used to study the Doppler broadening structure of the 5007 Å [O III] line (which is intrinsically narrow). Observations were made with the interferometer entrance aperture at twenty-five points across the nebula's face. It was found that the red-shifted component was generally weaker than the blue-shifted one, an effect that they attribute to internal dust extinction. Atherton estimates that a mean visual extinction of ≈ 0.34 magnitudes across the diameter of the H II region would explain the discrepancy.

Atherton *et al.* also detected a low surface brightness reflection nebula surrounding NGC 7027. This was interpreted as an extended cloud of low-density dust. It was found that the change in brightness of the nebula with radius could be easily modelled if the density of the dust drops off as r^{-3} outside the H II region. This supports the idea that the mass that formed the nebula was lost at an increasing rate until the ionization of the inner nebula.

Telesco and Harper were able to detect thermal emission from the nebula's dust in 1977 with the Kuiper Airborne

Observatory (KAO). The infrared radiation was observed with a 0.91 m telescope and detectors that scanned the region from $\lambda = 28\,\mu m$ to $\lambda = 320\,\mu m$. They fitted the observed IR irradiance from NGC 7027 to a two component model, with a cooler component of $T \approx 100\,K$ making up the bulk of the dust, mixed with 200 K to 300 K grains comprising a few percent of the dust mass.

Infrared observations of NGC 7027 were also made with the KAO by Moseley (1980), which he originally published in a paper that served as his Doctoral dissertation. Dust was observed as thermal emission at $\lambda = 37\,\mu m$ to $\lambda = 108\,\mu m$ over an angular extent of $\leq 20"$.

The small size of the 90 K dust region was confirmed by Bentley in 1982, who showed that the dust is almost certainly cospatial with the ionization region. Bentley also found that the dust emission spectra is adequately represented by a model particle composition of 8% silicon carbide, 45% graphite, and 47% consisting of an unidentified "Orion bar" dust component that is responsible for 8.6 and 11.3 μm IR emission features. Sellgren *et al.* (1983) have tentatively identified the "Orion bar" component as very small (≈ 50 atom) graphite grains which have been excited by a single UV photon (see also Leger and Puget, 1984). It is unlikely that the "Orion bar" dust is a simple oxide of silicon, so Thronson's 1982 suggestion that significant quantities of SiO are locked in grains is not

supported. It now seems quite certain that NGC 7027 is highly carbon rich.

Both Bentley and Moseley found that the size of the observed 90 K dust emission region is considerably smaller than the CO cloud. Moseley suggested that the dust in the bulk of the molecular envelope must have a temperature of $T \leq 35$ K, and recommended that observations at 350 μm be made to detect this dust.

These observations were carried out by Gee *et al.* (1982), who mapped NGC 7027 at wavelengths of $\lambda = 370$ μm, 780 μm, and 1090 μm. The cold gas component predicted by Moseley was indeed observable as excessive emission at 370 μm. The cold dust has a temperature of $T = 20$ K, and its distribution is cospatial with the CO molecular gas. Gee *et al.* estimate of the mass of the molecular cloud as $M_{envelope} > 5 M_{\odot}$. The mass of the progenitor star would then necessarily be $M_{star} > 6.5 M_{\odot}$. The maximum mass of stars that develop into planetary nebulae (and not into supernovae) would thus be at least this high. This is consistent with the theoretical and observational work discussed by Weidemann and Koester (1983), who suggest an upper limit to the white dwarf progenitor mass of $\approx 8 M_{\odot}$.

CHAPTER 3

THE CHEMISTRY OF THE H_3 MOLECULE

The triatomic hydrogen molecule is at present a mere laboratory curiosity. It can be fleetingly observed in hydrogen discharge tubes, but is otherwise undetected in nature. Nevertheless, chemical reactions in the interstellar medium might lead to the creation and subsequent detection of H_3. Computer models of the chemical abundances in the planetary nebula transition zone (TZ) and the molecular envelope (ME) will be discussed in this chapter, as will the reactions that lead to the formation of H_3.

3.1 FORMATION OF H_2

The first step in the reaction chain that creates H_3 is the formation of the H_2 molecule out of free hydrogen atoms. This reaction is exceedingly well studied and so it will not be discussed in detail here. However, the process's pertinent details must be presented.

The chemical combination of hydrogen atoms in deep interstellar clouds is believed to occur on chemisorptive grain surfaces. In order for the atoms to react on the grain surfaces before they evaporate, the grain's temperature must be $T_{grain} \leq T_{critical}$, where $10\,K < T_{critical} < 100\,K$. Dust grain

reactions are certainly the dominant route of H_2 production in the molecular envelope, where grain temperatures are $\approx 20\,K$.

The H_2 molecule may also be formed inside the nebula's ionization region, where temperatures are far too high for the dust grain reactions. Black (1978,1983) suggests that the coexistence of free atoms and electrons in the PN transition zone results in formation of H_2 by associative detachment of H^-. H_2 production is started by the reaction

$$H + e \rightarrow H^- + h\nu \qquad (R1)$$

which is followed by the subsequent reaction

$$H^- + H \rightarrow H_2 + e. \qquad (R2)$$

The reaction rate coefficient for Reaction 1 is given by the expression $k_1 \approx 10^{-18}\ T\ cm^3\,s^{-1}$ (Black,1978) where T is kinetic gas temperature. Consequently the parameter k_1 is linearly dependent on temperature. In contrast, the rate coefficient for Reaction 2 is relatively unaffected by temperature, and is known to be $k_2 = 2.7 \times 10^{-9}\,cm^3\,s^{-1}$ (Black, 1978). Thus the rate of H_2 formation in the Black model transition zone is

$$R_{2(TZ)} = k_{2(TZ)}\,n(H)\,n(H^-) = 2.7 \times 10^{-9}\,cm^3\,s^{-1}\,n(H)\,n(H^-)$$

where n(X) is the number density of the chemical species "X" in cm^{-3}.

In order to determine the rate of H_2 production, we must therefore know the density of H^- and H. The determination of

these values is complicated by the fact that the H^- ion is removed by photodetachment

$$H^- + h\nu \rightarrow H + e, \qquad \text{(R3)}$$

and by mutual neutralization with the arbitrary ion X^+,

$$H^- + X^+ \rightarrow H + X. \qquad \text{(R4)}$$

In Black's model (1978), the number density of H_2 reaches a maximum of $\approx 10^{-2}\,cm^{-3}$ at a radial distance of 2.9×10^{15} m from the central star. The model nebula has a constant total density of $n = 7000\,cm^{-3}$, and a central star with an effective temperature $T_e = 100000\,K$. This temperature is smaller than, but of the same order as, the effective temperature of NGC 7027's star, and so his results can be taken as at least qualitatively correct.

The H_2 molecules in the transition zone are subject to photodestruction while in the electronic ground state by photons of energy $\geq 4.48\,eV$. At this energy the ionized nebula is nearly transparent, and so the lifetime of H_2 molecules inside the nebular transition zone is very short ($\tau \approx 10^5$ to 10^6 seconds according to Black, 1983). The H_2 gas in the molecular envelope manages to survive for longer periods by relying heavily on self-shielding and dust grain extinction to prevent photodissociation.

3.2 Formation of H_2^+

In addition to being dissociated, the H_2 molecule can be singly ionized to form H_2^+ in a reaction requiring a photon with energy ≥ 15.4 eV,

$$H_2 + h\nu \rightarrow H_2^+ + e. \qquad \text{(R5)}$$

Since 15.4 eV lies beyond the Lyman limit, the opacity of the nebula's transition zone is very much higher at this energy than at H_2's dissociation energy. The ionization of H_2 by UV photons must therefore occur within a highly restricted radius. The photoionization rate of H_2 in Black's model is

$$R_{5(TZ)} \approx 10^{-6}\, n(H_2)\ s^{-1} \approx 10^{-8}\ cm^{-3}\, s^{-1}$$

at $r = 2.9 \times 10^{15}$ meters from the central star.

The H_2^+ ion may be created by less direct means as well, such as radiative association of an H^+ ion and a free hydrogen atom,

$$H^+ + H \rightarrow H_2^+ + h\nu, \qquad \text{(R6)}$$

as well as in a proton transfer reaction with HeH^+,

$$HeH^+ + H \rightarrow H_2^+ + He. \qquad \text{(R7)}$$

The rate of Reaction 6 is highly temperature dependent, and for transition zone temperatures the rate coefficient is $k_{6(TZ)} \approx 10^{-20}\ cm^3\, s^{-1}$ (Black, 1978). The contribution of Reaction 6 to the H_2^+ density is consequently quite small. The reaction rate coefficient of Reaction 7 is very much larger, and is

given by Hutchins (1976) as $k_7 = 10^{-10}\,cm^3\,s^{-1}$. The rate of Reaction 7 is thus

$$R_{7(TZ)} \approx 6 \times 10^{-13}\,cm^{-3}\,s^{-1}$$

in Black's model at $r = 2.9 \times 10^{15}$ meters. Comparing the rates of Reaction 5 and Reaction 7, it is readily apparent that the production of H_2^+ is dominated by the photoionization process.

Cosmic rays can ionize H_2 just as the star's UV photons can. Duley and Williams (1984) state that cosmic rays interact with H_2 along one of the following pathways;

$$H_2 + \text{cosmic ray} \rightarrow H + H^+ + e + \text{cosmic ray} \qquad (R8)$$

$$H_2 + \text{cosmic ray} \rightarrow H + H + \text{cosmic ray} \qquad (R9)$$

$$H_2 + \text{cosmic ray} \rightarrow H_2^+ + e + \text{cosmic ray} \qquad (R10)$$

The reaction of interest is Reaction 10, which according to Duley and Williams occurs 88% of the time. Herbst and Klemperer (1973) show that cosmic ray protons of energy 100 MeV can penetrate even the largest interstellar clouds, and they estimate the cosmic ray ionization rate as $\zeta \approx 10^{-17}$ s^{-1} per H_2 molecule. The H_2^+ production rate from cosmic ray ionization is thus $R_{10(TZ)} \approx 9 \times 10^{-18}\, n(H_2)\, s^{-1}$. Comparing the expression for $R_{10(TZ)}$ to that of the H_2 photoionization reaction rate $R_{5(TZ)}$, we see that cosmic ray ionization is insignificant inside the nebula transition zone.

This is however not the case outside the transition zone since the central star's ionizing radiation cannot penetrate the molecular envelope. This was shown by Mitchell, Ginsburg

and Kuntz (1978) who determined that the transition from a photoionized to an optically thick nebula occurs at a molecular density of $50\,000\,cm^{-3}$ for a $10 M_{\odot}$ cloud. The preshock molecular gas in NGC 7027 is one or two orders of magnitude denser than this optically thin limit (see Section 2.5) and so is most certainly self-shielding against photodestruction.

If we adopt the value of the preshock H_2 density determined in Section 2.5, we find that the H_2^+ production rate in the molecular envelope is $R_{10\,(ME)} \approx 2 \times 10^{-12}\,cm^{-3}\,s^{-1}$. This value is considerably smaller than the H_2^+ production rate in the transition zone, but it should be remembered that the molecular envelope is far more massive than the transition zone, and that the average lifetime of molecules in the molecular envelope is far greater as well. Consequently, the column density of H_2^+ ions in the transition zone is not vastly greater in the transition zone than in the molecular envelope.

Black's model predicts the number density of H_2^+ inside the transition zone to be $n(H_2^+) = 6.3 \times 10^{-4}\,cm^{-3}$ (at $r = 2.9 \times 10^{15}\,m$), while Mitchell, Ginsburg and Kuntz (1978) find that in a model molecular cloud of density $10^5\,cm^{-3}$, the value is $n(H_2^+) = 6 \times 10^{-8}\,cm^{-3}$.

Mitchell, Ginsburg and Kuntz also find the number density ratio of $n(H_2^+)/n(H_2)$ for total gas densities in the range of $n = 10\,cm^{-3}$ to $10^5\,cm^{-3}$. This ratio obtains a maximum value of 10^{-10} at a total gas density of $10^2\,cm^{-3}$. If we accept this derived maximum value of $n(H_2^+)/n(H_2)$ for the entire molecular envelope, and assume a density dependence of r^{-3}, we can find an upper limit to the molecular envelope's H_2^+ column density. This is found to be $\sim 6 \times 10^{13}\,cm^{-2}$ by integrating from $r = 5 \times 10^{18}$ cm to $r = \infty$. The column density of molecular envelope H_2^+ as seen in emission would be twice this value. We can similarly find the largest possible value of the column density of H_2^+ in the transition zone by adopting Black's peak value of $n(H_2^+)$ and assuming that this value is constant through the transition zone. The derived value is $\sim 10^{14}\,cm^{-2}$ (or $\sim 2 \times 10^{14}$ cm^{-2} in emission).

The H_2^+ ion has been observed in absorption over the ultraviolet radiation of several PN nuclei. The first observational evidence of the ion was obtained by Pottasch *et al.* (1978) using the Astronomical Netherlands Satellite. They found that the ultraviolet radiation from the nuclei of NGC 3242 and NGC 7662 deviates from a black-body curve between $\lambda = 2500$ Å and $\lambda = 1500$ Å. They offered no explanation for this anomaly. Data from the International Ultraviolet Explorer were then used by Heap and Stecher (1980) to show that the nebulae NGC 6210 and NGC 1535 have UV spectra similar to those

of Pottasch's nebulae. They attributed the anomalous spectra to photodissociation of H_2^+, and proposed that the ion is distributed in a shell with a line of sight column density of about $8 \times 10^{16}\,cm^{-2}$. Feibleman *et al.* (1981) extended the list of PN showing characteristic H_2^+ absorption to eight nebulae. Unfortunately, H_2^+ cannot be seen in absorption in NGC 7027 since its nucleus is shrouded by dust.

3.3 Formation of H_3^+

The photodissociative process observed in planetary nebulae destroys the H_2^+ ion by the reaction

$$H_2^+ + h\nu \rightarrow H^+ + H. \qquad \text{(R11)}$$

The H_2^+ ion may also be removed by dissociative recombination

$$H_2^+ + e \rightarrow H + H \qquad \text{(R12)}$$

which is quite rapid, or possibly by radiative recombination

$$H_2^+ + e \rightarrow H_2 + h\nu \qquad \text{(R13)}$$

which is very much slower. Electron transfer may remove H_2^+ as well, along the route

$$H_2^+ + H \rightarrow H^+ + H_2\ . \qquad \text{(R14)}$$

Finally, proton transfer processes may also destroy H_2^+. These include the high temperature (*i.e.* important for $T > 5000\,K$) reaction

$$H_2^+ + He \rightarrow HeH^+ + H. \qquad \text{(R15)}$$

The HeH^+ ion[1] may then be destroyed by a subsequent proton transfer with H_2,

$$HeH^+ + H_2 \rightarrow H_3^+ + He \qquad (R16)$$

which creates the important H_3^+ ion and is an important reaction in dense molecular regions such as Jupiter's ionosphere (Johnsen and Biondi, 1974). H_3^+ is also created by direct proton transfer with H_2^+ in the reaction

$$H_2^+ + H_2 \rightarrow H + H_3^+. \qquad (R17)$$

This reaction is facilitated by the low proton affinity of the H atom relative to the H_2 molecule (2.69 eV versus 4.34 eV). This reaction is therefore quite rapid in regions of sufficient H_2 density, with the product formation rate given by $R_{17} = k_{17}\, n(H_2^+)\, n(H_2)$.

We can roughly determine k_{17} by classical orbital theory since H_2 possesses no permanent electrical dipole moment. We assume that the H_2^+ ion induces an electric dipole moment in

---

[1] The HeH^+ ion (which has a large dipole moment) may also be created by the reaction

$$He^* + H_2 \rightarrow HeH^+ + H + e,$$

and in larger quantities by the reaction

$$H^+ + He \rightarrow HeH^+ + h\nu.$$

The HeH^+ ion has been tentatively identified in NGC 7027 by Dabrowski and Herzberg (1977) as the source of sharp emission features at 3.09 μm and 3.4 μm, but the match between the laboratory and astronomical spectra is quite poor, and can hardly be considered convincing. Furthermore, subsequent observations have cast considerable doubt on Dabrowski and Herzberg's identification (see Scrimger *et al.* 1978; Tokunaga and Young, 1980).

the molecule, which will in turn interact with itself with an interaction energy given by $E = -\alpha e^2/2(4\pi\varepsilon_o)^2 r^4$, where α is the average polarizability[1] of the molecule, e is the ionic charge and r is the ion-molecule distance.

The r^{-4} proportionality of the interaction energy between the molecule and the ion can now be compared to the $E \propto r^{-1}$ rule for gravitationally interacting bodies in Newtonian mechanics. We can treat the problem as one of classical mechanics with the inverse square law of gravity replaced with a steeper inverse fifth power law.

If two point particles approach from infinity, they will collide only if their "impact parameter" (b) is given by

$$b < b_o \equiv \frac{1}{\sqrt{4\pi\varepsilon_o}} \left(\frac{4\alpha e^2}{\mu v^2}\right)^{1/4}$$

where v is the relative particle velocity (at $r = \infty$) and $\mu^{-1} = m_{ion}^{-1} + m_{molecule}^{-1}$.

If the impact parameter is given precisely as $b = b_o$, then the two particles will not collide but will enter a circular orbit of radius $b_o(2)^{-1/2}$. The cross section of the collision

---

[1] The "average polarizability" is defined as $\alpha \equiv (\alpha_{\parallel} + 2\alpha_{\perp})/3$ where $\alpha_{\parallel}$ and $\alpha_{\perp}$ are respectively the parallel and perpendicular components of the molecular polarizability.

is therefore πb_o^2 and the rate coefficient for particles at velocity v is given by:

$$k = \pi b_o^2 v = \frac{\pi v}{4\pi\varepsilon_o}\sqrt{\frac{4\alpha e^2}{\mu v^2}} = \frac{e}{2\varepsilon_o}\sqrt{\frac{\alpha}{\mu}}$$

which is independent of v, and is consequently independent of temperature.

Therefore the value of k_{17} (and hence the creation rate of H_3^+ by Reaction 17) is also independent of gas temperature. Numerically, we find the value of k_{17} to be $\approx 3 \times 10^{-9}\,cm^3\,s^{-1}$. This is the so-called Langevin value of the rate coefficient, which is confirmed by a more rigorous quantum mechanical approach. The Langevin rate coefficient will generally hold for exothermic reactions of the type

$$A^+ + BC \rightarrow A + BC^+$$

that involve non-polar molecules.

We can now very roughly estimate the rate of the H_2^+ destructive reactions 11 through 17 using the published reaction rate coefficients (see Table 5). The transition zone and the molecular envelope will be considered separately. The values of n(H), $n(H_2)$, $n(H_2^+)$, n(He), $n(HeH^+)$, n(e) and the ionization rate for the transition zone are taken from the model by Black (1978) at a radius of 2.9×10^{15} m. The corresponding values for the molecular envelope are taken from Herbst and Klemperer (1973). The adopted abundances are shown in Table 4.

TABLE 4

ASSUMED NUMERICAL ABUNDANCES OF CHEMICAL SPECIES IN THE PN TRANSITION ZONE AND THE MOLECULAR ENVELOPE (in cm^{-3})

SPECIES	TRANSITION ZONE [1]	MOLECULAR ENVELOPE [2]
e	1600	0.007
H	6300	1
H^-	5×10^{-4}	
H_2	0.01	3×10^{5}
H_2^+	6×10^{-4}	6×10^{-8}
H_3^+		7×10^{-6}
He	600	8.4×10^{4}
He^+		2×10^{-6}
HeH^+	10^{-6}	
OH	5×10^{-7}	7×10^{-5}
CO		225
CN		3×10^{-4}
N_2		12
O		40
C		0.02
H_2O		0.012
NH_3		5×10^{-4}
HCN		10^{-4}
H_2CO		10^{-4}

[1] Adapted from Black,J.H. (1978) *Ap.J.***222**,125.

[2] Adapted from Herbst,E.,Klemperer,W. (1973) *Ap.J.***185**,505.

TABLE 5

ADOPTED REACTION RATE COEFFICIENTS FOR NUMBERED CHEMICAL REACTIONS

	REACTION	K VALUE	REFERENCE
1	$H + e \rightarrow H^- + h\nu$	3.9×10^{-15} cm^3 s^{-1} (@ 10 000 K)	1
2	$H^- + H \rightarrow H_2 + e$	2.7×10^{-9} cm^3 s^{-1} (@ 10 000 K)	1
3	$H^- + h\nu \rightarrow H + e$	$5.34 \times 10^{-6}[1+0.33 \exp(-1.4 \times 10^{-18} n(H))]$ s^{-1}	1
4	$H^- + X^+ \rightarrow H + X$	$4 \times 10^{-6} T^{-1/2}$ cm^3 s^{-1}	1
5	$H_2 + h\nu \rightarrow H_2^+ + e$	$3.75 \times 10^{-6} T^{-1/2} \exp(-4.61 \times 10^{-19} n(H))]$ s^{-1}	1
6	$H^+ + H \rightarrow H_2^+ + h\nu$	$(2.325\,T - 1875) \times 10^{-20}$ cm^3 s^{-1}	1
7	$HeH^+ + H \rightarrow H_2^+ + He$	10^{-10} cm^3 s^{-1}	1
8	$H_2 + cr$ [1] $\rightarrow H + H^+ + cr$	2×10^{-19} s^{-1}	2,3
9	$H_2 + cr \rightarrow H + H + cr$	10^{-18} s^{-1}	2,3
10	$H_2 + cr \rightarrow H_2^+ + cr$	9×10^{-18} s^{-1}	2,3
11	$H_2^+ + h\nu \rightarrow H^+ + H$	1.81×10^{-6} s^{-1}	1
12	$H_2^+ + e \rightarrow H + H$	$4.2 \times 10^{-8} T^{-1/2}$ cm^3 s^{-1}	1
13	$H_2^+ + e \rightarrow H_2 + h\nu$	10^{-12} cm^3 s^{-1}	2
14	$H_2^+ + H \rightarrow H^+ + H_2$	10^{-11} cm^3 s^{-1}	1
15	$H_2^+ + He \rightarrow HeH^+ + H$	$3.0 \times 10^{-10} \exp(6717/T)$ cm^3 s^{-1}	1
16	$HeH^+ + H_2 \rightarrow H_3^+ + He$	10^{-9} cm^3 s^{-1}	1
17	$H_2^+ + H_2 \rightarrow H_3^+ + H$	2.1×10^{-9} cm^3 s^{-1}	3
18	$H_3^+ + O \rightarrow OH^+ + H_2$	2.0×10^{-9} cm^3 s^{-1}	3
19	$H_3^+ + C \rightarrow CH^+ + H_2$	2.0×10^{-9} cm^3 s^{-1}	3
20	$H_3^+ + CO \rightarrow HCO^+ + H_2$	1.4×10^{-9} cm^3 s^{-1}	3
21	$H_3^+ + N_2 \rightarrow HN_2^+ + H_2$	1.5×10^{-9} cm^3 s^{-1}	3

Table continued next page…

[1] The letters "cr" designate a cosmic ray.

TABLE 5 (CONTINUED)

ADOPTED REACTION RATE COEFFICIENTS FOR NUMBERED CHEMICAL REACTIONS

	REACTION	K VALUE	REFERENCE
22	$H_3^+ + OH \rightarrow H_2O^+ + H_2$	$2.0 \times 10^{-9}\ cm^3\ s^{-1}$	3
23	$H_3^+ + CN \rightarrow HCN^+ + H_2$	$2.0 \times 10^{-9}\ cm^3\ s^{-1}$	3
24	$H_3^+ + H_2O \rightarrow H_3O^+ + H_2$	$3.0 \times 10^{-9}\ cm^3\ s^{-1}$	3
25	$H_3^+ + NH_3 \rightarrow NH_4^+ + H_2$	$3.6 \times 10^{-9}\ cm^3\ s^{-1}$	3
26	$H_3^+ + HCN \rightarrow H_2CN^+ + H_2$	$2.0 \times 10^{-9}\ cm^3\ s^{-1}$	3
27	$H_3^+ + H_2CO \rightarrow H_3CO^+ + H_2$	$2.0 \times 10^{-9}\ cm^3\ s^{-1}$	3
28	$H_3^+ + e \rightarrow H_3^* \rightarrow H + H + H$	see text	(Section 3.4)
29	$H_3^+ + e \rightarrow H_3^* \rightarrow H_2 + H$	see text	(Section 3.4)
30	$H_3^+ + h\nu \rightarrow H + H + H^+$	"	
31	$H_3^+ + h\nu \rightarrow H_2 + H^+$	"	
32	$H_3^+ + h\nu \rightarrow H_2^+ + H$	"	
33	$H_3^+ + H^- \rightarrow H_2 + H_2^* \rightarrow H_2 + H + H$	"	
34	$H_3^+ + H^- \rightarrow H_2 + H_2^* \rightarrow H_2 + H_2 + h\nu$	"	
35	$H_3^+ + H^- \rightarrow H_3^* + H \rightarrow H + H + H + H$	"	
36	$H_3^+ + H^- \rightarrow H_3^* + H \rightarrow H_2 + H + H$	"	

REFERENCES: 1) Black,J.H. (1978) *Ap.J.***222**,125.
2) Duley,W.W.,Williams,D.A. (1984) *Interstellar Chemistry*. Academic Press.
3) Herbst,E.,Klemperer,W. (1973) *Ap.J.***185**,505

The rates of the H_2^+ destruction reactions in the transition zone (T = 10000 K) are found to be

$$R_{11(TZ)} = k_{11(TZ)} n(H_2^+) = 1.1 \times 10^{-9} \text{ cm}^{-3} \text{ s}^{-1}$$

$$R_{12(TZ)} = k_{12(TZ)} n(H_2^+) n(e) = 1.3 \times 10^{-8} \text{ cm}^{-3} \text{ s}^{-1}$$

$$R_{13(TZ)} = k_{13(TZ)} n(H_2^+) n(e) = 1.2 \times 10^{-11} \text{ cm}^{-3} \text{ s}^{-1}$$

$$R_{14(TZ)} = k_{14(TZ)} n(H_2^+) n(H) = 3.2 \times 10^{-10} \text{ cm}^{-3} \text{ s}^{-1}$$

$$R_{15(TZ)} = k_{15(TZ)} n(H_2^+) n(He) = 5 \times 10^{-10} \text{ cm}^{-3} \text{ s}^{-1}$$

$$R_{17(TZ)} = k_{17(TZ)} n(H_2^+) n(H_2) = 6 \times 10^{-15} \text{ cm}^{-3} \text{ s}^{-1}.$$

The removal of H_2^+ in the molecular envelope proper (at T = 20 K) occurs with the reaction rates

$$R_{11(ME)} = k_{11(ME)} n(H_2^+) = 1.1 \times 10^{-13} \text{ cm}^{-3} \text{ s}^{-1}$$

$$R_{12(ME)} = k_{12(ME)} n(H_2^+) n(e) = 1.4 \times 10^{-17} \text{ cm}^{-3} \text{ s}^{-1}$$

$$R_{13(ME)} = k_{13(ME)} n(H_2^+) n(e) = 1.4 \times 10^{-21} \text{ cm}^{-3} \text{ s}^{-1}$$

$$R_{14(ME)} = k_{14(ME)} n(H_2^+) n(H) = 8 \times 10^{-21} \text{ cm}^{-3} \text{ s}^{-1}$$

$$R_{15(ME)} = k_{15(ME)} n(H_2^+) n(He) = 10^{-156} \text{ cm}^{-3} \text{ s}^{-1}$$

$$R_{17(ME)} = k_{17(ME)} n(H_2^+) n(H_2) = 6 \times 10^{-11} \text{ cm}^{-3} \text{ s}^{-1}.$$

Comparing the rates derived for Reaction 17 in the two regions, we find the interesting result that the H_3^+ ion is created by Reaction 17 ten thousand times faster outside the transition zone than in. This is surprising because the H_2^+ ions from which H_3^+ is formed are ten thousand times more abundant inside the transition zone than out. This strange result can be easily understood by comparing $R_{12(TZ)}$ with $R_{12(ME)}$. The electron density is so high in the transition

zone that most H_2^+ is destroyed by dissociative recombination (Reaction 12) before it can create H_3^+ via Reaction 17.

The relative abundance of H_3^+ to H_2 in the molecular envelope was found by Mitchell, Ginsburg and Kuntz to be nearly constant for various values of $n(H_2)$. The column density of H_3^+ can consequently be easily determined by assuming a maximum value of $n(H_2)$ of $2.5 \times 10^5\ cm^{-3}$ at $r = 5 \times 10^{18}$ cm and an r^{-3} dependence of density with radius. We find that the column density of H_3^+ in the molecular envelope is $\approx 2 \times 10^{15}\ cm^{-2}$.

The equilibrium abundance of H_3^+ in the transition zone was not determined by Black, but this may be worked out from the abundances he does include. An unfortunate complication does however arise since photodestruction and recombination with negative ions are important processes in the transition zone. In the next section we take a closer look at the H_3^+ destruction reactions to determine the TZ number density of this important ion.

3.4 Formation of H_3

The H_3^+ ion is extremely chemically reactive and the formation of this ion initiates many subsequent reactions. The importance to interstellar chemistry of the H_3^+ molecule was discussed by Herbst and Klemperer (1973) and by Watson

(1973). The H_3^+ ions interact with other species in proton transfer reactions of the type

$$H_3^+ + X \rightarrow XH^+ + H_2$$

where X may denote the species O, OH, CO, N_2, H_2O, NH_3 *etc.*. Reactions of this type dominate over reactions of the form

$$H_3^+ + X \rightarrow XH + H_2^+$$

because of the relatively low proton affinity of H_2 (4.34 eV). The species X almost always has a higher proton affinity than molecular hydrogen, making reactions of the second type quite rare. The rate coefficients for these reactions are found to be both temperature independent and in close agreement with the Langevin value (see Section 3.3).

The ion-molecule reactions that proved most efficient in removing H_3^+ in the models of Herbst and Klemperer and of Mitchell, Larson and Fink are:

$$H_3^+ + O \rightarrow OH^+ + H_2 \qquad \text{(R18)}$$

$$H_3^+ + C \rightarrow CH^+ + H_2 \qquad \text{(R19)}$$

$$H_3^+ + CO \rightarrow COH^+ + H_2 \qquad \text{(R20)}$$

$$H_3^+ + N_2 \rightarrow N_2H^+ + H_2 \qquad \text{(R21)}$$

$$H_3^+ + OH \rightarrow H_2O^+ + H_2 \qquad \text{(R22)}$$

$$H_3^+ + CN \rightarrow HCN^+ + H_2 \qquad \text{(R23)}$$

$$H_3^+ + H_2O \rightarrow H_3O^+ + H_2 \qquad \text{(R24)}$$

$$H_3^+ + NH_3 \rightarrow NH_4^+ + H_2 \qquad \text{(R25)}$$

$$H_3^+ + HCN \rightarrow H_2CN^+ + H_2 \qquad \text{(R26)}$$

$$H_3^+ + H_2CO \rightarrow H_3CO^+ + H_2 \qquad \text{(R27)}$$

The ions produced in these reactions are then involved in subsequent reactions that synthesize progressively larger polyatomic molecules. These reactions also serve to destroy H_3^+ ions before they can react with free electrons in the dissociative recombination processes:

$$H_3^+ + e \rightarrow H_3^* \rightarrow H + H + H \qquad \text{(R28)}$$

$$H_3^+ + e \rightarrow H_3^* \rightarrow H_2 + H \qquad \text{(R29)}$$

where the intermediate product H_3^* is an electronically excited H_3 molecule.

Reactions 28 and 29 can be considered together because they do not contribute significantly to the densities of H and H_2, and so it does not matter that their ultimate products are different. The reaction rate is given by

$$R_{28} + R_{29} = (k_{28} + k_{29})\, n(H_3^+)\, n(e).$$

We now have a very serious problem. The coefficients k_{28} and k_{29} are simply not known. We *do* know that dissociative recombination reactions of this type tend to have a roughly $T^{-1/2}$ dependence. This can be seen from a classical Boltzmann analysis of the particle velocities. Unfortunately, this treatment does not account for the quantum mechanical dependence of the reaction cross-section with the ion's energy state.

Work by Smith and Adams (1984) has shown that the dissociative recombination coefficient of ground state H_3^+

ions has an upper limit of $2 \times 10^{-8}\,cm^{-3}\,s^{-1}$. In their 1973 paper, Herbst and Klemperer had accepted a very much larger value of $(k_{28} + k_{29})$ of $3 \times 10^{-7}\,cm^{-3}\,s^{-1}$.

At the low temperatures and high densities of the molecular envelope, the H_3^+ ion is expected to be in the ground state because of collisional deexcitation. Herbst and Klemperer's $(k_{28} + k_{29})$ value in the low temperature molecular envelope is therefore a serious overestimate. We also have no reliable way of determining the value of $(k_{28} + k_{29})$ in the high temperature transition zone, since the degree of H_3^+ excitation in this regime is unknown.

This may have serious repercussions for the whole model. The equations for R_{28} and R_{29} are two in the system of differential equations that need to be solved when deriving the equilibrium number densities. An error in the rate coefficients for reactions 28 and 29 would affect the equilibrium number density of H_3^+, and hence the rates of reactions 18 through 27, and subsequently change the predicted number densities of all the molecules.

It will now be argued however that the erroneous reaction rate coefficients used by Herbst and Klemperer (and also by Mitchell, Larson and Fink) do *not* radically affect the calculated molecular abundances in their models. It is found that even if one uses the erroneously high value of $(k_{28} + k_{29})$, the

two reactions 28 and 29 destroy very little of the H_3^+ because nearly all the ions partake in reactions 18 through 27. The numerical evidence is as follows: Adopting the number densities of Table 4, we find;

$$R_{18(ME)} = k_{18(ME)}\, n(O)\, n(H_3^+) = 8 \times 10^{-8}\, n(H_3^+)\ s^{-1}$$

$$R_{19(ME)} = k_{19(ME)}\, n(C)\, n(H_3^+) = 4 \times 10^{-11}\, n(H_3^+)\ s^{-1}$$

$$R_{20(ME)} = k_{20(ME)}\, n(CO)\, n(H_3^+) = 3 \times 10^{-7}\, n(H_3^+)\ s^{-1}$$

$$R_{21(ME)} = k_{21(ME)}\, n(N_2)\, n(H_3^+) = 2 \times 10^{-8}\, n(H_3^+)\ s^{-1}$$

$$R_{22(ME)} = k_{22(ME)}\, n(OH)\, n(H_3^+) = 1.4 \times 10^{-14}\, n(H_3^+)\ s^{-1}$$

$$R_{23(ME)} = k_{23(ME)}\, n(CN)\, n(H_3^+) = 6 \times 10^{-13}\, n(H_3^+)\ s^{-1}$$

$$R_{24(ME)} = k_{24(ME)}\, n(H_2O)\, n(H_3^+) = 3.6 \times 10^{-11}\, n(H_3^+)\ s^{-1}$$

$$R_{25(ME)} = k_{25(ME)}\, n(NH_3)\, n(H_3^+) = 2 \times 10^{-12}\, n(H_3^+)\ s^{-1}$$

$$R_{26(ME)} = k_{26(ME)}\, n(HCN)\, n(H_3^+) = 2 \times 10^{-13}\, n(H_3^+)\ s^{-1}$$

$$R_{27(ME)} = k_{27(ME)}\, n(H_2CO)\, n(H_3^+) = 2 \times 10^{-13}\, n(H_3^+)\ s^{-1}$$

$$R_{28(ME)} = k_{28(ME)}\, n(e)\, n(H_3^+) = 10^{-9}\, n(H_3^+)\ s^{-1}$$

$$R_{29(ME)} = k_{29(ME)}\, n(e)\, n(H_3^+) = 10^{-9}\, n(H_3^+)\ s^{-1}$$

The total rate of the nine ion-molecule reactions is therefore $\approx 4 \times 10^{-7}\, n(H_3^+)\ s^{-1}$, while the two dissociative recombination reactions proceed at a rate of $\approx 2 \times 10^{-9}\, n(H_3^+)\ s^{-1}$. The dissociative recombination reactions 28 and 29 remove only 0.5% of the H_3^+ ions in the model molecular cloud of Herbst and Klemperer. It is therefore suggested that the adoption of a more realistic lower rate coefficient for reactions 28 and 29 would not seriously affect Herbst and Klemperer's model,

and that their value of $n(H_3^+)$ for the molecular envelope is acceptable for this discussion.

To estimate the H_3 formation rate in the molecular envelope, we will accept the upper limit to the value of $(k_{28} + k_{29})$ of Smith and Adams; $(k_{28} + k_{29}) = 2 \times 10^{-8}\,cm^3\,s^{-1}$. We then have for the preshock molecular gas

$$\begin{aligned} R_{28(ME)} + R_{29(ME)} &= [k_{28(ME)} + k_{29(ME)}]\, n(H_3^+)\, n(e) \\ &\leq (2 \times 10^{-8}\,cm^3\,s^{-1})\, n(H_3^+)\, n(e) \\ &\leq 10^{-17}\,cm^{-3}\,s^{-1}. \end{aligned}$$

Leaving the molecular envelope, we now wish to find the rate of H_3^+ destruction in the transition zone. We first find the rate of H_3^+ *formation*, since the two rates are equal. The reactions that produce H_3^+ are 16 and 17. The value of R_{17} has already been found, while R_{16} is given by

$$R_{16(TZ)} = k_{16(TZ)}\, n(H_2)\, n(HeH^+) \leq 10^{-17}\,cm^{-3}\,s^{-1}$$

The rate of H_3^+ formation in the transition zone is thus

$$R_{16(TZ)} + R_{17(TZ)} = 6 \times 10^{-15}\,cm^{-3}\,s^{-1}.$$

We now look at the *destruction* of H_3^+. We can be certain that reactions 28 and 29 completely dominate reactions 18 through 27 in the transition zone since the number density of electrons is nine orders of magnitude greater than any of the molecules. The destruction of H_3^+ in the transition zone will therefore occur by the dissociative recombination reactions 28 and 29, or by the photodissociative reactions

$$H_3^+ + h\nu \rightarrow H + H + H^+ \qquad \text{(R30)}$$

$$H_3^+ + h\nu \rightarrow H_2 + H^+ \qquad \text{(R31)}$$

$$H_3^+ + h\nu \rightarrow H_2^+ + H, \qquad \text{(R32)}$$

and possibly by the mutual neutralization reaction sequences

$$H_3^+ + H^- \rightarrow H_2 + H_2^* \rightarrow H_2 + H + H \qquad \text{(R33)}$$

$$H_3^+ + H^- \rightarrow H_2 + H_2^* \rightarrow H_2 + H_2 + h\nu \qquad \text{(R34)}$$

$$H_3^+ + H^- \rightarrow H_3^* + H \rightarrow H + H + H + H \qquad \text{(R35)}$$

$$H_3^+ + H^- \rightarrow H_3^* + H \rightarrow H_2 + H + H. \qquad \text{(R36)}$$

In order to calculate the H_3 formation rate we must adopt values of the reaction coefficients that are appropriate for the PN transition zone (T = 10 000 K). Unfortunately, there now exists considerable doubt as to the accuracy of published values of $(k_{28} + k_{29})$. Previous models of interstellar chemistry were based on measured $(k_{28} + k_{29})$ values of:

$$k_{28} + k_{29} = 2.0 \times 10^{-7}\ \mathrm{cm^3\,s^{-1}}\ @\ 400\ \mathrm{K},\ ^{(1)}$$

$$k_{28} + k_{29} = 2.3 \times 10^{-7}\ \mathrm{cm^3\,s^{-1}}\ @\ 300\ \mathrm{K},\ ^{(1)}$$

$$k_{28} + k_{29} = 2.9 \times 10^{-7}\ \mathrm{cm^3\,s^{-1}}\ @\ 205\ \mathrm{K},\ ^{(1)}$$

$$k_{28} + k_{29} = 3.0 \times 10^{-7}\ \mathrm{cm^3\,s^{-1}}\ @\ 200\ \mathrm{K},\ ^{(2)}$$

$$k_{28} + k_{29} = 7.2 \times 10^{-7}\ \mathrm{cm^3\,s^{-1}}\ @\ 100\ \mathrm{K},\ ^{(3)}$$

$$k_{28} + k_{29} = 1.1 \times 10^{-6}\ \mathrm{cm^3\,s^{-1}}\ @\ 40\ \mathrm{K}.\ ^{(3)}$$

---

[1] Leu,M.,Biondi,M.A,Johnsen,R. (1973) *Phys.Rev.***A8**,413.

[2] Black,J.H. (1978) *Ap.J.***222**,125.

[3] Duley,W.W.,Williams,D.A. (1984) *Interstellar Chemistry*, Academic Press

These data indicate a functional dependence of $(k_{28} + k_{29})$ with temperature of $(k_{28} + k_{29}) = 6.1 \times 10^{-6} T^{-1/2} \text{ cm}^3 \text{ s}^{-1}$, resulting in a transition zone value (T = 10 000 K) of

$$k_{28(TZ)} + k_{29(TZ)} = 6.0 \times 10^{-8} \text{ cm}^3 \text{ s}^{-1}.$$

The experimental data were collected with the "stationary afterglow" and "merged beam" techniques. Unfortunately, the stationary afterglow data were apparently contaminated by H_5^+ ions (Smith and Adams, 1984) and is consequently unreliable. The merged beam data are similarly suspect, as the H_3^+ ions produced in these experiments are expected to be vibrationally excited ($v > 3$). They would thus have very much larger collisional cross-sections than do the ground state H_3^+ ions. It is unclear to what degree the H_3^+ in the PN transition zone is vibrationally excited, so the data may or may not have a direct bearing on the problem at hand. Nevertheless, the derived value of $(k_{28(TZ)} + k_{29(TZ)})$ is accepted, but with the recognition that this may be a serious overestimate. We accept this value only as an upper limit.

The rates of reactions 33 through 36 are likewise not known from experiment, but a rough estimate may be made based on physical arguments. First, the reactions 33 and 34 are proton transfer reactions which are inherently less probable than the electron transfer reactions 35 and 36. The reaction rates of 33 and 34 are further reduced because the proton affinity of the H_2 molecule is 4.34 eV, while the electron

affinity of the H atom is only 0.754 eV. The proton is consequently much less likely to change partners than the electron is, and so proton transfer must occur at a negligibly small rate compared to electron transfer. The reactions 33 and 34 will then be completely neglected.

We can now derive an *upper limit* to the H_3 formation rate, by assuming that all H_3^+/H^- neutralization reactions results in the formation of H_3. The reaction rates of mutual neutralization reactions between oppositely charged ions is typically $k \sim 10^{-6} T^{-1/2}\,cm^3\,s^{-1}$. The adopted transition zone rate of reactions 35 and 36 is therefore $(k_{35(TZ)} + k_{36(TZ)}) \approx 10^{-8}\,cm^3\,s^{-1}$. This is of the same order of magnitude as the adopted rate coefficient of reactions 28 and 29, but these reactions will nevertheless occur at a very much faster rate than reactions 35 and 36 because of the low abundance of H^- relative to free electrons.

Since we are assuming chemical equilibrium, we require the formation and destruction rates of H_3^+ to be equal. If we neglect reactions 33 and 34 and also assume that reactions 18 through 27 are insignificant because of the relative scarcity of molecules, we can write

$$R_{16(TZ)} + R_{17(TZ)} = R_{28(TZ)} + R_{29(TZ)} + R_{30(TZ)} + R_{31(TZ)} + R_{32(TZ)} + R_{35(TZ)} + R_{36(TZ)}$$

We now replace the reaction rates with equivalent expressions, and drop the TZ subscripts to get

$$R_{16} + R_{17} = n(H_3^+)\left[(k_{28} + k_{29})\,n(e) + (k_{30} + k_{31} + k_{32}) + (k_{35} + k_{36})\,n(H^-)\right]$$

Replacing those terms in the previous equation which have numerical values listed in tables 4 and 5, we find that

$$n(H_3^+) = \frac{\left[(6 \times 10^{-8})\,(1600)\,s^{-1} + (10^{-5})\,s^{-1} + (10^{-8})\,(5 \times 10^{-4})\,s^{-1}\right]}{6 \times 10^{-15}\,cm^{-3}\,s^{-1}}$$

$$= 6 \times 10^{-11}\,cm^{-3}$$

We also find that the rate of those reactions that form H_3 as an intermediate product is

$$R_{28(TZ)} + R_{29(TZ)} + R_{35(TZ)} + R_{36(TZ)} = 3 \times 10^{-26}\,cm^{-3}\,s^{-1}$$

In order to find the density of H_3, we must now multiply this value by the lifetime of an H_3 molecule. As we shall see in the next chapter, the ground state of H_3 is repulsive and will break up in $\sim 10^{-13}$ s. The excited states of the molecule are not predissociated, and have a lifetime of at least 100 times greater than the repulsive ground state. We can now (very crudely) estimate the molecule's lifetime as $\sim 10^{-11}$ s. The density of H_3 in the transition zone would consequently be $\approx 3 \times 10^{-37}\,cm^{-3}$.

The density of H_3 in the molecular envelope can be found in a similar manner. An upper limit to the H_3 formation rate in the preshock molecular envelope was shown to be

$$R_{28(ME)} + R_{29(ME)} \leq 10^{-17}\,cm^{-3}\,s^{-1}.$$

The density of H_3 in the preshock molecular gas is therefore $10^{-28}\,cm^{-3}$. We can now find the column density of H_3 by integrating along the line of sight under an assumed r^{-3} density dependence in the molecular envelope. It is found that the column density of molecular envelope H_3 is on the order of $10^{-10}\,cm^{-2}$, while the corresponding value for the transition zone is on the order of $10^{-17}\,cm^{-2}$. We would consequently *not* expect to see H_3 emission from planetary nebulae.

3.5 Some Notes on the Validity of the Published Models

Black's transition zone model and the molecular envelope models are all in chemical equilibrium. It is therefore appropriate to comment on the validity of assuming time independence of the derived chemical abundances.

Different chemical species reach equilibrium concentrations at different times, and one might naively assume that relatively simple molecules such as the hydrogen compounds discussed here would reach equilibrium fairly quickly. This indeed appears to be the case in the transition zone, where reactions occur rapidly and complex molecules are prevented from forming.

We can estimate the time period required for chemical equilibrium by assuming that the precursor species of the molecule in question have already reached equilibrium. For

example, in the case of the H^- ion we assume that the H atoms, the electrons, and the positive atomic ions are at equilibrium concentration. We can then write under the additional assumption that $n(X^+) \approx n(e)$ that

$$\frac{dn(H^-)}{dt} = R_{1(TZ)} - R_{2(TZ)} - R_{3(TZ)} - R_{4(TZ)}$$

$$= k_{1(TZ)} n(H) n(e) - k_{2(TZ)} n(H^-) n(H) - k_{3(TZ)} n(H^-) - k_{4(TZ)} n(H^-) n(X^+)$$

$$\frac{dn(H^-)}{dt} = 3.9 \times 10^{-8}\,cm^{-3}\,s^{-1} - 8.8 \times 10^{-5}\,n(H^-)\,s^{-1}.$$

This is a simple first order differential equation, and can be easily integrated to yield

$$n(H^-) = \left[\frac{3.9 \times 10^{-8}\,cm^{-3}\,s^{-1}}{8.8 \times 10^{-5}\,s^{-1}}\right] \left[1 - e^{[-8.8 \times 10^{-5}\,s^{-1} t]}\right].$$

After a time of $[8.8 \times 10^{-5}]^{-1}$ seconds, the value of $n(H^-)$ would consequently reach $(1 - e^{-1}) = 0.63$ times its equilibrium value. In this case, the required time interval is $\approx 1.1 \times 10^4$ seconds, or about 3 hours. A similar argument determines the steady state time interval of H_2 in the transition zone as $\approx 2.7 \times 10^7$ seconds (2.5 years), while the corresponding values for H_2^+ and H_3^+ are respectively ≈ 4 days and ≈ 6 months.

It is apparent that the e folding time scales of the molecules in question are very much less than evolutionary time scales. Steady state calculations are therefore acceptable for the PN transition zone. It is however not readily apparent that this is also the case in the cold molecular

envelope. We can fortunately determine the equilibrium time scale of the ME by making a few simplifying assumptions.

In the molecular envelope, the vast majority of H_2^+ is destroyed by collision with H_2 (Reaction 17), while proton transfer with CO (Reaction 20) is most important in the removal of H_3^+. If we assume that all the H_2^+ and H_3^+ ions are respectively removed by these two reactions, we can find an *upper limit* to the e folding time scales of H_2^+ and H_3^+. We need only make the additional assumption that the number densities of H_2 and CO are constant over one H_2^+ and H_3^+ equilibrium time scale and are given by their observed values (see Sections 2.5 and 2.6). It is found that H_2^+ reaches 0.63 times its steady state concentration in <30 minutes, while H_3^+ takes <40 days. It is again found that steady state models should be sufficiently accurate.

The models published by Black are structurally simplified. Black assumes a monotonically decreasing ionization gradient within a dust free H II region. The total particle density is radius independent and has a value of 7000 cm^{-3}. Analysis of NGC 7027's forbidden and recombination line spectrum (Section 2.4) does however show this to be unrealistic. The real nebula is highly structured with zones of high density and lowered ionization within its H II region. Internal dust extinction is also known to be significant. The true molecular density could consequently be enhanced in the high

density knots, making the derived abundances serious underestimates.

The observations of H_2^+ absorption in other planetary nebulae provide indirect evidence that this indeed may be the case. The maximum value of the total column density of H_2^+ predicted for NGC 7027 by adding the column densities derived from Mitchell *et al.*'s model molecular envelope and Black's transition zone is $\sim 10^{14}\,cm^{-2}$. The real value would be expected to be less, as this number was found by adding the most absurdly high values suggested in Section 3.2. However, the column density of H_2^+ that is actually observed by Heap and Stecher in the other PN is 2 to 3 orders of magnitude greater. We would expect these PN to have, if anything, a *smaller* H_2^+ column density than NGC 7027, since they all have far less prominent molecular emission lines. This strongly suggests that the models grossly underestimate the number density of ionized H_2.

The reasons for this discrepancy are not readily seen, since there seems to be no plausible ways of forming H_2^+ besides those reactions already discussed. The dust grain reactions that produce H_2 (and subsequently H_2^+) in the cold molecular envelope are completely shut down at transition zone temperatures. Although dust cannot contribute significantly to the *production* of transition zone molecules, it may however be important in preventing their *destruction*.

The internal dust extinction is measured to be 0.34 magnitudes at 5007 Å across the diameter of the ionized nebula (Atherton, 1979), or 0.17 magnitudes across its radius (assuming a radially symmetric dust distribution). Therefore the stellar radiance at 5007 Å in the transition zone has only 86% of its value in a dust free nebula.

In order to find the effect of dust extinction on H_2 destruction, we must first determine how much the central star's UV light is attenuated at the edge of the H II region. We make use of the general relation

$$L_\lambda = L_\lambda(0)\, e^{(-\tau_\lambda)}$$

where L_λ is the stellar radiance at the transition zone, $L_\lambda(0)$ is the radiance at the stellar surface and τ_λ is the optical depth.

We next convert optical depth to extinction in stellar magnitudes with the formula

$$A_\lambda = 1.086\,\tau_\lambda.$$

We also make use of Mie scattering theory, where the light intensity at a distance r is given by

$$L_\lambda = L_\lambda(0)\, e^{(-Q_\lambda \pi a^2 n\, r)}$$

where Q_λ is the Mie extinction parameter, n is the number density of grains (in units of cm^{-3}), and a is the radius of the grains. The dust grains are assumed to be spherical, uniform in size, and small. We find that

$$A_\lambda = -1.086 Q_\lambda \pi a^2 n r.$$

We can now determine the dust extinction coefficient at a photon energy of 4.48 eV, which is the dissociation energy of H_2. A photon of this energy has a wavelength of 2770 Å, and so we can write

$$\frac{A_{2770Å}}{A_{5007Å}} = \frac{-1.086 Q_{2770Å} \pi a^2 n r}{-1.086 Q_{5007Å} \pi a^2 n r} = \frac{Q_{2770Å}}{Q_{5007Å}}$$

We now find in Wickramasinghe (1967) that $Q_{2770Å}$ is ≈ 1.2 and $Q_{5007Å}$ is ≈ 0.3, assuming a grain radius of $a = 0.02\,\mu m$. We thus find that $Q_{2770Å}/Q_{5007Å}$ is ≈ 4, and so the dust extinction at 4.48 eV across the radius of the H II region is roughly 0.7 magnitudes.

The H_2 dissociating radiation is consequently attenuated to about 55% of its unreddened radiance. The UV shielding by dust would therefore significantly contribute to the lifetime of transition zone H_2 molecules.

However, it is clearly seen that 0.02 μm dust cannot increase the molecules' lifetimes by several orders of magnitude, since over half of the dissociating ultraviolet reaches the edge of the H II region. We therefore conclude that the addition of 0.02 μm dust would not increase the observed molecular concentrations by several orders of magnitude either.

Hence it is found that adding of dust grains of typical interstellar size to the nebula's H II region will not raise molecular abundances to the high levels suggested by ultraviolet H_2^+ absorption.

Another possible way to raise molecular abundances is to add *very small* dust grains such as those suggested by Sellgren *et al.* (1983). Sellgren's hypothetical grains are made of graphite and have a radius of only ~5Å. These grains are a proposed source of unidentified IR emission features at 8.6 and 11.3μm. The infrared emission would come from CH radicals which are created by ambient hydrogen atoms bonding to the particles' surfaces. The stretching modes of the CH groups produce the IR emission bands when the grain is excited by a single UV photon.

The graphite grains absorb ultraviolet light, but are also responsible for Rayleigh scattering of incident radiation. Rayleigh scattering is proportional to λ^{-4}, and so the blue end of the spectrum is far more susceptible to its effects than the red. The soft UV flux at the transition zone could therefore be seriously diminished by these very small grains of graphite. A dusty planetary nebula might then be radically different from the purely gaseous models that have been written to date. It would be very interesting to compute a model PN that accounts for dust grain extinction by a wide range of grain sizes.

CHAPTER 4

THE SPECTRUM OF THE H_3 MOLECULE

The H_3 molecule was largely ignored by theoretical and experimental spectroscopists alike for much of the era of modern spectroscopy. This occurred because nobody could even find it before the late 1970's. However, a rash of papers appeared in the latter half of the seventies and into the early eighties after scientists discovered this relatively simple, but as yet unstudied, molecule. These publications culminated in a series of four papers by G. Herzberg and collaborators which presented the first actual observations of the H_3 spectrum.

4.1 SYMMETRY OF THE H_3 MOLECULE

H_3 is the simplest non-linear molecule, and so its spectrum makes a fine introduction to the theory of symmetric top molecular spectra. H_3 is of course homonuclear, with its three atoms arranged in an equilateral triangle. Ergo, the H_3 molecule is classified in the *molecular point group* $\mathbf{D}_{3h}$. The point group classification system is based on molecule symmetry, with the $\mathbf{D}_{3h}$ group including all equilateral triangular molecules of the chemical formula "X_3", as well as many other polyatomics.

In order to be a member of the $\mathbf{D}_{3h}$ point group, a molecule must have three axes about which a rotation of 180° would leave the atom's coordinates unchanged with respect to any laboratory stationary coordinate system. A fourth axis of symmetry (orthogonal to the first three) must also be present. Rotations about the fourth axis through 120° does not alter the atom's positions.

The three non-orthogonal axes of symmetry are referred to as the C_2 symmetry elements, since a rotation about each of these axes by an angle of $360° \div 2 = 180°$ does not result in a change of the atomic positions. The fourth axis of symmetry carries the appellation C_3 since the molecule's atomic arrangement is unaltered by a rotation of $360° \div 3 = 120°$. The C_3 axis is also referred to as the *principal* or *figure axis of symmetry* of the $\mathbf{D}_{3h}$ point group.

In addition to the axes of symmetry, there must also be four *planes of symmetry*, one of which is orthogonal to the first three. The atomic coordinates are not altered by a reflection through any of these planes. The planes of symmetry are denoted by the symbol σ, and carry the subscripted designations σ_h or σ_v depending on whether they are horizontal or vertical to the atomic plane.

The H_3 molecule is represented schematically with its symmetry elements in both Cartesian and cylindrical coordinates in Figure 1.

FIGURE 1

SYMMETRY ELEMENTS OF THE H_3 MOLECULE

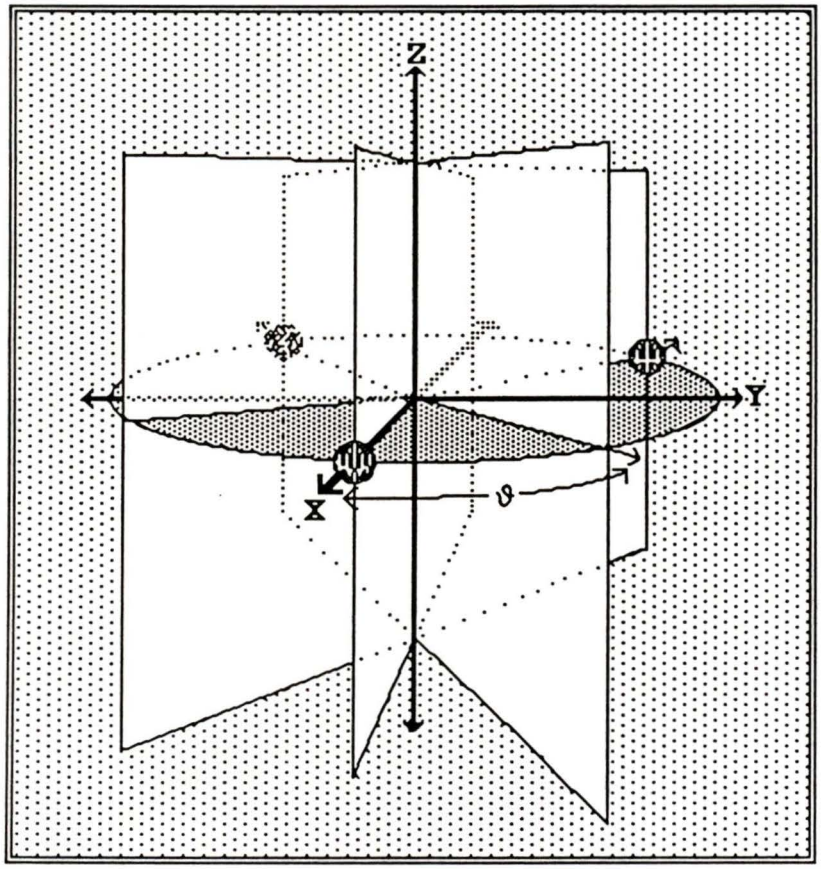

Atoms:
$\vartheta = 0°, r = R$
$\vartheta = 120°, r = R$
$\vartheta = 240°, r = R$

C_2:
$\vartheta = 0°, Z = 0$
$\vartheta = 120°, Z = 0$
$\vartheta = 240°, Z = 0$

C_3:
Z axis

σ_h:
XY plane

σ_v:
$\vartheta = 0°$
$\vartheta = 120°$
$\vartheta = 240°$

The symmetry elements C_2, C_3, σ_h, and σ_v are also used to define quantum mechanical operators. The operators they define are

$C_2 \leftrightarrow$ Rotation through 180° about a C_2 axis.

$C_3 \leftrightarrow$ Rotation through 120° about the C_3 axis.

$\sigma \leftrightarrow$ Reflection through a plane of symmetry.

The operator C_3 can be either a rotation in the counterclockwise, or the clockwise direction; or equivalently a rotation of 120° or 240° in the counterclockwise (positive ϑ) direction. In order to distinguish the two rotations, they will be denoted by

$C_3 \leftrightarrow$ Counterclockwise rotation of 120° about the C_3 axis,
$C_3^2 \leftrightarrow$ Counterclockwise rotation of 240° about the C_3 axis.

The three σ_v planes must also be distinguished, and will carry the designations

$\sigma_v \leftrightarrow$ Reflection through the σ_v plane at $\vartheta = 0°$,
$\sigma_v' \leftrightarrow$ Reflection through the σ_v plane at $\vartheta = 120°$,
$\sigma_v'' \leftrightarrow$ Reflection through the σ_v plane at $\vartheta = 240°$.

A set of superscripts similar to those used on the σ_v operators will be used on the three C_2 operators to distinguish between rotations about the C_2 axes at $\vartheta = 0°, 120°,$ and 240°.

Another operator that needs to be mentioned is a rotation about a p-fold axis of symmetry followed by a reflection through a plane perpendicular to this axis. This operator is denoted S_p, with the subscript p replaced by the subscript on the axis type. The specific rotation-reflection operator that concerns us here is S_3. The same superscripts are used to distinguish the two S_3 operators as are used for the two C_3 operators.

In addition to these operators, there exists the so-called identity operator which is usually designated by I (but sometimes by E). The identity operator does not alter the atomic coordinates in any way, but is included so the set of operators defines a true mathematical group.

One can prove that these operators form a mathematical group by simple application of the following definition of a group: In order to be a true mathematical group, four requirements must be met;

1) There must exist a rule for combining (multiplying) any two members of the group and the result (product) is likewise a member of the group. That is, the expression $PQ=R$, can be written where P, Q and R are all members of the group.

2) The associative law must hold. That is, $P(QR) = (PQ)R$.

3) There must exist an identity element I, with the property $IP=PI=P$ for P equal to any member of the group.

4) There exists an inverse element for P, designated by P^{-1}, with the property that $P^{-1}P=PP^{-1}=I$ for all members P of the group.

It is easy to see that the first condition is met by our set of operators. For instance, one can easily verify that

the first condition holds in such examples as $C_3 \sigma_h = S_3$, $I C_3 = C_3$ *etc*. The second rule may be seen to hold as well by investigating such combinations as

$$\sigma_v (C_3 \sigma_v') \ ? \ (\sigma_v C_3) \sigma_v'$$

We see that the left hand side is equal to $\sigma_v (C_3 \sigma_v') = \sigma_v (\sigma_v) = I$, while the right hand side is $(\sigma_v C_3) \sigma_v' = (\sigma_v) \sigma_v = I$, and hence the associative law holds. Finally, we see that the fourth rule holds by examining equations like $C_2 \sigma_v = I$.

The defined quantum mechanical operators can be represented by matrices, and so their actions can be determined mathematically as well as diagrammatically. For example, let us define T_x as translation in the positive X direction and R_x as rotation about the X axis. Operating on T_x with C_3 will change T_x to a translation along the $\vartheta = 120°$ line. In Cartesian coordinates, this can be written

$$C_3 (T_x) = -\frac{1}{2} T_x - \frac{\sqrt{3}}{2} T_y$$

while performing the same operation on T_y is written as

$$C_3 (T_y) = \frac{\sqrt{3}}{2} T_x - \frac{1}{2} T_y .$$

We see that both the X and Y coordinates are present in each of these equations. We can then form the matrix relation

$$C_3 \begin{pmatrix} T_x \\ T_y \end{pmatrix} = \begin{pmatrix} -\frac{1}{2} & -\frac{\sqrt{3}}{2} \\ +\frac{\sqrt{3}}{2} & -\frac{1}{2} \end{pmatrix} \begin{pmatrix} T_x \\ T_y \end{pmatrix} = \begin{pmatrix} T_x' \\ T_y' \end{pmatrix}$$

The trace of the C_3 matrix is -1, and this value is usually displayed along with the matrix traces of the other operators in a *character table*. The name "character table" is traditional, but is somewhat anachronistic since a character is now called a matrix trace. The character table for the D_{3h} point group is presented in Table 6.

TABLE 6 [1]

TRACES OF TRANSFORMATION MATRICES FOR THE D_{3h} POINT GROUP SYMMETRY OPERATORS

D_{3h}	I	C_3	C_3^2	C_2	C_2'	C_2''	σ_h	S_3	S_3^2	σ_v	σ_v'	σ_v''	
	+1	+1	+1	+1	+1	+1	+1	+1	+1	+1	+1	+1	
	+1	+1	+1	+1	+1	+1	-1	-1	-1	-1	-1	-1	
	+1	+1	+1	-1	-1	-1	+1	+1	+1	-1	-1	-1	R_z
	+1	+1	+1	-1	-1	-1	-1	-1	-1	+1	+1	+1	T_z
	+2	-1	-1	0	0	0	+2	-1	-1	0	0	0	T_x, T_y
	+2	-1	-1	0	0	0	-2	+1	+1	0	0	0	R_x, R_y

The matrix representation of an operator is not unique. In the derivation of the C_3 matrix, we made implicit use of the molecule's symmetry and the knowledge that a rotation about the C_3 axis (Z axis) does not involve a change in Z.

---

[1] Adapted from Herzberg,G. (1945) *Infrared and Raman Spectra* :Princeton:D.Van Nostrand Company Inc.

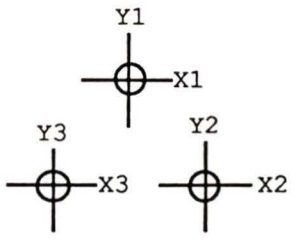

We could take the very much more general approach and apply separate sets of coordinate axes to each of the three atoms. We then write the transformation equation as the product of a 9x9 matrix with a 9x1 matrix. To illustrate, the simplest example of this sort of representation will be given; that of the identity operator I.

$$I\begin{pmatrix} X_1 \\ Y_1 \\ Z_1 \\ X_2 \\ Y_2 \\ Z_2 \\ X_3 \\ Y_3 \\ Z_3 \end{pmatrix} = \begin{pmatrix} 1 & 0 & 0 & 0 & 0 & 0 & 0 & 0 & 0 \\ 0 & 1 & 0 & 0 & 0 & 0 & 0 & 0 & 0 \\ 0 & 0 & 1 & 0 & 0 & 0 & 0 & 0 & 0 \\ 0 & 0 & 0 & 1 & 0 & 0 & 0 & 0 & 0 \\ 0 & 0 & 0 & 0 & 1 & 0 & 0 & 0 & 0 \\ 0 & 0 & 0 & 0 & 0 & 1 & 0 & 0 & 0 \\ 0 & 0 & 0 & 0 & 0 & 0 & 1 & 0 & 0 \\ 0 & 0 & 0 & 0 & 0 & 0 & 0 & 1 & 0 \\ 0 & 0 & 0 & 0 & 0 & 0 & 0 & 0 & 1 \end{pmatrix} \begin{pmatrix} X_1 \\ Y_1 \\ Z_1 \\ X_2 \\ Y_2 \\ Z_2 \\ X_3 \\ Y_3 \\ Z_3 \end{pmatrix} = \begin{pmatrix} X_1 \\ Y_1 \\ Z_1 \\ X_2 \\ Y_2 \\ Z_2 \\ X_3 \\ Y_3 \\ Z_3 \end{pmatrix}$$

This matrix representation of the identity operator can be reduced by the application of similarity transformations of the type $I' = \beta^{-1} I \beta$ for a series of orthonormal matrices β. The smallest matrix that can be derived that represents the identity operator acting on translations in the XY plane is the so-called *irreducible representation* of the identity operator.

The matrix of the irreducible representation is included in the equation

$$I\begin{pmatrix} T_x \\ T_y \end{pmatrix} = \begin{pmatrix} 1 & 0 \\ 0 & 1 \end{pmatrix} \begin{pmatrix} T_x \\ T_y \end{pmatrix} = \begin{pmatrix} T_x \\ T_y \end{pmatrix}$$

which of course has the trace of +2. It is the traces of only the irreducible representations that are included in the point group's character table.

The final column of Table 6 refers to the type of motion represented. The blank entries are vibrational motions that have not yet been discussed, but their matrix traces are included here for the sake of completeness.

It is seen in Table 6 that the traces of the three C_2 operator matrices are identical, as are the traces of the two C_3 operators, and the three σ_v operators. This situation is typical, and we say that operators with identical column entries in the character table define a *class* of operators. It is convenient to adopt the condensed notation of $2C_3$ for C_3 and C_3^2; $3\sigma_v$ for σ_v, σ_v' and σ_v''; *etc.*.

We also introduce the notation of *symmetry types*. A molecular motion (translation, vibration or rotation) is said to be of symmetry type A if a rotation about the principal axis of the point group leaves the motion unchanged both in sign and in absolute value. This is equivalent to saying that the motion is symmetric about the C_3 axis (as opposed to anti-symmetric) or that the entry in the C_3 column of its row in the character table is +1.

We also define the subtypes A_1 and A_2 by requiring that the transformation matrices of a symmetry type A_1 be symmetric

to all rotations, while allowing the type A_2 to be antisymmetric with respect to rotation about the C_2 axes. By this convention, the motion represented in the first row of Table 6 is of type A_1 while second row is of type A_2.

We have the additional need to distinguish degenerate and non-degenerate motions. Degenerate motion arise because the moment of inertia of $\mathbf{D_{3h}}$ point group molecules about the X and Y axes are the same (more on this later). Degenerate motions are given the designation E (from the German "entartet") and are distinguishable from non-degenerate motions by the fact that they define transformation matrices of order larger than one. The previously discussed translation and rotation motions T_x and R_x are of this type.

TABLE 7

CONDENSED D_{3h} CHARACTER TABLE

D_{3h}	I	$2C_3$	$3C_2$	σ_h	$2S_3$	$3\sigma_v$	
A_1'	+1	+1	+1	+1	+1	+1	
A_1''	+1	+1	+1	-1	-1	-1	
A_2'	+1	+1	-1	+1	+1	-1	R_z
A_2''	+1	+1	-1	-1	-1	+1	T_z
E'	+2	-1	0	+2	-1	0	T_x, T_y
E''	+2	-1	0	-2	+1	0	R_x, R_y

Motions are further distinguished by their symmetry to the σ_h plane. Symmetric motions are denoted by a single quotation mark (') while antisymmetric transformations are labelled with double quotation marks (").

Table 7 is a copy of the character table of the D_{3h} point group, but with the operators grouped in classes and the symmetry type notation added. The reader will notice that tabulating only one member of each class reduces the character table to a square array.

4.2 Vibration of the H_3 Molecule

The number of vibrational degrees of freedom in a non-linear polyatomic molecule with N atoms is 3N - 6. The H_3 molecule therefore has three fundamental vibrations. The fundamental vibrations are also referred to as the molecule's *normal vibrations*. A normal vibration is one in which all atoms move with the same frequency and in such a way that the Cartesian coordinates of the displacements change sinusoidally with time. We will be able to use the character table of the D_{3h} point group to deduce the direction of the normal vibrations.

We can see that the entries in the character table behave as orthogonal vectors. If we let the letter F represent one of the operators, and $t_i(F)$ be the trace of that operator in the i^{th} row of Table 6, we see that for any two rows i and j,

$$\sum_F t_i(F)\, t_j(F) = 0 \text{ for } i \neq j,$$

$$\sum_F t_i(F)\, t_i(F) = g$$

where g is the order of the mathematical group of the defined operators. In the case of the D_{3h} point group, g = 12.

We will now recall the previously demonstrated fact that an operator can be represented by many matrices (actually an infinite number of them), but by only a few irreducible matrices (the traces of which make up that operator's column in the character table). It can be shown that the set of matrices whose traces form one row of the character table are an irreducible representation of the group of operators. Each of the infinite number of reducible representation is a linear combination of these irreducible representations.

We can determine the number of times each irreducible representation occurs in a given reducible representation, and hence determine what linear combination of irreducible representations make up the reducible one. We let r_i be the number of times that the representation given in the character table's i^{th} row occurs in a reducible representation. Group theory tells us that

$$r_i = \frac{1}{g} \sum_F t_r(F)\, t_i(F),$$

where $t_r(F)$ is the trace of the transformation matrix of the reducible representation, while $t_i(F)$ is the entry under F in the i^{th} row of the character table. We traditionally write this equation as a summation over all classes instead of over all operators since the character tables are usually

condensed into one column per class (as is Table 7). In this form the equation becomes

$$r_i = \frac{1}{g} \sum_C n_C t_r(C)\, t_i(C), \qquad \text{(E1)}$$

where C is an operator representative of its class and n_C is the number of operators in that class.

We now apply this equation to the 9x9 matrix representations of the symmetry operators. Using the 9x9 representations we will be able to deduce the symmetry properties of the molecule's normal vibrations.

The diagonal elements of the 9x9 matrix of the identity operator (I) are easily added to yield its trace of 9. We can similarly find the traces of the 9x9 matrices of the other operator classes to be

$$t_{9x9}(2C_3) = 0$$

$$t_{9x9}(3C_2) = -1$$

$$t_{9x9}(\sigma_h) = 3$$

$$t_{9x9}(2S_3) = 0$$

$$t_{9x9}(3\sigma_v) = 1.$$

We thus find that the values of the r_i's are given by the equation

$$r_i = \frac{1}{12} \left[(1)(9)t_i(I) + (2)(0)t_i(2C_3) + (3)(-1)t_i(3C_2) + (1)(3)t_i(\sigma_h) + (2)(0)t_i(2S_3) + (3)(1)t_i(3\sigma_v) \right]$$

with the result that the values of the r_i's are

$$r_1 = \frac{1}{12} \left[(9) + (0) + (-3) + (3) + (0) + (3) \right] = 1$$

$$r_2 = \frac{1}{12}\left[(9) + (0) + (-3) + (-3) + (0) + (-3)\right] = 0$$

$$r_3 = \frac{1}{12}\left[(9) + (0) + (3) + (3) + (0) + (-3)\right] = 1$$

$$r_4 = \frac{1}{12}\left[(9) + (0) + (3) + (-3) + (0) + (3)\right] = 1$$

$$r_5 = \frac{1}{12}\left[(18) + (0) + (0) + (6) + (0) + (0)\right] = 2$$

$$r_6 = \frac{1}{12}\left[(18) + (0) + (0) + (-6) + (0) + (0)\right] = 1$$

These results can be summarized by the equation

$$\Gamma_{9x9} = A_1' + A_2' + A_2'' + 2E' + E''$$

where Γ_{9x9} is the group representation given by the 9 x 9 matrix. The symbols on the right hand side denote the irreducible representations whose traces make up the character table.

This equation means that the molecule has a total of 3 non-degenerate normal motions, as well as 3 pairs of degenerate normal motions. However, it is known from the final column of the character table that two of the non-degenerate motions are translation and rotation of the Z axis (T_z and R_z). We have also determined (and included in the character table) that two of the pairs of degenerate motions are T_x, T_y and R_x, R_y. Hence there remains one non-degenerate motion (of symmetry type A_1') and one pair of degenerate motions (of symmetry type E') that are unaccounted for.

One can easily use the process of elimination to see that these motions must be vibrations since all rotational and translational motions have been found. The vibration of symmetry type A_1' must be symmetric with respect to all symmetry elements (by definition of the A_1' type). The only conceivable vibration that fits this requirement is a "radial" pulsation of the type shown in Figure 2. This vibration carries the designation ν_1.

FIGURE 2

ν_1 VIBRATION OF H_3 MOLECULE (SYMMETRY TYPE A_1')

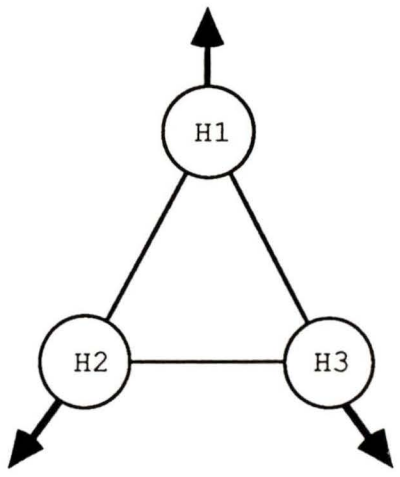

The two degenerate motions are of symmetry type E', and are therefore not symmetric with respect to the C_3 axis. It is very difficult to determine the direction of these vibrations from the character table alone, although one could conceivably do so by systematically eliminating vibrational modes until one happens upon two that work.

One can also determine the direction of the degenerate vibrations by first realizing that an infinite number of degenerate modes would fit the definition of a normal vibration. Each of the infinite number of normal vibrations

can be represented by a linear combination of elements of a basis set. The problem now becomes one of finding two linearly independent vibrations to make up the basis set.

Being degenerate, the two vibrations have the same energy, and so have the same frequency. If we add two vibrations of the same frequency and amplitude that are 90° out of phase, the result is circular motion. Circular motion can easily be shown to be a normal vibration, and since two phase shifted sinusoidal vibrations are linearly independent we have found our basis set.

There is of course an infinite number of orthogonal vibrations that are phase-shifted 90° to each other, and we must use the symmetry properties of the E' symmetry type to determine which two are the ones we want. In practice, this can be done by simply rotating a diagram of the molecule through its C_3 axis.

FIGURE 3

ADDITION OF ORTHOGONAL VIBRATIONS WITH 90° PHASE SHIFT

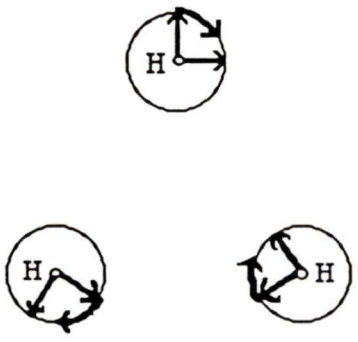

The two vibrations that make up the basis set for all degenerate normal vibrations of the H_3 molecule are designated v_{2a} and v_{2b}. They are shown individually in Figure 4. One can

easily verify that they do transform according to the rules of the E' symmetry type.

FIGURE 4

v_2 VIBRATIONS OF H_3 (SYMMETRY TYPE E')

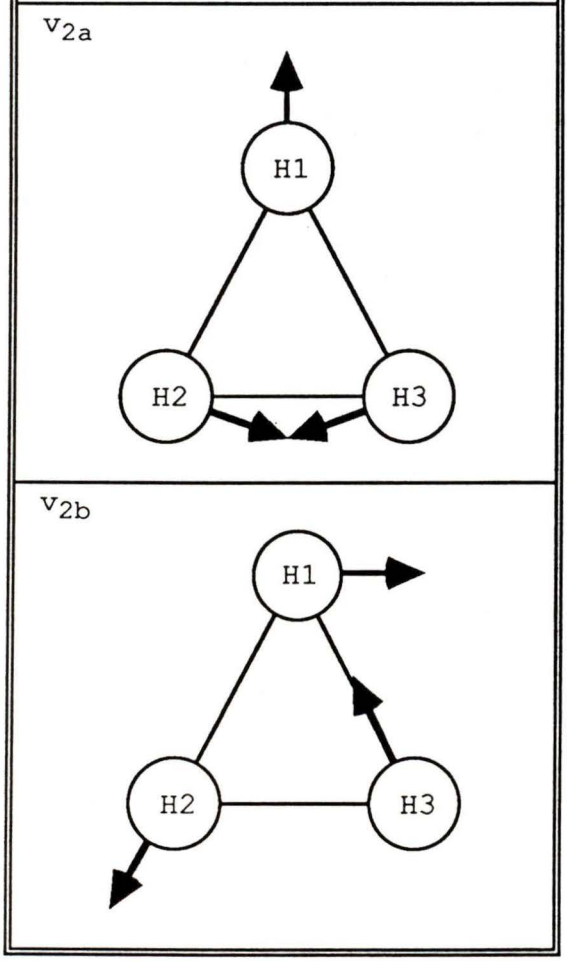

The effect of operating on a degenerate pair of vibrations by a symmetry operator may be more than a simple change of sign. That is, a degenerate vibration need not be either symmetric or antisymmetric with respect to a symmetry operator. To illustrate, the effect of the C_3 operator (120° rotation) and the C_3^2 operator (240° rotation) is shown in Figure 5.

The molecule can vibrate in any or all modes at once, with the restriction that the total vibrational eigenfunction must transform according to a linear combination of the point group's symmetry types.

It is easy to determine the symmetry properties of the total vibrational eigenfunction (or, for that matter, the symmetry type of the total rotational and electronic eigenfunctions). If a state is the sum of non-degenerate eigen-

functions only, then the total eigenfunction is symmetric with respect to a given operator if and only if the product of the traces of the substates that make it up is +1.

FIGURE 5
BEHAVIOR OF DEGENERATE v_2 VIBRATIONS UNDER C_3 AND C_3^2 TRANSFORMATIONS

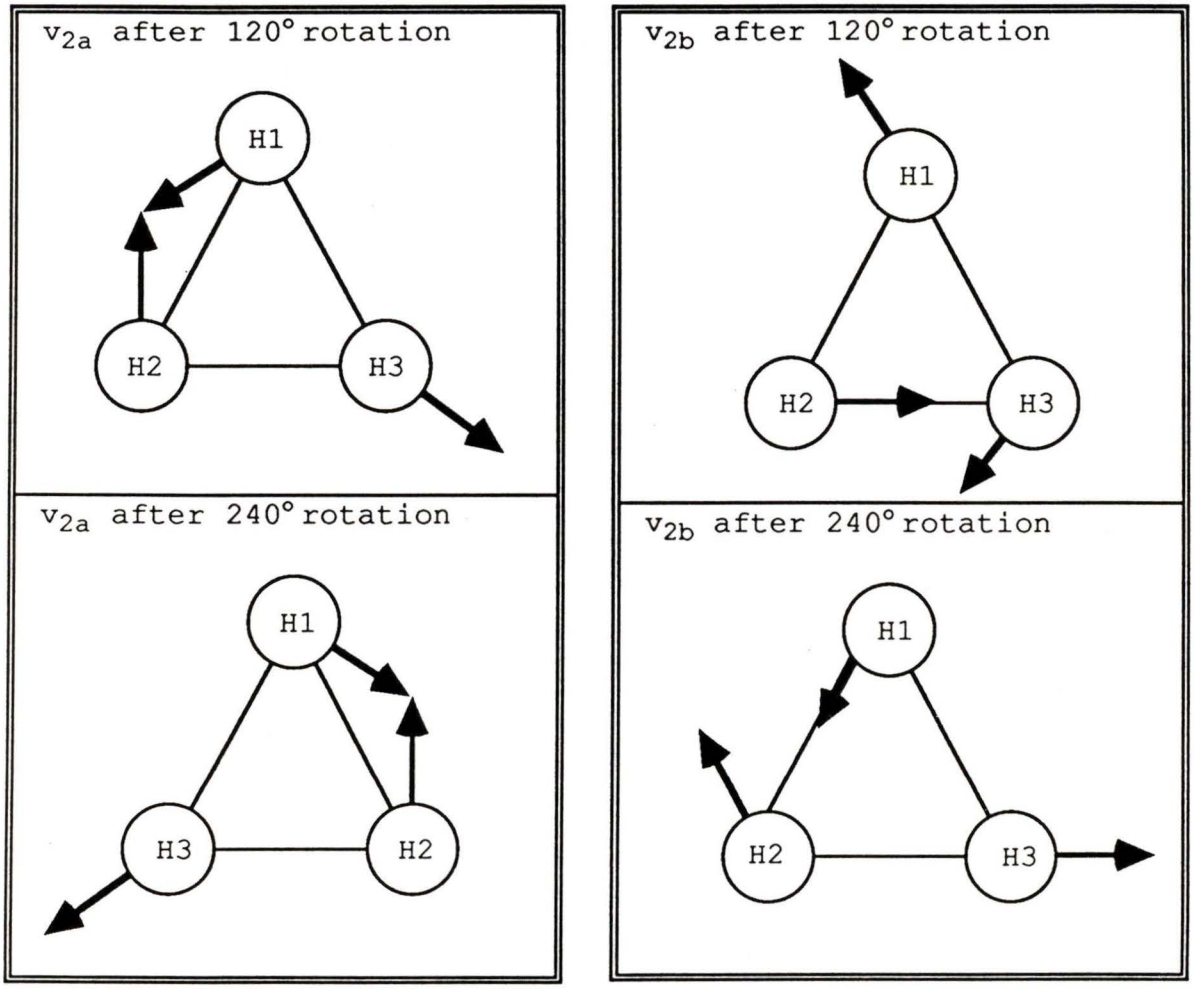

For example, we can find the symmetry species of the eigenfunction of a molecule that is vibrationally excited in

the v_1 mode and is also rotationally excited in the R_z mode. The v_1 vibration is of symmetry type A_1', while the R_z rotation is of symmetry type A_2'. We can now find the symmetry of the total eigenfunction with respect to the six operator classes by multiplying the entries in the A_1' and A_2' rows of the D_{3h} character table (Table 7).

The pertinent part of the Table 7 is reproduced here along with the table entries of the resultant eigenfunction.

	I	$2C_3$	$3C_2$	σ_h	$2S_3$	$3\sigma_v$
A_1'	1	1	1	1	1	1
A_2'	1	1	-1	1	1	-1
$A_1'A_2'$	1	1	-1	1	1	-1

Thus it is found that the total vibrational-rotational eigenfunction is symmetric to I, symmetric to $2C_3$, antisymmetric to $3C_2$, symmetric to σ_h, symmetric to S_3, and antisymmetric to $3\sigma_v$. The final state is therefore of the symmetry type A_2'. In group theory jargon, the $A_1'A_2'$ representation is called the *direct product* of the irreducible representations A_1' and A_2'. We can write the direct product as the equation

$$A_1'A_2' \equiv A_2'$$

If the molecule is excited in both a degenerate and a nondegenerate mode, then the symmetry type of the resultant eigenfunction is just as easily found. For example, if the

molecule vibrates in the v_1 mode (symmetry type A_1'), and simultaneously vibrates in the v_{2a} mode (symmetry type E'), then the resultant vibration has the traces of $1 \times 2 = 2$ for I, $1 \times -1 = -1$ for $2C_3$, $1 \times 0 = 0$ for $3C_2$, $1 \times 2 = 2$ for σ_h, $1 \times -1 = -1$ for $2S_3$, and $1 \times 0 = 0$ for $3C_2$.

These are the traces of the species E', and so the symmetry type of the total eigenfunction is found. We can write the superposition of the A_1' species and the E' species symbolically by the equation

$$a_1' \; e' = E'.$$

where we have adopted the convention of denoting the symmetry type of the substates by lower-case letters.

Difficulties arise when finding the symmetry type that results from the superposition of two (or more) degenerate eigenfunctions. One at first follows the same method as for non-degenerate modes, but unfortunately the derived symmetry for the total eigenfunction is generally not an irreducible representation of the point group. However, in such cases the derived representation is a linear combination of the irreducible representations. It is therefore necessary to reduce the derived state to its basis components.

For example, assume the v_{2a} vibration (symmetry type E') is excited by three quanta ($v = 3$), and both the v_1 vibration (symmetry type A_1') and the R_x rotation (symmetry type E") are

excited by one quantum. The resulting eigenfunction has the symmetry table:

I	$2C_3$	$3C_2$	σ_h	$2S_3$	$3\sigma_v$
16	1	0	-16	-1	0

The final state is therefore 16-fold degenerate. Using the method of reduction for reducible representations that was previously demonstrated, it is found that this eigenfunction is composed of the substates A_1', A_1', A_1', A_2', A_2' A_2', E', E', E', E' and E'. This result is summarized by the equation

$$a_1' \; 3e' \; e'' = 3A_1' + 3A_2' + 5E'.$$

We shall see that an important example of this kind of superposition of vibrational states arises from the degenerate v_2 vibrations when excited to $v_2 > 1$. The results of superpositions of this type are summarized in Table 8. The reader will see that all the highly excited v_2 vibrational modes have a completely symmetric component of symmetry species A_1'.

TABLE 8

SYMMETRY SPECIES OF HIGHER ORDERS OF v_2 VIBRATIONS

v_2	
2	$A_1' + E'$
3	$A_1' + A_2' + E'$
4	$A_1' + 2E'$
5	$A_1' + A_2' + 2E'$
6	$2A_1' + A_2' + 2E'$

We now ask how much energy would be contained in such a superposition of vibrational states. The total energy contained in molecular vibration is given by the relation

$$E_{vib} = h\nu_1(v_1+\tfrac{1}{2}) + h\nu_{2a}(v_{2a}+\tfrac{1}{2}) + h\nu_{2b}(v_{2b}+\tfrac{1}{2}). \quad \text{(E2)}$$

where ν_i represents the frequency of the vibration designated by v_i when excited by v_i quanta.

This equation is more useful when expressed as a *term value*, G. The term value is an expression of energy in units of cm^{-1}, and is derived from the previous equation by dividing by hc

$$G_{v_1v_{2a}v_{2b}} = \frac{\nu_1}{c}(v_1+\tfrac{1}{2}) + \frac{\nu_{2a}}{c}(v_{2a}+\tfrac{1}{2}) + \frac{\nu_{2b}}{c}(v_{2b}+\tfrac{1}{2}). \quad \text{(E3)}$$

This equation is usually condensed by the substituting ω_i for $\frac{\nu_i}{c}$. In our case, the vibrations v_{2a} and v_{2b} are degenerate, and therefore have the same frequency. Consequently, we can substitute $\omega_{2a}=\omega_{2b}\equiv\omega_2$ and $v_{2a}+v_{2b}\equiv v_2$ to hence find that

$$G_{v_1v_2} = \omega_1(v_1+\tfrac{1}{2}) + \omega_2(v_2+1). \quad \text{(E4)}$$

The parameters ω_1 and ω_2 accurately represent the frequency of an infinitesimally small vibration, but since a real molecule is not a true harmonic oscillator, higher order terms arise for vibrations of finite amplitude. In order to more accurately represent the vibrational energy of the H_3 molecule, we introduce the vibrational anharmonicity constants, x_{ii}.

We now write the term value to the higher approximation

$$G_{v_1 v_2} = \omega_1 (v_1 + \tfrac{1}{2}) + \omega_2 (v_2 + 1) + x_{11}(v_1 + \tfrac{1}{2})^2 + x_{22}(v_2 + 1)^2 + x_{21}(v_1 + \tfrac{1}{2})(v_2 + 1) + g_{22}(l_2)^2 . \quad \text{(E5)}$$

where g_{22} is a small constant of interaction between the degenerate v_2 vibrations. The symbol l_2 denotes a new quantum number that can take on the values $l_2 = v_2, v_2 - 2, v_2 - 4, \ldots, 1 \text{ or } 0$.

4.3 Rotation of the H_3 Molecule

The H_3 molecule is an oblate symmetric top molecule. An oblate symmetric top molecule is one that has two equal principal moments of inertia, with the third being larger than the first two. The unique moment of inertia of an oblate top is generally represented by I_C, while the two equal moments are designated I_A and I_B. In this case, $I_C > I_A = I_B$. If an oblate symmetric top molecule is also planar (as is H_3), then

$$I_C = 2I_A = 2I_B \quad \text{(E6)}$$

The rotational energy of a rigid molecule is given by the general equation

$$E_{Rot} = \tfrac{1}{2} I_A \omega_A^2 + \tfrac{1}{2} I_B \omega_B^2 + \tfrac{1}{2} I_C \omega_C^2$$

$$= \frac{p_A^2}{2I_A} + \frac{p_B^2}{2I_B} + \frac{p_C^2}{2I_C} \quad \text{(E7)}$$

We can now make use of the fact that $I_A = I_B$, and also that the total angular momentum is quantized, with values given by

$$p_{total} = \sqrt{J(J+1)}\frac{h}{2\pi}, \qquad J = 0, 1, 2, \ldots \tag{E8}$$

We also assume that the angular momentum about the figure axis is also quantized, with permitted values given by

$$p_C = k\frac{h}{2\pi}, \qquad k = 0, \pm 1, \pm 2, \ldots, \pm J \tag{E9}$$

Substituting the equations for the angular momenta into the rotational energy equation yields the result

$$E_{Rot} = \frac{h^2}{8\pi^2 I_A} J(J+1) + \left(\frac{h^2}{8\pi^2 I_C} - \frac{h^2}{8\pi^2 I_A}\right)k^2. \tag{E10}$$

As before, we convert this relation to term values by division by hc

$$F_{Jk} = \frac{h}{8\pi^2 c I_A} J(J+1) + \left(\frac{h}{8\pi^2 c I_C} - \frac{h^2}{8\pi^2 c I_A}\right)k^2.$$

We now introduce the rotational constants B and C, where B and C have the units of cm^{-1} and are given by

$$B = \frac{h}{8\pi^2 c I_B} \qquad C = \frac{h}{8\pi^2 c I_C} \tag{E11}$$

The rotational term value is then given the value of

$$F_{Jk} = B J(J+1) + (C-B) k^2,$$

while the inclusion of higher order terms (that result from centrifugal stretching) gives the result

$$F_{Jk} = B J(J+1) + (C-B) k^2 - D_J J^2(J+1)^2 - D_{Jk} J(J+1) k^2 - D_k k^4. \tag{E12}$$

Dowling (1961) has shown that for axially symmetric planar molecules, we can relate the centrifugal distortion constants by the equation

$$D_{Jk} = -\frac{2}{3}(D_J + 2D_k) \qquad \text{(E13)}$$

Only quadratic and quartic terms of k appear in the equation for F_{Jk}, and so states with $k \neq 0$ are doubly degenerate. We also see that only the absolute value of k is of interest, and so we generally make the substitution $|k| = K$. The previous equations for the rotational term values may now be written with k replaced by K.

The permanent dipole moment of the H_3 molecule points along its figure axis, which is also the Z axis. In order for dipole electromagnetic radiation to be produced by a pure rotational transition, the rotation must therefore shift the Z axis. A rotation about the Z axis consequently has no effect on the production of dipole radiation. Since K is the absolute value of the figure axis component of the angular momentum, rotational transitions are subject to the dipole selection rule $\Delta K = 0$.

The wavenumber produced by a rotational transition is the difference between the term values of the upper and lower states (respectively designated by $F_{J'K'}$ and $F_{J''K''}$). That is

$$\sigma = F_{J'K'} - F_{J''K''} = 2B(J''+1) - 2D_{J''K}(J''+1)K^2 - 4D_{J''}(J''+1)^3 \qquad \text{(E14)}$$

where we made implicit use of the fact that $K' = K'' \equiv K$.

The values of D_{JK} and D_K are always much less than the corresponding value of B, and so we find that the lines of pure rotational spectrum are very nearly equally spaced.

The eigenfunctions for $K=0$ are completely symmetric for even values of J, and so have symmetry type A_1. The eigenfunctions are of symmetry type A_2 for odd values of J. This occurs because $K=0$ rotations do not involve the figure axis and 180° rotations about an axis perpendicular to the figure axis will change the sign of the eigenfunction only if J is odd.

Rotational levels with $K>0$ are made up of two equal energy states with $k=\pm K$. We know that $K\neq 0$ rotations involve the figure axis, which happens to be of the C_3 type. Since rotations about a C_3 figure axis through $360°\div 3=120°$ leaves the molecule unaltered, values of $K=3q$ (for $q=0,1,2,3,\ldots$) will result in a pair of equal energy eigenfunctions of types A_1 and A_2. Values of $K=3q\pm 1$ result in a pair of degenerate eigenfunctions (of overall symmetry type E).

4.4 Vibrational-Rotational Interaction

In order to treat a molecule that undergoes simultaneous rotation and vibration, it is necessary to modify the rotational term value equation given in the previous section. We replace the molecule's equilibrium values of the rotational

constants B and C with the average values of B and C over one vibration period. If we use the subscripts "e" and "[v]" to respectively designate the equilibrium and time averaged values of B and C, we can write

$$B_{[v]} = B_e - \sum_i \alpha_{i(B)} \left(v_i + \frac{d_i}{2} \right) + \ldots$$

$$C_{[v]} = C_e - \sum_i \alpha_{i(C)} \left(v_i + \frac{d_i}{2} \right) + \ldots \qquad \text{(E15)}$$

where d_i is the degeneracy of the v_i vibration. In our case, $d_i = 1$ if $i = 1$, and $d_i = 2$ if $i = 2$. The value of α_i is always small and positive for non-degenerate vibrations, but may be negative for degenerate vibrations.

We can then find the total energy (in cm^{-1} units) of vibration and rotation, which is given by

$$T = F_{[v]JK} + G_{v_1 v_2}$$

where we now substitute the above terms with equations 5 and 12 to yield the result

$$\begin{aligned} T = {} & B_{[v]} J(J+1) + (C_{[v]} - B_{[v]}) K^2 - D_J J^2 (J+1)^2 - \\ & D_{JK} J(J+1) k^2 - D_K K^4 + \omega_1 (v_1 + \tfrac{1}{2}) + \omega_2 (v_2 + 1) + \\ & x_{11} (v_1 + \tfrac{1}{2})^2 + x_{22} (v_2 + 1)^2 + x_{21} (v_1 + \tfrac{1}{2})(v_2 + 1) + \\ & g_{22} (l_2)^2 . \end{aligned} \qquad \text{(E16)}$$

Unfortunately, a major problem occurs for the degenerate vibrations v_{2a} and v_{2b}. The Coriolis force created by rotation results in an interaction between the degenerate components. Since the degenerate vibrations have the same frequency, a

transition from one to the other vibrational mode (and back) can occur very quickly. The coupling between the two modes is therefore very strong. A rotating molecule in a v_{2a} vibration must consequently undergo simultaneous v_{2b} vibration.

This can easily be seen by inspection of Figure 6. The direction of the Coriolis force on the v_{2a} is perpendicular to the direction of vibration, and is therefore in the direction of the v_{2b} vibration.

The effect of this is to slightly remove the degeneracy of the two vibrations. The amount of splitting increases linearly with K.

FIGURE 6

CORIOLIS FORCE ON THE DEGENERATE v_{2a} VIBRATION

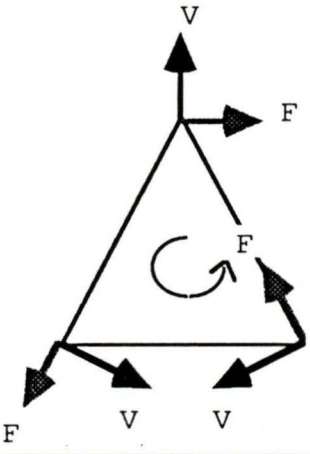

F: Direction of Coriolis force
V: Direction of vibrational motion

The formula for the rotational energy levels must therefore be modified if degenerate vibrations are present. The modified equation can be written

$$F_{[v]JK} = B_{[v]}J(J+1) + (C_{[v]} - B_{[v]})K^2 \pm -2C_{[v]}K\sum_i\left(\pm l_i\zeta_{vi}\right) \qquad \text{(E17)}$$

which differs from the non-degenerate equation by the addition of the third term. The factor ζ_{vi} is the Coriolis

coupling constant of the v_i vibration excited by v_i quanta. l_i (letter "l") is the previously mentioned quantum number that is constrained to the values $l_i = v_i, v_i - 2, v_i - 4, \ldots, 1 \text{ or } 0$.

The third term of the equation gives the term value two energy levels, which are labelled the (+l) and (-l) states. The parentheses are used to avoid confusion with the quantum number l, which is always non-negative. The (-l) state has the higher energy of the two states. The designations $(+\Lambda)$ and $(-\Lambda)$ are sometimes used as synonyms for (+l) and (-l).

The third term's summation runs only from i = 1 to 2, since we only have the v_1 vibration and the pair of v_2 vibrations to worry about. However, ζ_{vi} is zero if v_i is a non-degenerate vibrational mode, and so the first term of the summation drops out. We can then replace the summation by a single term involving ζ_{v2}.

In the very special case of an X_3 molecule the value of ζ_{v2} is equal to 1 if $v_2 = 1$. More generally, ζ_{vi} is a very complicated function of the atomic masses, the geometrical dimensions, and the potential constants.

We can then simplify the final term of Equation 17 to the form

$$\pm -2 C_{[v]} K l_2 \zeta_{v2} \approx \pm -2 C_{[v]} K l_2$$

Garing, Nielsen and Rao (1959) have shown that in higher approximation, the vibrational interaction with the centrifu-

gal distortion constants must be taken into account. They propose that one must also add to the rotational term value the additional terms

$$+2K\left(\sum \pm l_i \zeta_{v_i}\right)\left((2D_J + D_{JK})J(J+1) + 2(D_K + D_{JK})K^2\right) \qquad \text{(E18)}$$

We now define the term *transition moment* to be the change of the dipole moment in a transition. If the transition moment is parallel to the figure axis (||band), then the transition does not involve a change in K. Thus the selection rules for rot-vib transitions within an electronic state are

$$\Delta K = 0,\ \Delta J = 0, \pm 1 \quad \text{if } K \neq 0$$

$$\Delta K = 0,\ \Delta J = \pm 1 \quad \text{if } K = 0.$$

If the transition moment is perpendicular to the figure axis then we must have a change in K, and so for a ⊥ band

$$\Delta K = \pm 1,\ \ \Delta J = 0, \pm 1.$$

In the case of a parallel transition with $K \neq 0$, we have three simple branches, which carry the designations

$$P \leftrightarrow \Delta J = -1$$

$$Q \leftrightarrow \Delta J = 0$$

$$R \leftrightarrow \Delta J = +1$$

while if $K = 0$, the Q branch would be missing for a rot-vib transitions within one electronic state.

4.5 Vibronic Interaction in the H_3 Molecule

The electronic eigenfunctions have symmetric properties just as the vibrational and rotational eigenfunctions do. For the electronic eigenfunctions, we must also take into account the spin of the electron.

An electron is a spin $s=\frac{1}{2}$ particle, with the direction of the vector **s** either parallel or antiparallel to any preferred direction. The sum of the **s** vectors is labelled **S**, which can take on integral and odd-half integral values. To account for the spin function we must introduce *extended point groups* (or *double groups*). An extended point group includes the heretofore unmentioned symmetry operator R. It is difficult to assign a physical analogy to the R operator, but it can be thought of as a rotation through a complete turn of 360°. The difficulty in this interpretation is that the spin function is *not* symmetric with respect to this operator, but is symmetric to (*i.e.* can only be turned back onto itself by) the operator R^2 (or two complete turns).

In addition to the R operator, we introduce the operators $RC_3 \equiv C_3^4$, $RC_3^2 \equiv C_3^5$, $RS_3 \equiv S_3^4$, $RS_3^2 \equiv S_3^5$. There are three new operator classes defined by the addition of these operators; R itself, the class $2C_3^2$ made up of C_3^2 and C_3^5, and the class S_3^2 made up of S_3^2 and S_3^5.

TABLE 9 [1]

EXTENDED CHARACTER TABLE OF THE D_{3h} POINT GROUP

D_{3h}	I	$2S_3$	$2C_3$	σ_h	$3C_2$	$3\sigma_v$	R	$2S_3^2$	$2C_3^2$	
A_1'	+1	+1	+1	+1	+1	+1	+1	+1	+1	
A_2'	+1	+1	+1	+1	-1	-1	+1	+1	+1	R_z
A_1''	+1	-1	+1	-1	+1	-1	+1	-1	+1	
A_2''	+1	-1	+1	-1	-1	+1	+1	-1	+1	T_z
E''	+2	+1	-1	-2	0	0	+2	+1	-1	R_x, R_y
E'	+2	-1	-1	+2	0	0	+2	-1	-1	T_x, T_y
$E_{1/2}$	+2	$+\sqrt{3}$	+1	0	0	0	-2	$-\sqrt{3}$	-1	
$E_{3/2}$	+2	0	-2	0	0	0	-2	0	+2	
$E_{5/2}$	+2	$-\sqrt{3}$	+1	0	0	0	-2	$\sqrt{3}$	-1	

[1] Adapted from Herzberg,G. (1966) *Electronic Spectra of Polyatomic Molecules* : Princeton:D.Van Nostrand Company Inc.

The extended character table for the D_{3h} point group is included in Table 9. The addition of the new operators to the character table creates three new irreducible representations of the point group. These representations are all doubly degenerate and carry the subscripts 1/2, 3/2, or 5/2.

TABLE 10 (1)

SYMMETRY OF SPIN FUNCTIONS OF THE D_{3h} POINT GROUP

S	Symmetry Type
0	A_1'
$\frac{1}{2}$	$E_{1/2}$
1	$A_2' + E''$
$\frac{3}{2}$	$E_{1/2} + E_{3/2}$
2	$A_1' + E' + E''$
$\frac{5}{2}$	$E_{1/2} + E_{3/2} + E_{5/2}$

The electronic states of the D_{3h} point group (including spin) are characterized by S. The symmetry types of these eigenfunctions have been found by Herzberg (1966), and are listed in Table 10. If however the spin is only slightly coupled to the orbital angular momentum, then the spin may be treated as a second order perturbation, and so the original character table will suffice.

The value of S is of course constrained to $|S| \leq \frac{3}{2}$ in the case of an H_3 molecule (which has only three electrons). The final two entries in Table 9 therefore have no relevance to

---

[1] Adapted from Herzberg,G. (1966) *Electronic Spectra of Polyatomic Molecules* : Princeton:D.Van Nostrand Company Inc.

the problem at hand, but are included for the sake of completeness.

In order to find the symmetry type of the total vibrational-electronic eigenfunction (or the *vibronic state function*) we must multiply the characters of the spin function, the vibration function and the electronic function. That is, we must find the direct product of the irreducible representations of these eigenfunctions. The procedure for finding direct products was presented in the discussion of the superposition of vibrational eigenfunctions.

We now run into a complication. The total eigenfunction (Ψ) cannot be considered the simple direct product of the electronic spin function (ψ_s), the electronic eigenfunction (ψ_e) and the vibrational eigenfunction (ψ_v) because of coupling between the vibrational and electronic states. This interaction results in the so-called vibronic interaction, which is also known as the *Jahn-Teller interaction*.

The Jahn-Teller interaction effectively shifts the electronic potential minimum (*i.e.* the equilibrium point of the vibrations) away from the symmetrical position of the molecule. Therefore, when the Jahn-Teller interaction is very large, the vibrating molecule is not a member of its non-vibrational point group. Fortunately, it is usually practical to consider the Jahn-Teller interaction as a mere second

order perturbation of the molecule's vibronic state, allowing one to use the stationary point group classification.

Let us now take a detailed look at the effect of the Jahn-Teller interaction on the H_3 molecule by following the derivation of Herzberg (1966). First, we inspect the degenerate vibrational modes v_{2a} and v_{2b} (Figure 4). If the X axis is drawn through the H1 atom and the molecule's center, and if the Z axis comes out of the paper, then the vibration v_{2a} is symmetric to the XZ plane, while v_{2b} is antisymmetric to the XZ plane.

We now assume that the electronic state is of the symmetry type E'. The electronic state is therefore two-fold degenerate, with the two eigenfunctions $\Psi_{e(a)}$ and $\Psi_{e(b)}$ sharing the same energy. Let q be the coordinates of the electrons, and let Q_{2a} and Q_{2b} be the normal coordinates of the degenerate vibrations.

For convenience, we also introduce the complex normal coordinates and electronic eigenfunctions

$$Q_2^+ \equiv Q_{2a} + iQ_{2b} \equiv re^{+i\varphi}$$

$$Q_2^- \equiv Q_{2a} - iQ_{2b} \equiv re^{-i\varphi}$$

$$\Psi_e^+ \equiv \Psi_{e(a)} + i\Psi_{e(b)}$$

$$\Psi_e^- \equiv \Psi_{e(a)} - i\Psi_{e(b)}$$

We know that the electronic Hamiltonian of the eigenfunctions has the form $H_e = T_e + V_e$. To find the energy E, we first convert the Hamiltonian to the complex coordinate system.

In the new coordinates, the secular equation is given by

$$\begin{vmatrix} H_{++} - E & H_{+-} \\ H_{-+} & H_{--} - E \end{vmatrix} = 0$$

where the elements of the matrix are

$$H_{++} = \int \psi_e^{+*} H_e \psi_e^{+} dq \qquad H_{+-} = \int \psi_e^{+*} H_e \psi_e^{-} dq$$

$$H_{-+} = \int \psi_e^{-*} H_e \psi_e^{+} dq \qquad H_{--} = \int \psi_e^{-*} H_e \psi_e^{-} dq$$

We now write H_e as a power series of the complex normal coordinates Q_2^+ and Q_2^-

$$H_e = H_o + H_1^+ Q_2^- + H_1^- Q_2^+ + H_2^+ Q_2^{-2} + H_2^- Q_2^{+2} + \ldots$$

Substitution into the equations for the matrix element H_{++} yields the result

$$H_{++} = \int \psi_e^{+*} H_o \psi_e^{+} dq + Q_2^- \int \psi_e^{+*} H_1^+ \psi_e^{+} dq + Q_2^+ \int \psi_e^{+*} H_1^- \psi_e^{+} dq + \ldots$$

Analogous expressions can be found for H_{-+}, H_{+-}, and H_{--}.

The Hamiltonian must be symmetric to all of the point groups operators. Since a rotation of 120° is one of the point

groups symmetry elements (C_3), it follows that H_1^+, H_1^-, *etc.* must also be symmetric to a rotation of 120°.

A C_3 rotation is equivalent to multiplication by $\omega \equiv e^{+2\pi i/3}$ or $\varpi \equiv e^{-2\pi i/3}$, and so it can be found that multiplication by ω or ϖ will leave the Hamiltonian unchanged if and only if the linear terms of Q_2^+ and Q_2^- in H_{++} and H_{--} are zero, and the first terms of H_{+-} and H_{+-} are also zero. We now neglect quadratic and higher order terms, and find the results:

$$H_{++} = \int \psi_e^{+*} H_o \psi_e^+ dq \equiv W_o \qquad H_{--} = \int \psi_e^{-*} H_o \psi_e^- dq \equiv W_o$$

$$H_{+-} = CQ_2^+ \qquad H_{-+} = CQ_2^-.$$

Substitution into the original determinant yields

$$\begin{vmatrix} W_o - E & CQ_2^+ \\ CQ_2^- & W_o - E \end{vmatrix} = 0$$

$$\therefore \quad E = W_o \pm C(Q_2^+ Q_2^-)^{1/2} \tag{E19}$$

We rewrite Equation 19 to get the result $E = W_o \pm Cr$ where C is some constant and $r = \sqrt{Q_{2a}{}^2 + Q_{2b}{}^2}$. In this first order approximation, the electronic energy varies linearly with displacement. We also find that energy (E) increases with r for one of the component states but decreases with r for the other, and so the minimum value of the potential energy does not occur at $r = 0$.

By including quadratic and higher terms, it can be shown that the potential energy has three minima, none of which are exactly coincident with the geometrical points of an equilateral triangle. There are consequently three non-symmetrical equilibrium configurations of an H_3 molecule in a degenerate electronic state. These are shown in Figure 7.

FIGURE 7
EQUILIBRIUM CONFIGURATIONS OF DEGENERATE ELECTRONIC STATES UNDERGOING VIBRATION

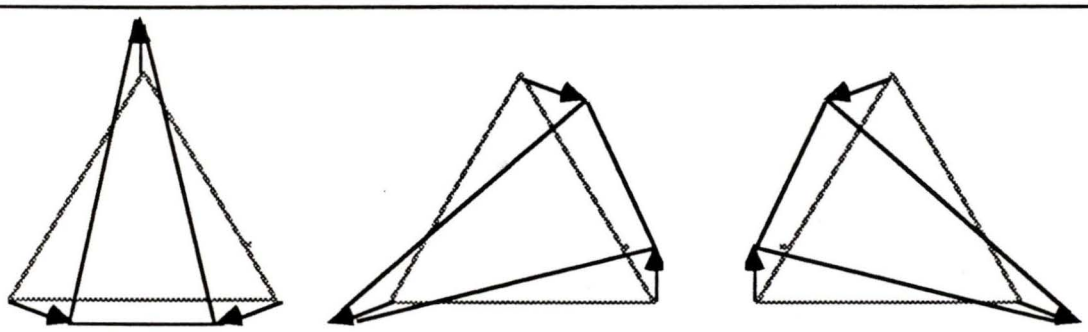

With no Jahn-Teller interaction, the vibrations are about the vertices of the gray (equilateral) triangles. If Jahn-Teller interaction is significant, the center of the vibrations are shifted to the black (isosceles) triangles

When the Jahn-Teller coupling is small, the molecule's deviation from symmetry may be treated more simply as a perturbation of the vibronic wavefunction. Such a treatment was performed by Child (1963), who derived an expression for the term value for the degenerate v_2 vibrations of an X_3 molecule. For very small Jahn-Teller coupling, it is found that

$$G_{v_2} = \omega_2(v_2+1) \pm (-2)D\,\omega_2(l_2 \pm 1) \qquad \text{(E20)}$$

where D is a small coupling parameter, and as before, the quantum number l_2 can take on the values $l_2 = v_2, v_2 - 2, \ldots, 1 \text{ or } 0$. In order for the equation to be sufficiently accurate, the value of D must be < 0.05.

For larger values of D, this formula is no longer even approximately correct since l is no longer a good quantum number. Longuet-Higgins *et al.* (1958) have introduced the new quantum number j, and found that the angular momentum of the motion induced by a strong Jahn-Teller coupling is

$$p_j = j\frac{h}{2\pi} \qquad j = \frac{1}{2}, \frac{3}{2}, \frac{5}{2}, \ldots, v_i + \frac{1}{2} \; . \tag{E21}$$

Now that the symmetry types of the vibronic states have been discussed, we can determine the selection rules of vibronic transitions. In general, the probability of a transition between two vibronic states is very small unless the symmetry species of the two states differ by the species of one of the normal vibrations.

In our case, the normal vibrations are of the species A_1' and E'. We can therefore expect transitions from a vibronic state of the symmetry type "X" only to vibronic states of symmetry types $(A_1')(X)$ and $(E')(X)$. The reader may have noticed that a transition between states of the same species is permitted by this rule, since $(A_1')(X) \equiv X$. Those transitions that are permitted are listed in Table 11.

TABLE 11

SYMMETRIC TYPES OF PERMITTED VIBRONIC TRANSITIONS OF THE H_3 MOLECULE

Original Species	Permitted Final Species	
A_1'	A_1'	E'
A_2'	A_2'	E'
A_1''	A_1''	E''
A_2''	A_2''	E''
E'	E'	$A_1' + E'$
E''	E''	$A_1'' + A_2'' + E''$
$E_{1/2}$	$E_{1/2}$	$E_{3/2} + E_{5/2}$
$E_{3/2}$	$E_{3/2}$	$E_{1/2} + E_{5/2}$
$E_{5/2}$	$E_{5/2}$	$E_{1/2} + E_{3/2}$

4.6 Rovibronic Interaction in the H_3 Molecule

It has been shown that the rotational term value of a molecule in non-degenerate vibration is given by Equation 12;

$$F_{[v]JK} = B_{[v]}\,J(J+1) + (C_{[v]} - B_{[v]})\,K^2 - D_J\,J^2(J+1)^2 - D_{JK}\,J(J+1)K^2 - D_K\,K^4$$

We have neglected the extremely small dependence of the centrifugal distortion constants (D_J, D_K, and D_{JK}) on the vibrational quantum number.

For the case of a degenerate vibrational mode, we must also account for the Coriolis interaction, which we have done by adding to the previous equation the term

$$-2\,C_{[v]}\,K \sum_i \left(\pm l_i \zeta_{v_i}\right)$$

where ζ_{v_i} is the Coriolis coupling constant of the v_i vibration (when excited by v_i quanta), and $l_i = v_i, v_i - 2, v_i - 4, \ldots, 1 \text{ or } 0$.

We can now define the quantity $\left(\zeta_{v_2} \frac{h}{2\pi}\right)$ given by

$$\zeta_{v_2} \frac{h}{2\pi} \equiv \sum_i \left(\pm l_i \zeta_{v_i}\right) \frac{h}{2\pi} = \pm l_2 \zeta_{v_2} \frac{h}{2\pi} \qquad \text{(E22)}$$

to be the *vibrational angular momentum* of the degenerate vibrational mode v_2. When we have *rovibronic* coupling (*i.e.* coupling of the rotation with the electronic state as well as the vibrational mode), we must modify the value of ζ_{v_2} slightly. If we let ζ_e be $h/2\pi$ times the *electronic angular*

momentum, then Child and Longuet-Higgins (1961) have shown that for an X_3 molecule, we must replace ζ_{v_2} with ζ_t, where

$$\zeta_t \equiv B(\zeta_e - \tfrac{1}{2}\zeta_{v_2})d - j\zeta_{v_2} \qquad \text{(E23)}$$

The letter d signifies the "quenching parameter", and $j = \frac{1}{2}, \frac{3}{2}, \frac{5}{2}, \ldots, v_i + \frac{1}{2}$. Note that ζ_t may be non-zero even if the molecule is not vibrating.

We therefore find that the rotational energy level of an H_3 molecule in a degenerate vibronic state is given by (neglecting centrifugal stretching terms),

$$F_{[v]JK} = B_{[v]}J(J+1) + (C_{[v]} - B_{[v]})K^2 \pm (-2C_{[v]}\zeta_t K) \qquad \text{(E24)}$$

We now look at the effect of electron spin on this energy. To do this, we introduce the new vector **N** (the magnitude of which is the quantum number N). **N** takes the place of the previously used vector **J**, and is defined as the total angular momentum excluding the spin angular momentum **S**. **J** is defined to be the sum of *all* angular momenta. Thus

$$\mathbf{J} \equiv \mathbf{N} + \mathbf{S}$$

and the corresponding quantum number J has the values $J = N+S, N+S-1, \ldots, |N-S|$. We now replace the letter J in rotational term value equation with N (*i.e.* $F_{[v]JK} \rightarrow F_{[v]NK}$). Each level defined by a given N is split into $2S+1$ components (unless $N<S$).

If we let $F_{[v]JK}$ be the rotational term value neglecting electron spin (designated by $F_{o[v]NK}$) then we have for non-degenerate vibronic species

$$F_{o[v]NK} = B_{[v]}N(N+1) + (C_{[v]} - B_{[v]})K^2 \qquad \text{(E25)}$$

and for degenerate vibronic states,

$$F_{o[v]NK} = B_{[v]}N(N+1) + (C_{[v]} - B_{[v]})K^2 \pm (-2C_{[v]}\zeta_t K). \qquad \text{(E26)}$$

When $S=\frac{1}{2}$ we have a *doublet state* (since $2S+1=2$). The term values of the two components of a doublet have been determined by Henderson (1955) to be

$$F_{1[v]NK} = F_{o[v]NK} + \frac{1}{2}\left(\kappa\frac{K^2}{N(N+1)} + \mu\right)N$$

$$F_{2[v]NK} = F_{o[v]NK} - \frac{1}{2}\left(\kappa\frac{K^2}{N(N+1)} + \mu\right)(N+1). \qquad \text{(E27)}$$

where κ and μ are the spin rotation coupling constants, and F_1 and F_2 are respectively the term values for $J=N+\frac{1}{2}$ and $J=N-\frac{1}{2}$. For triplet and higher states, additional terms arise because of spin-spin interaction. These need not be dealt with here.

The rovibronic functions have their own symmetry properties, and are consequently classed into symmetry types just as the vibrational functions are. There is however a very extensive list of rovibronic species that arise from all of the possible rotational, vibrational, and electronic functions, and in the pursuit of brevity we will only discuss those species resulting from the A_1', A_2'', and E' electronic states. In doing so, we anticipate the last sections of this

chapter where spectra resulting from transitions between the A_1', A_2'', and E' electronic states are discussed.

The symmetry properties of rovibronic species are determined by taking the direct product of the rotational, the vibrational and the electronic symmetry types. This procedure has already been extensively dealt with, and so only the results will be presented here.

If an electronic eigenfunction is totally symmetric (of species A_1'), then the resulting rovibronic state will have two non-degenerate levels for every quantum number N if K is a multiple of 3 and greater than zero (*i.e.* K=3, 6, 9, ...). If K is every second number of this sequence (*i.e.* K=6, 12, 18, ...) then the two non-degenerate levels will be one of type A_1' and one of type A_2'. If, on the other hand, K=3, 9, 15, ..., then the two non-degenerate states will be of the species A_1'' and A_2''. If K is not a multiple of three, then there will be one pair of degenerate rovibronic states of type E' for even K and type E" for odd K. Finally, if K=0, the K degeneracy is lost and only one rovibronic eigenfunction results. This state is of type A_1' for even N and A_2' for odd N.

If the electronic state is of symmetry type A_2'', then the resulting rovibronic states are identical to those of the A_1' electronic state except that the superscripts " and ' and the subscripts 1 and 2 must be interchanged (*i.e.* A_1'' becomes A_2' *etc.*).

If the electronic state is of the degenerate species E' and if $K=0$, then the resulting rovibronic state is also of the species E'. If $K\neq 0$, we must account for Coriolis splitting, which results in the (+1) and the (-1) substates. If K is not a multiple of 3, then one of the two Coriolis components will be two non-degenerate states, while the other will be a pair of degenerate ones. The ' and " superscripts alternate with K. If $K=3, 6, 9, 12, \ldots$ then the resultant states are degenerate for both (+1) and (-1). The superscripts of the degenerate species (*i.e.* E' or E") alternate with K as well.

The results of the last three paragraphs are summarized in tables 12 to 14. The reader is urged to examine these tables carefully in order to understand the recent deluge of information.

The *statistical weights* of the different rovibronic states can now be determined with one additional piece of information: the nuclear spin of the atoms. The nuclear spin is of course dependent on isotopic number, but the abundance of deuterium relative to simple hydrogen is negligibly small in chemically evolved astronomical objects (such as planetary nebulae), and so we will ignore such things as H_2D, D_2H, and D_3. The spin of the ^1H isotope hydrogen atom is $I=\frac{1}{2}$, and so the H_3 nuclei must obey Fermi statistics. We may now proceed.

TABLE 12

SYMMETRIC TYPES OF ROVIBRONIC STATES RESULTING FROM THE A_1' ELECTRONIC STATE

K	0	1	2	3	4	5	6
N 0	A_1'						
1	A_2'	E''					
2	A_1'	E''	E'				
3	A_2'	E''	E'	A_2' A_1''			
4	A_1'	E''	E'	A_1'' A_2''	E'		
5	A_2'	E''	E'	A_2'' A_1''	E'	E''	
6	A_1'	E''	E'	A_1'' A_2''	E'	E''	A_1' A_2'

TABLE 13

SYMMETRIC TYPES OF ROVIBRONIC STATES RESULTING FROM THE A_2'' ELECTRONIC STATE

K	0	1	2	3	4	5	6
N 0	A_2''						
1	A_1''	E'					
2	A_2''	E'	E''				
3	A_1''	E'	E''	A_1' A_2'			
4	A_2''	E'	E''	A_2' A_1'	E''		
5	A_1''	E'	E''	A_1' A_2'	E''	E'	
6	A_2''	E'	E''	A_2' A_1'	E''	E'	A_2'' A_1''

TABLE 14

SYMMETRIC TYPES OF ROVIBRONIC STATES RESULTING FROM THE E' ELECTRONIC STATE

K	0	1 (+1)	1 (−1)	2 (+1)	2 (−1)	3 (+1)	3 (−1)	4 (+1)	4 (−1)	5 (+1)	5 (−1)	6 (+1)	6 (−1)
N													
0	E'												
1	E'	A_2'' A_1''	E''										
2	E'	A_1'' A_2''	E''	E'	A_1' A_2'								
3	E'	A_2'' A_1''	E''	E'	A_2' A_1'	E''	E''						
4	E'	A_1'' A_2''	E''	E'	A_1' A_2'	E''	E''	A_1' A_2'	E'				
5	E'	A_2'' A_1''	E''	E'	A_2' A_1'	E''	E''	A_2' A_1'	E'	E''	A_2'' A_1''		
6	E'	A_1'' A_2''	E''	E'	A_1' A_2'	E''	E''	A_1' A_2'	E'	E''	A_1'' A_2''	E'	E'

The complete eigenfunction (Ψ) can be considered to be the product of the rovibronic eigenfunction (Ψ_{evr}) and the nuclear spin eigenfunction (Ψ_i), if we neglect the coupling between the electron and the nuclear angular momenta.

FIGURE 8

POSSIBLE ORIENTATIONS OF SPIN VECTORS OF H_3

#	H1	H2	H3
I	↑	↑	↑
II	↑	↑	↓
III	↑	↓	↑
IV	↓	↑	↑
V	↑	↓	↓
VI	↓	↑	↑
VII	↓	↑	↓
VIII	↓	↓	↓

There are eight possible orientations for the nuclear spin vectors **I**. These are graphically illustrated in Figure 8. There are consequently eight different nuclear spin functions Ψ_i. The first and last of the spin functions are totally symmetric to all of the point group's symmetry operators, and are therefore one of the A_1 species.

There are also two linear combinations of the remaining six eigenfunctions that are symmetric to rotations, and are consequently of the general type A_1. These are

$$\Psi_i^{II} + \Psi_i^{III} + \Psi_i^{IV} \quad \text{and} \quad \Psi_i^{V} + \Psi_i^{VI} + \Psi_i^{VII}$$

There are four spin functions remaining that are linearly independent of Ψ_i^I, Ψ_i^{VIII} and the two sets of symmetric linear combinations. These remaining functions are degenerate.

We therefore have four symmetric spin eigenfunctions and two pairs of degenerate spin eigenfunctions.

We will now look at a rovibronic species that result from a rotating, non-degenerate electronic (or vibronic) state of species A_1'. The vibronic eigenfunction is symmetric to a 120° rotation, which is equivalent to two successive exchanges of two pairs of nuclei. The total (rovibronic) eigenfunction must however be anti-symmetric to such a rotation, since the nuclei obey Fermi statistics. The completely symmetric rovibronic states that result from the rotation of a completely symmetric vibronic state consequently remain unpopulated in an H_3 molecule (see Table 12). This means that only the odd N rotational levels of an A_1' electronic state are populated for $K=0$.

Furthermore, since there are two degenerate and four non-degenerate spin states, the ratio of the statistical weights of the A_2 (non-degenerate) species to the E (degenerate) species is 4:2. Since a non-degenerate rovibronic species only occurs for $K= 0, 3, 6, 9,\ldots$, we thus have an alternation of line intensities of the ratios $4,2,2,4,2,2,4,\ldots$.

Similar arguments apply to rovibronic states that result from A_2'' and E' vibronic species. Tables 15 to 17 list which of the rovibronic states of listed in Tables 12 to 14 are populated, along with their statistical weights.

TABLE 15

STATISTICAL WEIGHTS OF POPULATED ROVIBRONIC STATES RESULTING FROM THE A_1' VIBRONIC STATE

K	0	1	2	3	4	5	6
N							
0							
1	A_2' - 4	E'' - 2					
2		E'' - 2	E' - 2				
3	A_2' - 4	E'' - 2	E' - 2	A_2'' - 4			
4		E'' - 2	E' - 2	A_2'' - 4	E' - 2		
5	A_2' - 4	E'' - 2	E' - 2	A_2'' - 4	E' - 2	E'' - 2	
6		E'' - 2	E' - 2	A_2'' - 4	E' - 2	E'' - 2	A_2' - 4

TABLE 16

STATISTICAL WEIGHTS OF POPULATED ROVIBRONIC STATES RESULTING FROM THE A_2'' VIBRONIC STATE

K	0	1	2	3	4	5	6
N							
0	A_2'' - 4						
1		E' - 2					
2	A_2'' - 4	E' - 2	E'' - 2				
3		E' - 2	E'' - 2	A_2' - 4			
4	A_2'' - 4	E' - 2	E'' - 2	A_2' - 4	E'' - 2		
5		E' - 2	E'' - 2	A_2' - 4	E'' - 2	E' - 2	
6	A_2'' - 4	E' - 2	E'' - 2	A_2' - 4	E'' - 2	E' - 2	A_2'' - 4

TABLE 17

STATISTICAL WEIGHTS OF ROVIBRONIC STATES RESULTING FROM THE E' VIBRONIC STATE

K	0	1 (+1) (-1)	2 (+1) (-1)	3 (+1) (-1)	4 (+1) (-1)	5 (+1) (-1)	6 (+1) (-1)
N							
0	E' 2						
1	E' 2	A_2'' E'' 4 2					
2	E' 2	A_2'' E'' 4 2	E' A_2' 2 4				
3	E' 2	A_2'' E'' 4 2	E' A_2' 2 4	E'' E'' 2 2			
4	E' 2	A_2'' E'' 4 2	E' A_2' 2 4	E'' E'' 2 2	A_2' E' 4 2		
5	E' 2	A_2'' E' 4 2	E' A_2' 2 4	E'' E'' 2 2	A_2' E' 4 2	E'' A_2'' 2 4	
6	E' 2	A_2'' E'' 4 2	E' A_2' 2 4	E'' E'' 2 2	A_2' E' 4 2	E'' A_2'' 2 4	E' E' 2 2

4.7 Rovibronic Transitions in the H_3 Molecule

It is obvious that in order for a molecule to undergo a light emitting (or absorbing) electric dipole transition, the molecule's electric dipole moment must change. In quantum mechanical parlance, this requirement is written

$$\int \Psi_e'^{*}\, \mathbf{M}\, \Psi_e''\, d\tau_e \neq 0$$

for the upper and lower electronic eigenfunctions Ψ_e' and Ψ_e''. **M** is the electric dipole moment vector.

The components of the dipole moment vector (M_x, M_y, and M_z) have symmetry properties of their own. With some thought, one may see that each component is of the same symmetry species as its corresponding translational motion (*i.e.* the species of M_x is the same as T_x *etc.*). We now find from group theory that the above integral is not equal to zero if, and only if, one of the **M** components has the same symmetry as the product $\Psi_e'^{*}\Psi_e''$. Stated another way, we require that one of $\Psi_e'^{*} M_x \Psi_e''$, $\Psi_e'^{*} M_y \Psi_e''$, or $\Psi_e'^{*} M_z \Psi_e''$ must be totally symmetric.

However, since the electronic eigenfunction includes the effects of electron spin, we must also require that

$$\int \Psi_{es}'^{*}\, \mathbf{M}\, \Psi_{es}''\, d\tau_e \neq 0$$

for the total electron eigenfunctions Ψ_{es}'' and Ψ_{es}'.

In the approximation that the total electron eigenfunction is the simple product of the electronic and the spin eigenfunctions ($\Psi_{es} = \Psi_e \Psi_s$) we derive the additional selection rule that

$$\Delta S = 0.$$

This means that only doublet-doublet or triplet-triplet *etc.* transitions are allowed. In real molecules however, such intercombinations as singlet-triplet transitions may occur occasionally.

The vibrational eigenfunction (Ψ_v) also adds a selection rule. In the approximation that $\Psi_{esv} = \Psi_{es} \Psi_v$ we require that the so-called *overlap integral* be non-zero, that is

$$\int \Psi_v'^* \, \Psi_v'' \, d\tau_v \neq 0.$$

This is equivalent to saying that $\Psi_v'^*$ and Ψ_v'' must be of the same symmetry species.

It is therefore apparent that a molecule excited in the v_1 vibrational mode (symmetry type A_1') can undergo an electronic transition and maintain its vibration. The molecule may also end up in a highly excited v_2 vibrational mode, despite the fact that v_2 is of symmetry type E'. This can be seen from Table 8, where it is shown that highly excited v_2 vibrations always have a component of symmetry species A_1'. It is however found that $\Delta v = 0$ is by far the most probable transition, so a transition from a low excitation v_1 vibration to a high excitation v_2 vibration is unlikely.

For the degenerate v_2 vibrations, an additional complication arises due to vibronic interaction. We must take into account the quantum number l_2 (where $l_2 = v_2, v_2 - 2, \ldots, 1 \text{ or } 0$, see Section 4.4). It has been shown by Longuet-Higgins *et al.* (1958) that it is required that $\Delta l_2 = 0$.

It has been shown by Hougen (1962) that there is also an additional selection rule that is very stringent and is applicable to the complete rovibronic eigenfunctions. The direct product of the upper and lower states must be of the same *overall species* as the direct product $T_z R_z$. The product $T_z R_z$ happens to be of the species A_1'' in the $\mathbf{D}_{3h}$ point group, and so has the overall species A".

This means that only transitions between rovibronic eigenfunctions of the species

$$A_1' \leftrightarrow A_1''$$

$$A_2' \leftrightarrow A_2''$$

$$E' \leftrightarrow E''$$

are allowed by this rule. The reader should clearly understand that these selection rules refer only to *rovibronic* species. Transitions between two *vibronic* states are not subject to these selection rules.

If we inspect Table 15 to 17, we will see that the A_1' and the A_1'' rovibronic species are unpopulated in our $I = \frac{1}{2}$ molecule. Consequently, the first of these allowed transi-

tions does not actually occur in H_3 (although it does in the molecule's heavier isotopic species).

The restrictions introduced by the rotational eigenfunction have already been introduced (Section 4.4), but a transition involving change in the electronic state of the molecule (not just the vibrational state) introduces additional restrictions. These are for parallel transitions

$$\Delta K = 0,\ \Delta J = 0, \pm 1,\ \Delta N = 0, \pm 1 \qquad \text{if } K \neq 0$$

$$\Delta K = 0,\ \Delta J = \pm 1,\ \Delta N = \pm 1 \qquad \text{if } K = 0$$

Those transitions with $\Delta N = \Delta J$ are the most probable.

Parallel transitions can occur in symmetric top molecules that are symmetric tops because of physical symmetry only for transitions between non-degenerate vibronic states (such as $A_1' \leftrightarrow A_2''$). The *line strength* ($A_{KJ}$) of a parallel transition line is given by the Hönl-London formulae

$$\text{R branch } (\Delta J = +1):\ A_{KJ} = \frac{(J+1)^2 - K^2}{(J+1)(2J+1)}$$

$$\text{Q branch } (\Delta J = 0):\ A_{KJ} = \frac{K^2}{J(J+1)}$$

$$\text{P branch } (\Delta J = -1):\ A_{KJ} = \frac{J^2 - K^2}{J(2J+1)}. \qquad \text{(E28)}$$

The intensities of a line is proportional to the product of its A_{KJ} and the statistical weight of the line as found in tables 15 to 17.

A perpendicular transition involves a transition from a degenerate electronic state to a non-degenerate state (or

vice versa) since the transition moment is a right angles to the axis of symmetry. For perpendicular transitions the selection rules are

$$\Delta K = \pm 1, \quad \Delta J = 0, \pm 1, \quad \Delta N = 0, \pm 1.$$

However, a degenerate electronic state has (+l) and (-l) components, and it is found that an additional selection rule applies. For $\Delta K = +1$ transitions from a degenerate to a non-degenerate state it is necessary to be in the (+l) substate. A $\Delta K = -1$ transition can only occur if the molecule is in the (-l) state. For the reverse transition (from a non-degenerate to degenerate electronic state), the molecule must end up in the (+l) state if $\Delta K = -1$ or in the (-l) substate if $\Delta K = +1$.

The (+l) and (-l) substates give rise to two *subbands* for each K value, with each subbands having its own P, Q, and R branches. The subbands are labelled with the left superscript r or p, which in emission respectively correspond to the $\Delta K = +1$ and $\Delta K = -1$ cases.

It can be easily shown that origins of the r and p subbands are separated by a significant distance. If we let σ_o be the wavenumber produced by the non-rotating, non-vibrating transition, then the band origin of the r subband is given by

$$\sigma_r = \sigma_o + F'(0,K+1) - F''(0,K) \qquad \text{(E29)}$$

where F'(0,K+1) and F"(0,K) are respectively the rotational term values of the (non-vibrating) degenerate upper state and the non-degenerate lower state.

We have already seen that the rotational term value of a degenerate state is given by Equation 17;

$$F_{[v]NK} = B_{[v]}N(N+1) + (C_{[v]} - B_{[v]})K^2 \pm (-2)\,C_{[v]}K\sum_i \left(\pm l_i \zeta_{v_i}\right)$$

In our case we can rid ourselves of the summation since we a restricted to one (+1) substate only. We can also drop the vibration number subscripts and the ± sign since we are trying to find the origin ($v \equiv 0$) of the r subband. However we must add the ' and " superscripts to denote the rotational constants of the upper and lower states.

We then find that for a degenerate upper state

$$F'(0,K+1) = B' + (C' - B')(K+1)^2 + 2C'(K+1)\zeta_t', \qquad \text{(E30)}$$

while for the non-degenerate lower state,

$$F''(0,K) = B'' + (C'' - B'')(K)^2 .$$

If we make the approximations that $B' = B'' \equiv B$, $C' = C'' \equiv C$, and let $\zeta_t' \equiv \zeta_t$, then we can write that the origin of the r subband is

$$\sigma_r = \sigma_o + (C-B)(K+1)^2 - 2C(K+1)\zeta_t - (C-B)K^2$$

$$= \sigma_o + [(1-2\zeta_t)C - B] + 2[(1-\zeta_t)C - B]K. \qquad \text{(E31)}$$

We can similarly show that the origin of the p subband is $\sigma_p = \sigma_o + [(1-2\zeta_t)C - B] - 2[(1-\zeta_t)C - B]K$, and so the wavenumbers of the two subband origins differ by $4[(1-\zeta_t)C - B]K$.

The intensities of the subbands differ as well, as can be seen from the Hönl-London factors of $\perp$ transitions. These are

$$\text{R branch } (\Delta J=+1): A_{KJ} = \frac{(J+2\pm K)(J+1\pm K)}{(J+1)(2J+1)}$$

$$\text{Q branch } (\Delta J=0): A_{KJ} = \frac{(J+1\pm K)[J\pm(-K)]}{J(J+1)}$$

$$\text{P branch } (\Delta J=-1): A_{KJ} = \frac{[J-1\pm(-K)][J\pm(-K)]}{J(2J+1)}. \quad \text{(E32)}$$

except for the $K=0$, $\Delta K=+1$ case when the R branch has twice this weight. Each Hönl-London factor has two values which differ by 2K and which correspond to the r subband and p subbands. If you add the K's (or the -K's) in the numerators, you get the Hönl-London factor of the r subband, while subtraction yields the corresponding value for the p subband. It is seen that the R branch of an r subband is stronger than its P branch, and that the P branch of a p subband is stronger than the R branch.

Figure 9 shows a schematic representation of the r and p subbands with their P, Q, and R branches. It is assumed that the rotation constants are the same for the upper and lower states. The intensities are found from the Hönl-London factors alone, without the alternation in statistical weights created by the nuclear spin. Figure 9 is therefore applicable to the heavier isotopes of H_3.

FIGURE 9

ROTATIONAL STRUCTURE OF PERPENDICULAR TRANSITIONS ASSUMING IDENTICAL ROTATIONAL CONSTANTS FOR THE UPPER AND LOWER STATES

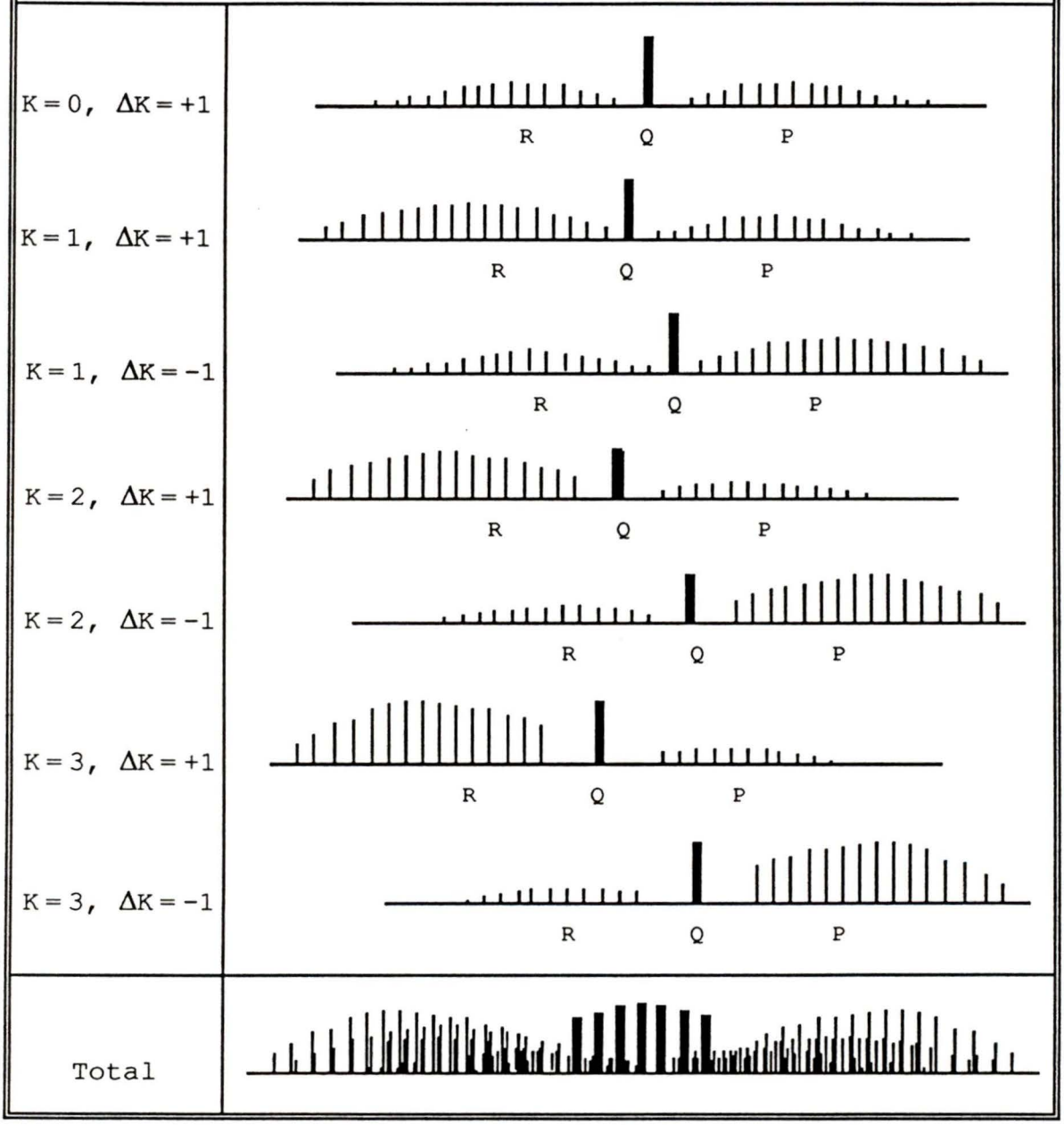

4.8 Electronic Configuration of the H_3 Molecule

The model of the electronic structure of H_3 is that of an H_3^+ core with a third (unpaired) electron added to the system. The electronic ground state configuration of H_3^+ is designated $[1s\,a_1']^2$ (1), and results from the addition of a proton to a ground state H_2 molecule. The addition of the third electron to the system populates one of the orbitals $(2s\,a_1')$, $(2p\,e')$, $(2p\,a_2'')$, $(3s\,a_1')$, $(3p\,e')$, … .

The electron configuration resulting from the unification of three ground state hydrogen atoms is a repulsive state of H_3. This state transforms according to the symmetry type E', and consequently carries the designation $^2E'$ (the left superscript has the value $2S+1$). This state must therefore correspond to the electron configuration $[1s\,a_1']^2(2p\,e')$. Ergo, the two lowest excited states of H_3 must have the configurations $[1s\,a_1']^2(2s\,a_1')$ and $[1s\,a_1']^2(2p\,a_2'')$, and hence carry the designations $2s\,^2A_1'$ and $2s\,^2A_2''$. The number 2 in these

---

[1] The notation that will be adopted is to signify filled orbitals by square brackets, while unfilled orbitals are surrounded by parentheses. The letter to the right of the letter of the "l" quantum number denotes the behavior of the wave function when operated upon by the symmetry operators. These letters are in lower case to signify that a single electron is referred to, not the total wave function. The right superscript outside the brackets (denoting the number of electrons in the orbital) will be understood to be equal to one if omitted. Higher values of the right superscript (2,3,…) will of course be written explicitly.

designations is the value of the quantum number n, which is analogous to the principal quantum number of atomic spectroscopy.

Higher excited states must have $n \geq 3$, and so transitions from such states as $3s\,^2A_1'$, $3p\,^2A_2''$ *etc.* down to the two $n=2$ states are to be expected.

4.9 Parallel Bands Near 5600 Å and 6025 Å

The first publication that featured a detailed description of the H_3 spectrum was produced in 1980, when Dabrowski and Herzberg (1980) observed Rydberg spectra of H_3 in emission at 5600 Å and 6025 Å.

In the 5600 Å band, the R branch line for $N=0$ is missing. We see from inspection of Table 15 that this means that the lower vibronic state must be of symmetry type A_1'.

In order to determine the species of the upper state, we must rely on the selection rules previously discussed. From Table 15 we see that the rovibronic species of the $K=0$, $N=1$ rotational levels of an A_1' vibronic species is A_2'. It is however known from Hougen's selection rules for rovibronic transitions that a transition between two rovibronic states of species A_2' cannot occur. A transition between the $K=0$ rotational levels of two A_1' vibronic states is therefore forbidden. However, the Q branch ($\Delta K = \Delta J = 0$) transitions for $K=0$

are observed and so the upper vibronic state cannot be of species A_1'. Hougen's selection rule insures that the upper vibronic state must have K=0 rotational levels of rovibronic species $A_2"$, and so from Table 16 we see that the upper vibronic state must also be of species $A_2"$.

Those 5600 Å line that are observed are listed in Table 18. The assignment notation in Table 18 shows the branch type (Q, R, or P) then the value of K in a left subscript. The upper and lower state values of K is the same in these ‖ transitions (according to the selection rule $\Delta K=0$). The value of N in the upper state follows the K subscript. For example, Q_11 refers to the Q branch transition with the K=1 and N=1 for both the upper and lower states.

TABLE 18 [1]

MAJOR EMISSION FEATURES OF THE H_3 MOLECULE NEAR 5600 Å

OBSERVED WAVELENGTH (Å)	ASSIGNMENT
5564.06	R_01, R_11
5622.80	$Q_11, Q_12, Q_13, Q_21, Q_22, Q_23, Q_31, Q_32, Q_33$
5649.43	P_01
5679.98	P_12
5711.04	P_03, P_13, P_23
5738.94	P_14, P_24, P_34

[1] Adapted from Dabrowski, I., Herzberg, G. (1980) *Can. J. Phys.* **58**:1238.

TABLE 19 [1]

MAJOR EMISSION FEATURES OF THE H_3 MOLECULE NEAR 6025 Å

OBSERVED WAVELENGTH (Å)	ASSIGNMENT
5926.74	$R_2 2$
5957.14	$R_1 1$
5988.17	$R_0 0$
6019.66	$Q_2 2$
6019.88	$Q_1 1$
6020.50	$Q_1 2$
6020.86	$Q_2 3$
6084.87	$P_1 2$
6084.61	$P_0 2$
6116.71	$P_2 3$
6117.04	$P_1 3$
6149.14	$P_1 4$
6148.93	$P_0 4$

The K structure of the 6025 Å band was resolved by Dabrowski and Herzberg, and it clearly seen that the odd N transitions are missing for K=0. The lower state of the 6025 Å band is therefore of symmetry type A_2" while the upper state is of species A_1'. We predicted an intensity alternation with N for K≥1 in the ratio 2:2:4 *etc.* (see Table 16) which is indeed observed.

The parallel transitions observed near 6025 Å are listed in Table 19.

The upper states of both the 5600 Å and the 6025 Å band is assumed to be n=3 states, while the lower states are n=2 states. The orbital assignments are therefore $3p\,^2A_2$" and $2s\,^2A_1$' for the upper and lower states of the 5600 Å band, and $3s\,^2A_1$' and $2p\,^2A_2$" for the upper and lower states of the 6025 Å band.

---

[1] Adapted from Dabrowski,I.,Herzberg,G. (1980) *Can.J.Phys.***58**:1238.

The rotational constants were determined by a least-squares fit program and by assuming that both the upper and lower states were not vibrating. The values of the rotational distortion constants could not be determined because of the inability to adequately resolve K structure. The value of D_N was however assumed to be the same as that of H_3^+, letting the values of D_K and D_{NK} be determined from Equation 13. The rotational constants determined from the 5600 Å and 6025 Å lines are listed in Table 20.

TABLE 20 (1)

ROTATIONAL CONSTANTS OF THE UPPER AND LOWER STATES OF THE PARALLEL BANDS OF H_3 NEAR 5600 Å AND 6025 Å

	$2s\,^2A_1'$	$2p\,^2A_2'$	$3s\,^2A_1'$	$3p\,^2A_2''$
B_o	46.8 cm^{-1}	44.530 cm^{-1}	44.158 cm^{-1}	45.5 cm^{-1}
C_o	23.4 cm^{-1}	22.266 cm^{-1}	22.9 cm^{-1}	22.75 cm^{-1}
r_o	0.8543 Å	0.8667 Å	0.8703 Å	0.8575 Å
D_N	0.0415 cm^{-1}	0.0539 cm^{-1}	0.0675 cm^{-1}	0.0415 cm^{-1}
D_{NK}		-0.0909 cm^{-1}	-0.110 cm^{-1}	
D_K		0.0412 cm^{-1}	0.1 cm^{-1}	

The width of the 5600 Å lines is 8 Å, while the 6025 Å lines are somewhat narrower at 5 Å. The cause of this great line width can only be predissociation of one of the

---

[1] Adapted from Dabrowski, I., Herzberg, G. (1980) *Can. J. Phys.* **58**:1238.

electronic states. Dabrowski and Herzberg argue that the predissociated state must be the lower one. If it is the upper state that is predissociated, it would not be significantly populated, and it would then be impossible to see the observed bands in emission. We find from Heisenberg's uncertainty principle that the lower level of the 5600 Å transition is $\approx 2 \times 10^{-13}$ s, while the lower state of the 6025 Å transition has a lifetime of $\approx 3.5 \times 10^{-13}$ s.

The superposition of Q branch lines at 5622.80 Å has been tentatively identified in emission in the spectrum of the planetary nebula NGC 7027 by Pritchet and Grillmair (1984).

4.10 Perpendicular Bands Near 7100 Å

Perpendicular transitions ($\Delta K = \pm 1$) of H_3 have been reported by Herzberg and Watson (1980). A perpendicular transition in an oblate symmetric tops involves degenerate and non-degenerate vibronic states. We must therefore be concerned with the Jahn-Teller interaction and the Coriolis coupling.

If we add the centrifugal distortion terms to Equation 26, we find that the rotational term values of a (non-vibrating) degenerate state are

$$F(N,K) = BN(N+1) + (C-B)K^2 \pm -2CK\zeta_t - D_N N^2(N+1) - D_{NK} N(N+1)K^2 - D_K K^4 \qquad (E33)$$

where the exact value of ζ_t is given by Equation 23, but is expected to be close to +1.

It is possible to account for the Jahn-Teller interaction to a higher order approximation than was discussed here by introducing the quantum number G. G is defined by the equation $G \equiv K - 1$ (letter "l"). Child and Strauss (1965) tell us to add to Equation 33 the terms

$$\pm \frac{1}{2} \sqrt{16\,[C(1-\zeta_t) - B]^2 G^2 + q^2 [N(N+1) - G(G-1)]\,[N(N+1) - G(G+1)]}$$

where the splitting constant q is the sum of contributions from the Coriolis splitting and the Jahn-Teller splitting.

A least squares program fit the parameters σ_o, B', ζ_t', q' for the upper state and B" for the lower state. It was assumed that $C = \frac{1}{2} B$. The centrifugal distortion constants were given theoretical values for the calculations, but could not be determined from the observations because of insufficient resolution. The values of the determined constants are included in Table 21.

The width of 7100 Å H_3 lines is roughly the same as the 5600 Å lines. This suggests that the two transitions may share a common lower state. The derived rotational constants of the lower state of the 7100 Å band shows that this is indeed the case. The upper state of the 7100 Å band has been identified

TABLE 21 [1]

ROTATIONAL CONSTANTS OF THE UPPER AND LOWER STATES OF THE 7100 Å BAND

	$2s\,^2A_1'$	$3p\,^2E'$
σ_o (cm^{-1})	-	14091.7
B_o (cm^{-1})	23.12	21.15
C_o (cm^{-1})	11.56	23.12
r_o (Å)	0.850	0.889
ζ_t	-	0.877
q	-	2.82

as the degenerate vibronic state $3p\,^2E'$. The upper state is not vibrationally excited.

A spectrophotometric search for the 7100 Å H_3 band in the spectrum of NGC 7027 was conducted by the author. It was hoped that this would confirm Pritchet and Grillmair's possible observation of the 5600 Å Q branch lines. The particulars and the results of this search are the

TABLE 22 [1]

MAJOR EMISSION FEATURES OF THE H_3 MOLECULE NEAR 7100 Å

WAVELENGTH (Å)	ASSIGNMENT	WAVELENGTH (Å)	ASSIGNMENT
7083.96	$^rR_03, {}^pQ_33$	7194.38	$^rR_66, {}^rQ_01, {}^rQ_03$
7101.27	$^rR_13, {}^pQ_34$	7227.26	$^pP_44$
7122.32	$^rR_12, {}^rR_01$	7249.69	$^rR_12, {}^pP_12, {}^pP_66$
7137.63	$^rR_34$	7261.64	$^pP_23$
7156.74	$^rR_11, {}^pQ_11,$ $^rR_22, {}^rR_33, {}^pQ_12$	7292.73	$^pP_56, {}^pP_13$
		7357.25	$^rP_03$

[1] Adapted from Herzberg,G.,Watson,J.K.G. (1980) *Can.J.Phys.* **58**:1250.

topics of the remaining chapters of this thesis.

4.11 Other Observed H_3 Emission Bands

A perpendicular emission band of H_3 has been observed in the infrared near 2.8 μm and reported by Herzberg, Lew, Sloan, and Watson (1981). The upper state of this band is apparently the same as the upper state of the 6025 Å band ($3s\,^2A_1'$), while its lower state is the upper state of the 7100 Å band ($3p\,^2E'$).

The widths of the infrared perpendicular lines are somewhat less than 1 Å, and so they are very much narrower than the lines of the 6025 Å and 7100 Å bands. This agrees with the idea that the lower states of the 6025 Å and 7100 Å bands are predissociated, while the upper states are stable.

Jahn-Teller splitting is observed in this band, and Herzberg *et al.* were able to determine that the Jahn-Teller interaction constant has a value of $D = 0.0301$. We thus find that Equation 20 holds at least as a first approximation.

If the recent improvement in infrared detectors continues, it is entirely possible that these lines may be someday be detected astronomically. In anticipation of this, the wavenumbers of Herzberg *et al.*'s paper are converted to wavelengths and are listed in Table 23.

TABLE 23 [1]

MAJOR EMISSION FEATURES OF THE H_3 MOLECULE NEAR 2.8 μm

WAVELENGTH (μm)	I (obs)	ASSIGNMENT	WAVELENGTH (μm)	I (obs)	ASSIGNMENT
3.14508	0.5		2.79130	1.1	
3.06364	0.7		2.77060	0.3	
2.91480	0.2		2.76521	0.5	
2.91050	0.4		2.76405	1.6	$^{p}P_{2}2$
2.89769	2.1		2.76404	0.9	$^{p}P_{3}3$
2.89360	0.4		2.76244	0.7	
2.88489	0.3		2.75973	1.8	$^{p}P_{4}4$
2.88454	0.5		2.75918	0.4	
2.87869	0.2		2.73110	0.4	
2.87494	0.4	$^{r}Q_{2}3$	2.72921	0.6	$^{p}Q_{1}3$
2.86679	0.5		2.71808	2.5	$^{p}Q_{1}1$
2.86556	0.7		2.70430	0.4	$^{r}R_{0}0$
2.86156	0.4	$^{p}P_{2}4$	2.69744	0.8	$^{r}R_{1}1$
2.81757	0.9	$^{p}P_{2}3$, $^{r}Q_{1}2$	2.69101	0.7	
2.81724	0.4		2.68295	0.9	$^{r}R_{2}2$
2.81103	3.2	$^{p}P_{1}2$	2.63665	0.3	$^{p}Q_{2}2$
2.80837	0.4	$^{r}Q_{1}3$	2.61755	0.5	
2.80625	0.2	$^{p}P_{4}5$	2.59848	0.3	

[1] Adapted from Herzberg,G.,Lew,H.,Sloan,J.J.,Watson,J.K.G. (1981) *Can.J.Phys.***59**:428.

Those lines that are unassigned probably do not belong to the $3s\,^2A_1' \rightarrow 3p\,^2E'$ transition, but instead belong to an as yet unidentified one. The entries under the **I** column are the lines' relative intensities in an arbitrary scale.

A fourth paper on the laboratory spectrum of H_3 was presented by Herzberg, Hougen and Watson (1982). This paper includes many sharp lines that have been assigned to Rydberg transitions from the 3d orbital.

The 3d orbital includes electronic states of symmetry A_1', E', and E", which consequently carry the respective designations $3d\,^2A_1'$, $3d\,^2E'$, and $3d\,^2E"$. These states undergo transitions to the $2p\,^2A_2"$ and the $3p\,^2E'$ states.

The wavelengths of the observed transitions from the 3d orbital are listed in tables 24 and 25 along with their intensities relative to an arbitrary scale (not the same scale as Table 23).

TABLE 24 [1]

H_3 SPECTRAL FEATURES OF THE $3d \rightarrow 2p\ ^2A_2''$ TRANSITION

WAVELENGTH (Å)	I (obs)	WAVELENGTH (Å)	I (obs)	WAVELENGTH (Å)	I (obs)
6144.5	3	5906.6	3	5778.2	1
6119.5	3	5898.4	1	5777.2	4
6107.2	5	5895.5	4	5774.0	1
6083.9	2	5873.6	6	5771.8	8
6049.6	0.5	5868.4	6	5762.7	5
6036.5	0.5	5849.3	6	5762.4	3
6033.0	2	5840.5	1	5753.3	3
6025.4	2	5834.7	1	5752.0	5
5997.1	2	5827.9	8	5750.3	1
5986.2	4	5824.4	2	5748.7	10
5976.4	2	5823.3	2	5739.5	7
5973.6	7	5821.0	1	5727.2	7
5971.5	1	5818.4	2	5726.6	3
5966.6	8	5817.7	?	5720.4	10
5961.9	7	5814.0	8	5715.6	1
5951.5	8	5811.2	2	5700.2	3
5929.9	10	5782.2	4	5686.8	2
5918.6	10	5782.1	4	5677.7	2
5908.3	3	5779.8	6		

[1] Adapted from Herzberg,G.,Hougen,J.T.,Watson,J.K.G. (1982) *Can.J.Phys.* **60**:1261.

TABLE 25[1]

H_3 INFRARED FEATURES OF THE $3d \rightarrow 2p\ ^2E'$ TRANSITION

WAVELENGTH (μM)	I (obs)	WAVELENGTH (μM)	I (obs)	WAVELENGTH (μM)	I (obs)
2.56945	3.5	2.50911	1.3	2.33781	1.3
2.54842	1.3	2.49777	1.9	2.32590	1.3
2.53666	0.6	2.48830	3.1	2.32257	1.0
2.53434	1.4	2.47878	0.7	2.30655	0.4
2.52885	1.6	2.46607	1.1	2.26857	0.8
2.52701	3.0	2.45283	0.8	2.25728	0.7
2.51529	2.9	2.44062	0.8	22513.8	0.4
2.51434	1.4	2.39077	0.9	22434.2	0.8
2.51193	1.1	2.38040	0.8		

[1] Adapted from Herzberg,G.,Hougen,J.T.,Watson,J.K.G. (1982) *Can.J.Phys.***60**:1261.

CHAPTER 5

THE OBSERVATIONS

The H_3 lines discussed in the previous chapter have never been positively identified in any planetary nebula. The planetary nebula NGC 7027 is thought to be a good candidate nebula for the search for these lines (as discussed in Chapter 2), and indeed, initial spectral searches proved promising. In 1984, a previously unidentified line was detected near 5624 Å by C.Pritchet and C.Grillmair and was tentatively identified as a parallel transition feature of H_3. As this was the only candidate H_3 line found, the identification remained unconfirmed. More observations were required to detect other H_3 lines, and the collection of the new data is the topic of this chapter.

5.1 AUGUST, 1984

Pritchet conducted a search for the 7100 Å lines of H_3 in August of 1984 with the 1.83 m telescope at the Dominion Astrophysical Observatory (DAO). The spectrograph used had a 1200 lines/mm grating, blazed at 7500 Å and equipped with an order filter to prevent ultraviolet contamination of the data. The telescope was fitted with extended red optics (enhanced silver coatings) in its 53 cm focal length F/5

camera mirror. The spectrographic resolution was 0.2 Å/pixel, and the observing slit was opened to 0.2 mm.

The spectra were recorded by a RETICON™ RL 1872 photodiode array, but no image intensifier was used in order to record the highest possible signal to noise (SN) ratio. With sufficient exposure times, this apparatus can easily generate SN ratios of several hundred for bright emission lines, and can record comparison arcs of full width-half maximum ≤ 1 Å.

The observations were made from August 7/8 to 10/11,1984. Sky conditions during the observing run were compromised by intermittent cloud, but the atmospheric "seeing" ranged from 3 arc seconds (3"), down to an outstanding 1". Full moon occurred on the night of the eleventh, so skies were bright throughout the observing run. This was not considered troublesome because of the extreme redness of the wavelength region under study.

Midnight culmination of NGC 7027 occurs on August 9, since its (1987.0) equatorial coordinates are:

$$\alpha = 21\text{h } 06\text{m } 32\text{s}$$

$$\delta = +42^\circ\ 11'\ 30"$$

The PN was consequently observable for the entire night. It should be noted that the interval between the astronomical twilights is only five hours at this time of year in Victoria. In practice it was however possible to make

observations for over an hour past astronomical dawn because of the observed wavelength region and the westerly apparent position of the nebula.

It was anticipated that the telluric absorption lines of the Earth's atmosphere would interfere strongly with the recorded data, and for that reason spectra of the hot stars ν Cygni and Vega (α Lyrae) were taken on the same nights. These spectra were to serve as "flat field" measures, for which the spectral response of the RETICON™ and the absorption function of the atmosphere were to be recorded. It was necessarily assumed that the spectra of these stars are both unsloped and featureless in the small wavelength interval between 7100 Å and 7300 Å.

The light of the night sky was also collected in order to identify emission features of terrestrial origins. Typical sky exposures were from 900 to 1800 seconds long. Finally, the spectrum of a neon-cadmium comparison arc was recorded on 6 frames.

A total of 62 frames were taken over the four nights, of which 17 were spectra of NGC 7027 taken near 7100 Å. Nebula exposures ranged from 3600 to 5400 seconds, for a total of integration time of nearly 62000 seconds. The data were recorded directly to a 1/2 inch format magnetic tape by a NOVA™

1200 computer. The data tape was recorded at a density of 800 bpi.

A complete listing of all exposures taken by Pritchet during the four nights of his observing run is included in Appendix 1.1.

5.2 August, 1986

Pritchet's observations were repeated by the author in the summer of 1986, using the same telescope and spectrophotometric apparatus as Pritchet. The author's observations covered a wavelength range of ≈6900 Å to 7300 Å, and were recorded under moonlit skies on the six nights of August 16/17 to 21/22, 1986.

Atmospheric seeing during this observing run was good, and ranged from 3" down to nearly 1" just before the dawn. Atmospheric transparency was also generally good, with no high altitude cirrus cover, but with some ground haze. As the apparent altitude of the nebula ranged from 42° to 84°, the low-altitude haze did not significantly obscure the nebula. However, the moon had reached full phase on August 19, so the ground haze scattered a great deal of moonlight as well as street-light. The sky was very bright, with a typical naked-eye stellar limit of 4.5 magnitudes at the zenith. It was hoped that this would not be a major problem because of the

sanguinary wavelength region under study. This appeared to be the case, as the telescope's exposure meter recorded a count rate nearly 10 times greater for the nebula than for the nearby sky.

The nebula was recorded with the various integration times ranging from 1200 to 15000 seconds. A total of 18 nebula frames were recorded during the six nights, for a total integration time of 81 600 seconds. Spectra of ν Cygni, Vega and the empty sky were taken as well. The spectrum of the Ne-Cd arc was recorded before and after each frame to determine the change in the pixel/wavelength correspondence with the telescope's hour angle.

The observing records for the six nights have been included in Appendix 1.2.

CHAPTER 6

REDUCTION OF THE DATA

In this day of digital recording devices and storage systems, computers play an important part in turning raw data into written conclusions. The purpose of this chapter is to describe the computer procedures used to reduce the data.

6.1 RETICENT

The raw data were reduced using the University of British Columbia's RETICENT spectrophotometric reduction package. This package was installed in the University of Victoria's VAX™ 11/750 mini-computer by Pritchet in 1982. An introductory description of RETICENT is found in a paper by Pritchet, Mochnacki and Yang (1982), to which the reader is urged to refer if necessary. Also, Appendix 2 contains a synopsis of the italicized RETICENT commands mentioned in this chapter.

RETICENT stores recorded spectra in individual data frames and allows them to be manipulated by simple one word commands or by command sequences. The command sequences are referred to as *Macros*, and are syntactically similar to programs in an unstructured version of FORTRAN.

The reduction procedure performed using RETICENT can be summarized as follows;

1) All frames aligned to the same pixel/wavelength correspondence.

2) The dispersion function of the frames determined.

3) Frames corrected for telluric absorption and sky contamination.

4) Frames coadded to detect very faint emission features by increasing the signal to noise ratio.

6.2 FRAME ALIGNMENT

A frame alignment procedure is required because of flexure in the 1.83 m telescope's optical assembly. This flexure results in a slow change in the pixel/wavelength correspondence with the telescope's hour angle. Furthermore, the grating rotation may be changed by tests and adjustments made between observing sessions, resulting in changes in the position of the spectral lines.

To align the emission spectrum frames, they were first displayed on a Tektronix™ graphics terminal using RETICENT's *Tek* command. *Tek* allows two (or more) frames to be simultaneously plotted on the terminal using the *O* (overplot) sub-

command. The difference between positions of emission lines on the overplotted frame and the base frame was then measured. The measured differences ranged from a fraction of a pixel (for frames taken sequentially) to 250 pixels for frames taken after the grating was deliberately rotated.

Next, the *Shift* command was used to roughly align the frames. The two frames were again displayed on the Tektronix™ terminal, and the process was repeated (if necessary) until the two frames were aligned as closely as possible.

The *Posn* command was then used to calculate any residual misalignment of the frames to the nearest tenth of a pixel. *Posn* works by searching the data for the center of an absorption or emission feature within a certain number of pixels (usually three) from a specified position. The average distance of the located line centers to the specified pixel positions is then calculated and displayed. It is necessary to align the frames visually before *Posn* is called to ensure that the program manages to find the right emission lines.

Shift was again called, using the mean shift value calculated by *Posn* as the shifting parameter. Displaying the aligned frames with the *Tek* command should then result in a complete superposition of the two frames.

The alignment was next checked with the *Sub* command, which subtracts one frame from the other. If the frames are

properly aligned, the height of the emission lines will be reduced after *Sub* is used. If the frames are misaligned the emission line will have a "mirror image" absorption line next to it on the subtracted frame. (See figures 10 and 11).

FIGURE 10

THE RESULT OF SUBTRACTING TWO MISALIGNED NGC 7027 FRAMES

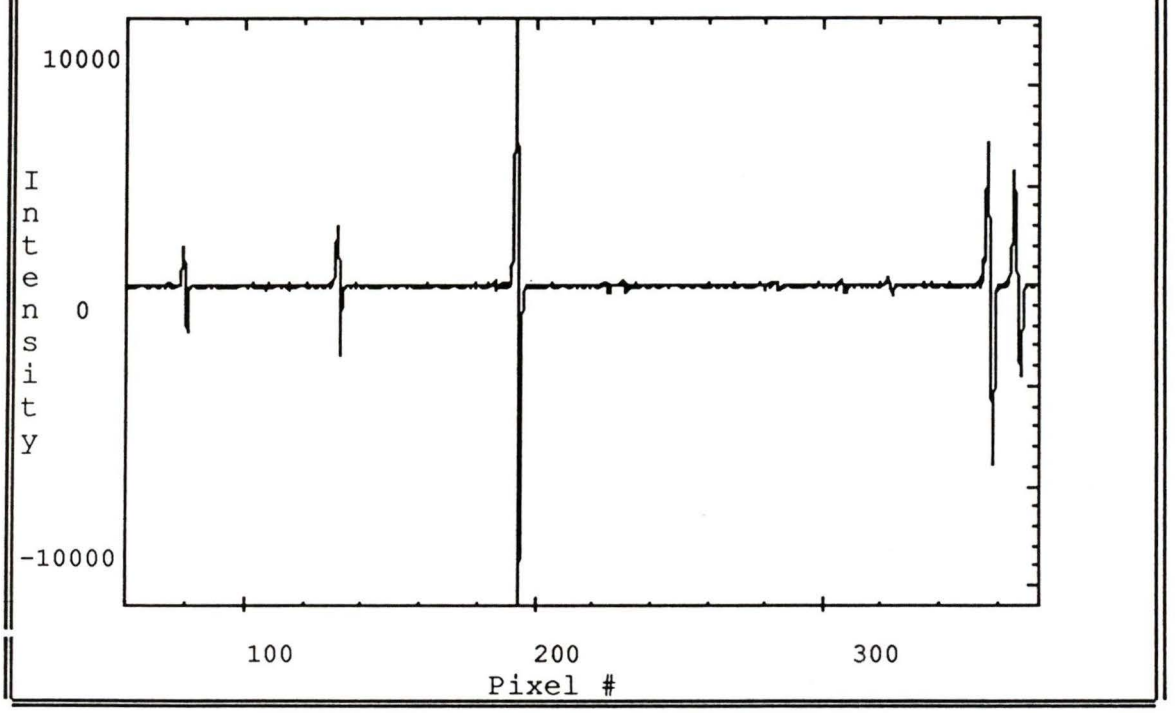

All the Ne-Cd comparison arc frames were aligned to a "base" frame, which was arbitrarily chosen to be the first frame taken on August 16,1986. A plot of "frame shift versus hour angle" was then made and found to be very nearly linear. The shift required to align the first NGC 7027 frame with the base frame was consequently determined by linearly interpolating the shifts of the two Ne-Cd frames taken before and

after it. All NGC 7027 frames were then aligned to the first planetary nebula frame.

FIGURE 11

THE RESULT OF SUBTRACTING TWO ALIGNED NGC 7027 FRAMES

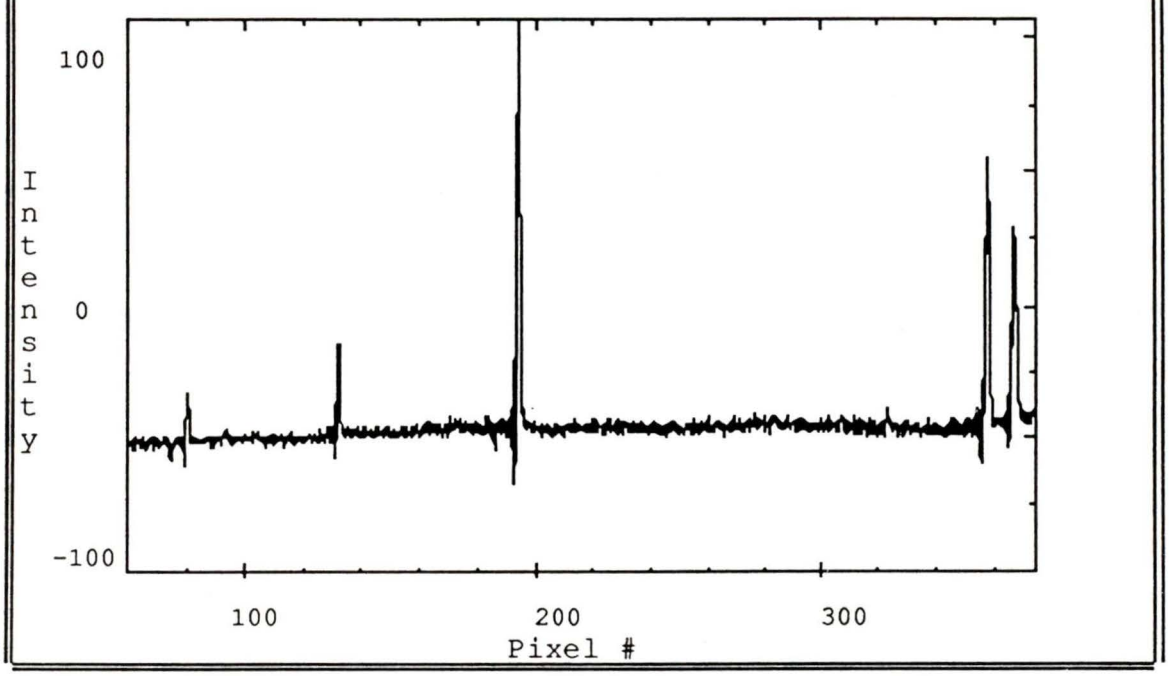

The spectra of the comparison stars lack sharp features, and so can not be precisely aligned to each other as can the nebula and the comparison arc frames. Instead, the required shift values were estimated by averaging the measured shift values of the spectrum's two comparison arc frames.

Using the *Shift* command to shift spectra by a non-integral number of pixels results in a Fourier reduction of the spectrum followed by an application of the Fourier shift theorem. Unfortunately, the Fourier reduction of an emission

spectrum introduces an oscillatory "ringing" that significantly alters the spectrum's noise characteristics near strong emission lines. This ringing can be seen by comparing figures 12 and 13.

This ringing is particularly troublesome in the 7100 Å frames, since the intense 7136 Å feature of [Ar III] lies in the middle of the sought after H_3 lines. To remove the ringing, one must use the *Filter* command.

FIGURE 12

AN ENLARGEMENT OF AN UNSHIFTED NGC 7027 FRAME ABOUT A BRIGHT EMISSION LINE

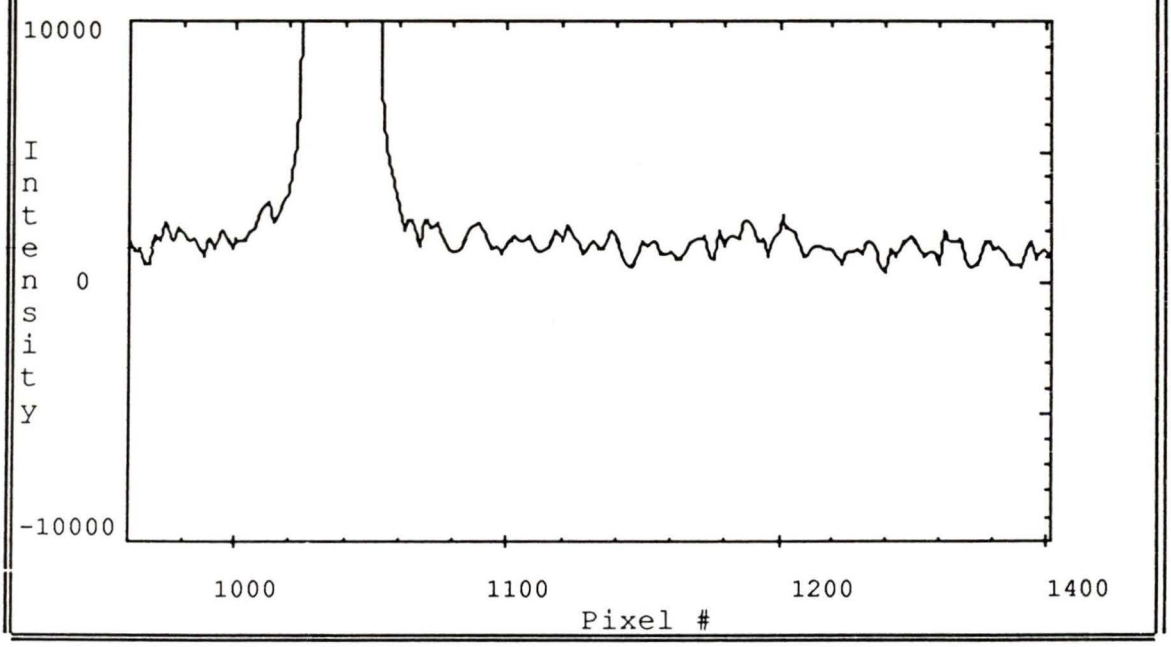

FIGURE 13

AN ENLARGEMENT OF AN NGC 7027 FRAME AFTER A NON-INTEGRAL SHIFT

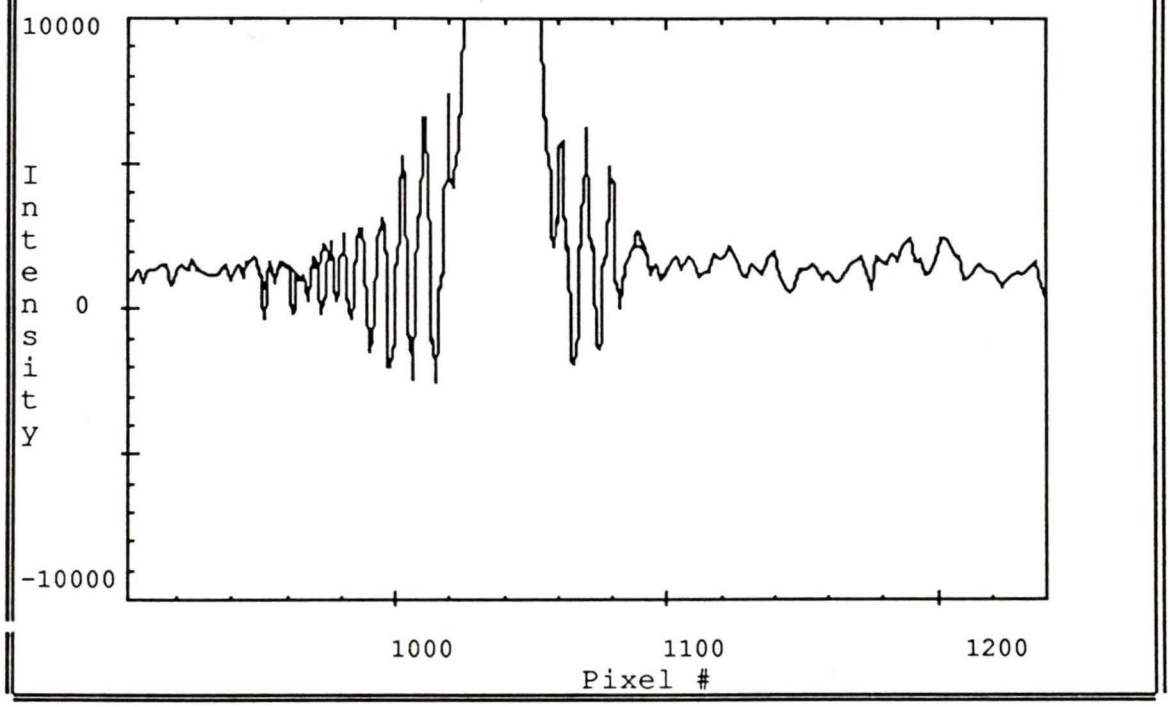

Filter employs a somewhat convoluted Fourier analysis procedure to quell the Fourier ringing. The filter that was used was defined by the command

FiltDef 32,64,0.25,0.3125,0.5,0.625,0.75,0.8125

(See Appendix 2 for an explanation of the *FiltDef* command.)

Filter reduces the ringing to simple oscillatory noise. These oscillations can now be suppressed with the *Smooth* command. The final result is a relatively noise free, properly aligned spectrum. The filtered spectrum is shown in Figure 14, while Figure 15 shows the smoothed version.

FIGURE 14

THE EFFECTS OF FILTERING A SHIFTED NGC 7027 FRAME:
AN ENLARGEMENT ABOUT A BRIGHT EMISSION LINE

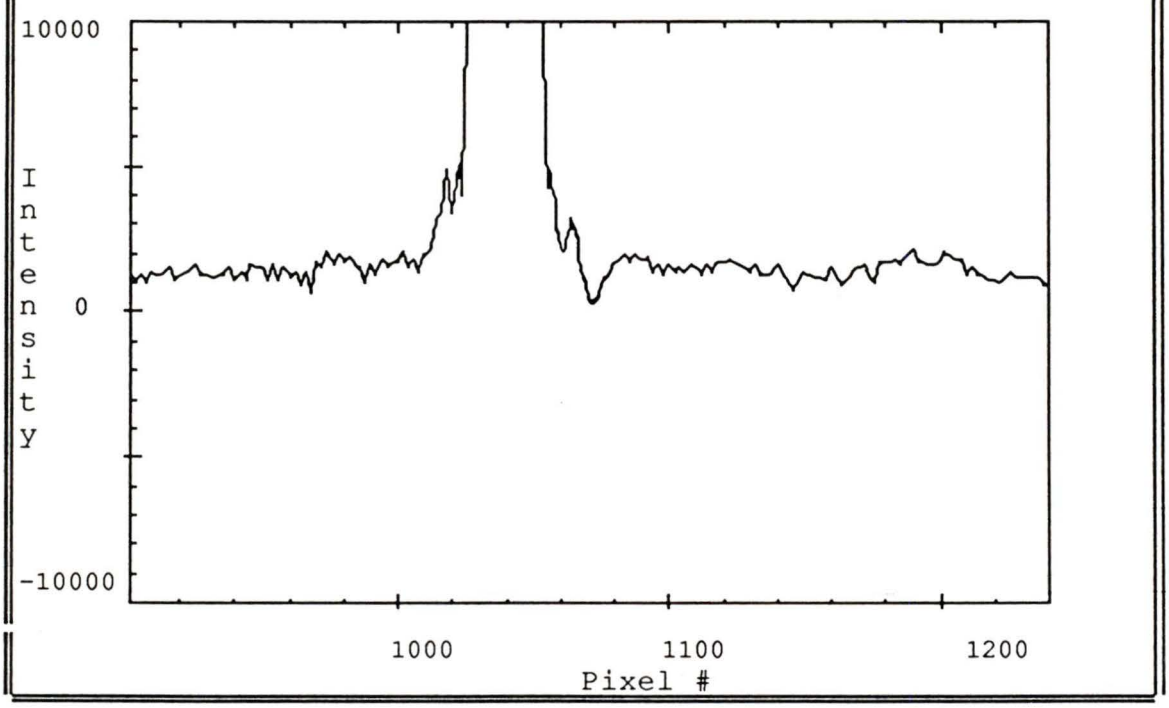

FIGURE 15

THE EFFECTS OF SMOOTHING A FILTERED AND SHIFTED NGC 7027 FRAME: AN ENLARGEMENT ABOUT A BRIGHT EMISSION LINE

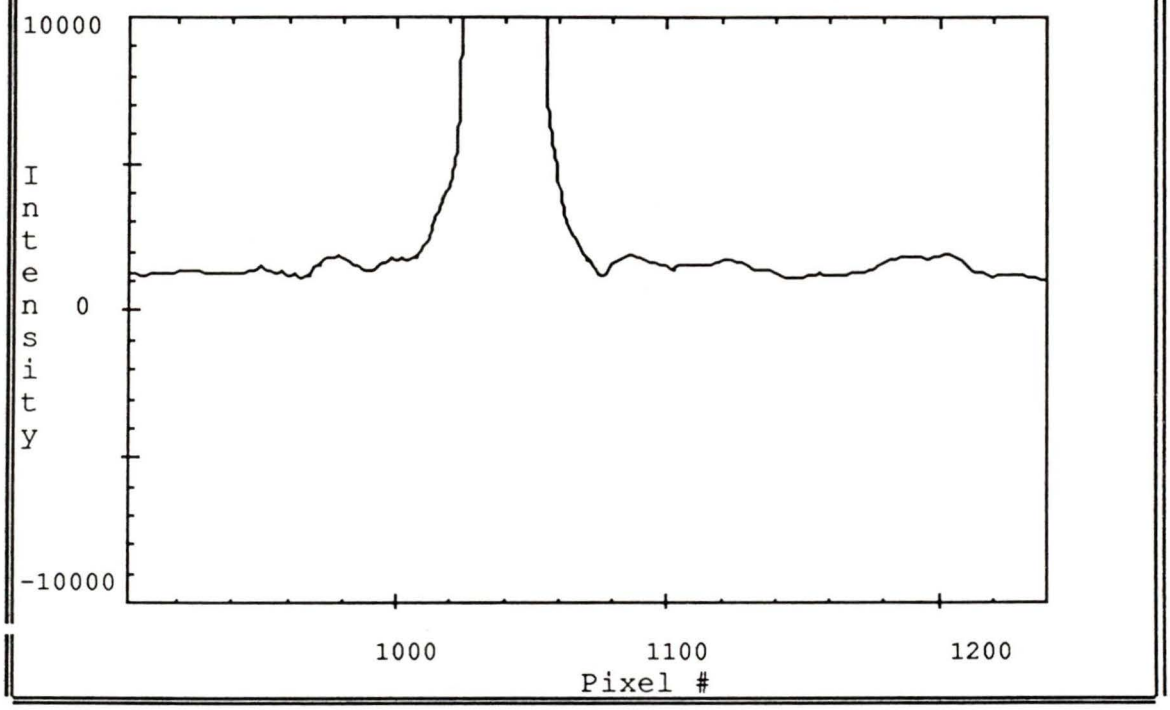

6.3 FRAME DISPERSION

To determine the frame dispersions, the wavelengths of the Ne-Cd arc lines and the prominent nebula lines were first entered into data arrays with the *Data* command. The *Tek* command was then used with an array name specified as a parameter to record the positions of the spectral features. Finally, the *Disp* command was used to determine the dispersion coefficients using the wavelength array and the pixel position array as parameters.

Using the *Sub* command to check the frame alignments also reveals differences in the dispersion of two frames. A change in the frame dispersion will result in some of the emission lines being properly aligned, but others (usually near the frame edges) being misaligned. If a noticeable change in the dispersion was found, then the *Stretch* command was used to place the frames on a common wavelength scale.

Stretch was used (more or less experimentally) on only a few frames as the dispersion of the various aligned frames did not appear significantly different. As an added check for variation in the dispersions, the dispersion coefficients of different frames were found. These were then used to calculate line wavelengths independently on several frames. The variation in the determined wavelengths using the different dispersion coefficients was ≤ 0.2 Å, which was considered acceptable.

6.4 Telluric Absorption

The 7100 Å frames are significantly affected by the atmosphere's telluric absorption bands. These bands are clearly visible as a series of sharp absorption lines at $\lambda \geq 7170$ Å on the spectra taken of the comparison stars (Figure 16). Correcting for these bands could be done by dividing the

planetary nebula frames by the comparison star frames with the *Div* command.

Dividing the comparison's star spectrum from the nebula will adversely affect the data unless the comparison star's spectrum is naturally unsloped and featureless in the required wavelength region. All irregularities in the stellar spectrum must be due to the Earth's atmosphere.

This requirement limits the choice of comparison stars to hot stars positionally close to NGC 7027. The comparison stars chosen were Vega (α Lyrae) and ν Cygni, which are both of the spectral type A0. Their optical spectra are quite featureless at wavelengths longer than Hα, and since 7100 Å lies well away from the peak of the Planckian curve for a $T \geq 10000$ K radiator, their spectra are also relatively flat over the small frequency interval of the spectrum.

The division procedure was at first unsuccessful, since the telluric absorption lines were incompletely removed. Frame division created emission-like bumps on the nebula frames (Figure 17). It was found that this problem could be largely corrected by adding a constant integer to each data point in the nebula frame before division by the stellar frame. A *Macro* was written that added sequential integers to the planetary nebula frames before division, and then

selected that integer that best minimized the bumps (Figure 18).

FIGURE 16

SPECTRUM OF VEGA SHOWING TELLURIC ABSORPTION BANDS

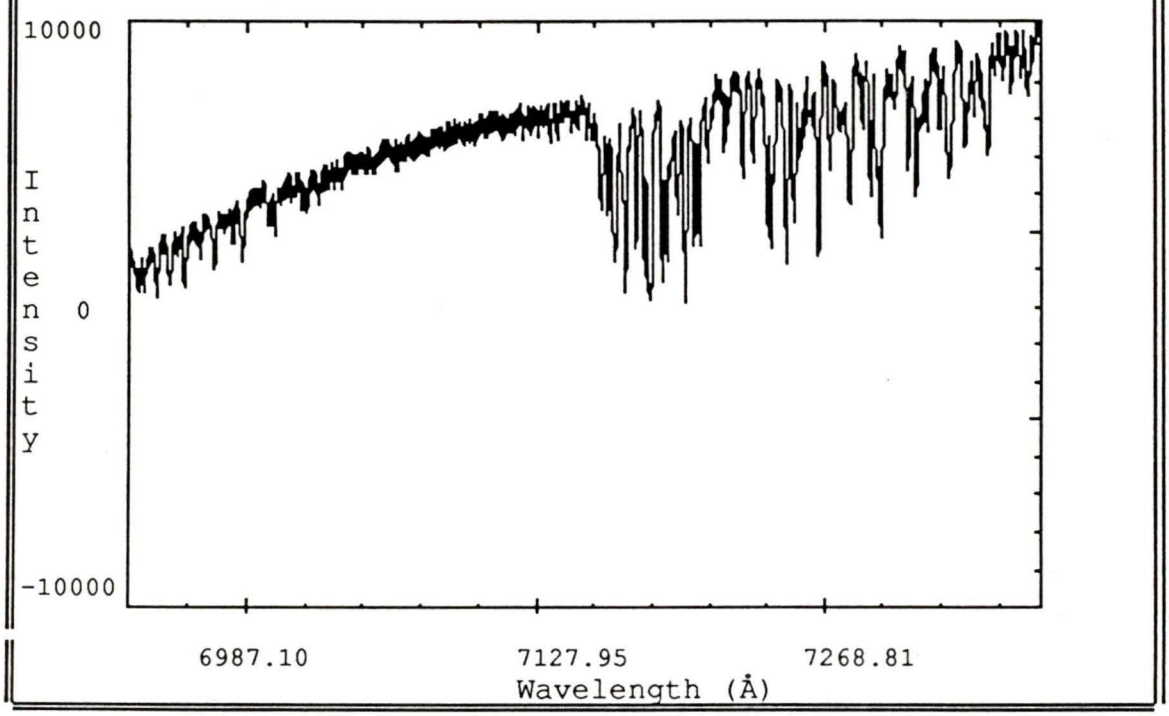

It is clearly seen in Figure 16 that telluric absorption is minimal or nonexistent in the wavelength interval $\lambda = 7100$ Å to 7170 Å. The brightest lines in H_3's perpendicular emission band all lie within this window, and so we would not expect the telluric absorption to significantly affect the detectability of the H_3 emission lines.

FIGURE 17

NGC 7027 FRAME AFTER DIVISION BY VEGA FRAME

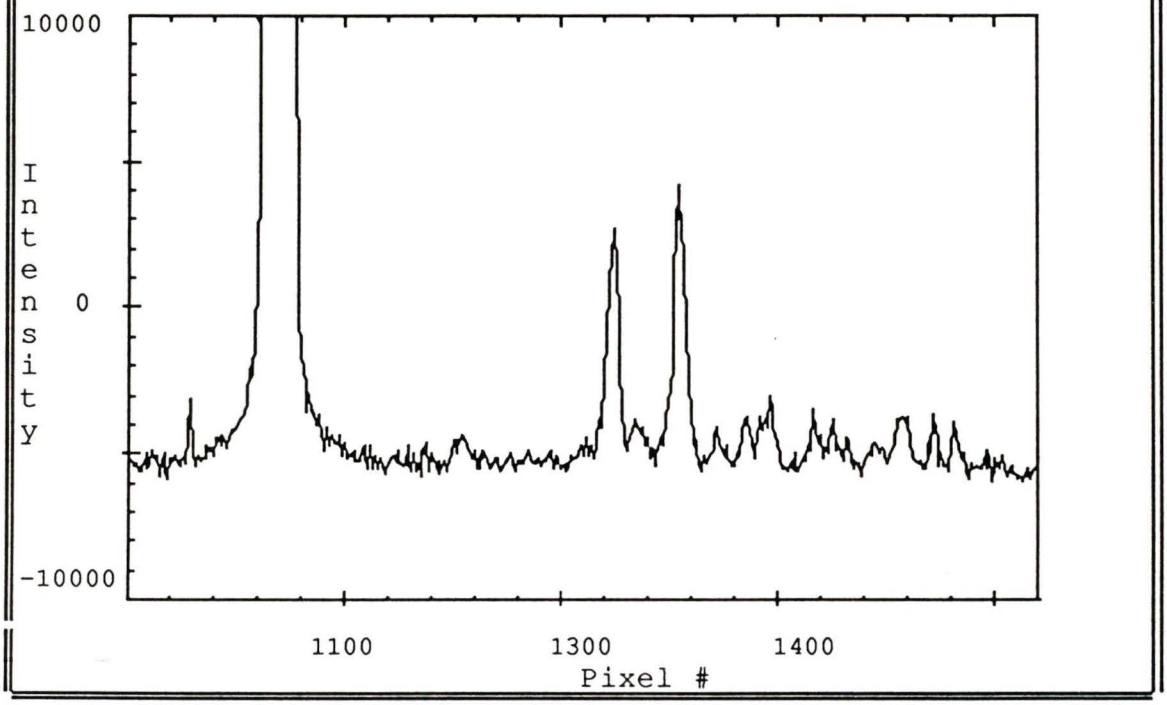

FIGURE 18

NGC 7027 FRAME AFTER DIVISION BY VEGA FRAME
THAT HAS HAD A CORRECTING INTEGER APPLIED

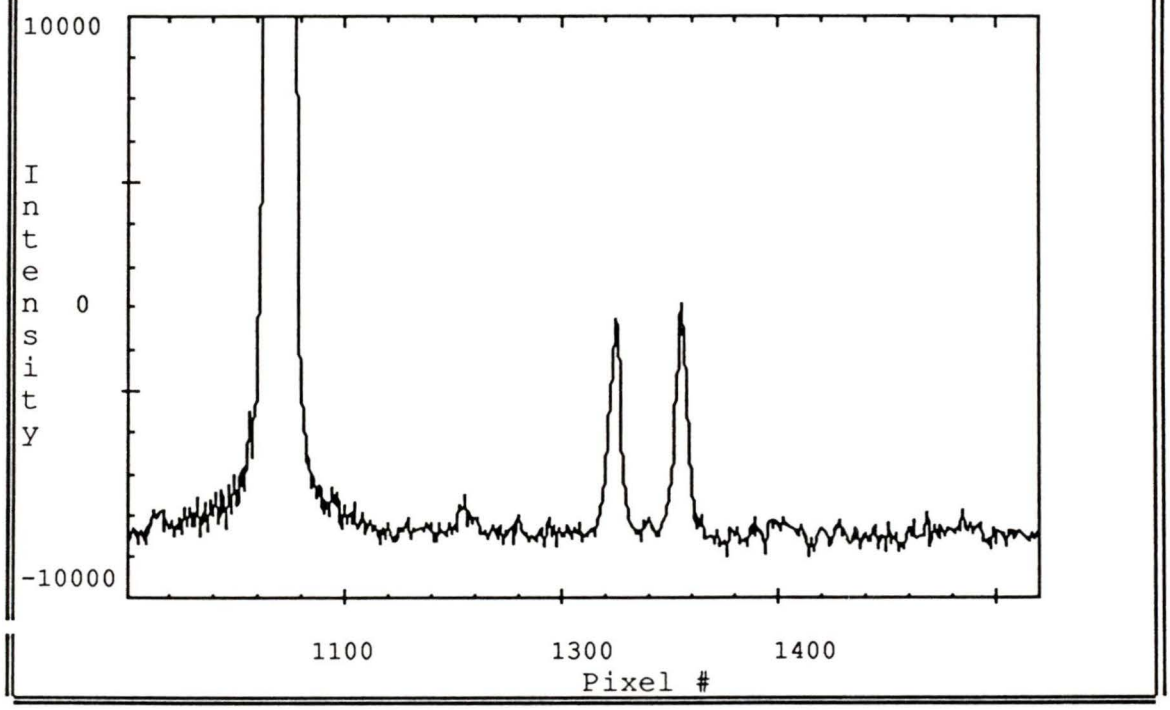

6.5 SKY EMISSION

It is very easy to correct for sky emission if exposures of the sky are taken with the observations. A simple subtraction (using the *Sub* command) of the sky frame from the nebula frame will remove the atmospheric light quite easily, provided that the exposure times of the two frames are similar. When the exposure time of the sky frame is some fraction of the exposure time of the nebula frame, the two frames are respectively multiplied by the denominator and by

the numerator of that fraction (using the *MultI* command) before they are subtracted.

6.6 Coaddition

If one assumes that signal noise is random (*i.e.* uncorrelated with pixel number), then the signal to noise ratio of two frames will tend to increase when the frames are added together. In fact, it can easily be shown using Poisson statistics that the signal to noise ratio of coadded frames increases with $\sqrt{N}$, where N is the number of coadded frames (provided that the SN ratio of each of the N frames is equal). The SN ratio of the 7100 Å frames can consequently be increased by almost a factor of 6 by coaddition, since there are 35 of them.

In addition to a simple suppression of random noise, an effectively longer exposure can be simulated by coadding separate frames while neatly side-stepping many of the practical problems of taking a single exposure. The major problem with long exposures is that emission lines recorded in a long exposure (*i.e.* an exposure taken while the telescope moves over several hours of angle) will appear artificially broadened because of flexure in the telescope apparatus. Taking several shorter exposures ameliorates this problem since each frame is aligned before coaddition. The

other difficulty resulting from taking a few long exposures is the inability to distinguish emission lines from freak occurrences, such as cosmic ray events.

The advantages of taking many smaller frames is lessened by the introduction of read-out noise at the end of every integration. However, each individual exposure was at least an hour long, and the read-out noise was very small compared to the strength of the signal collected in this time. Walker, Johnson and Yang (1987) have determined that the read-out noise is typically 370 electrons rms, resulting in a typical signal to read-out noise ratio of ≈ 10 on the continuum.

6.7 Flat Fielding

The response of the RETICON™ detector is not flat, but shows pixel-to-pixel variations as well as sensitivity variations with spectral region. This is potentially a very difficult problem, as artificial bumps in the nebula's continuum produced by variations in detector sensitivity could be misidentified as faint emission features.

The RETICON™ software at the DAO will automatically measure the detector bias and subtract this from the data before it is stored on disk (or tape).

The response characteristics of the RETICON™ after bias subtraction were determined from incandescent lamp spectra, which is of course free of emission lines. It was proposed that the lamp frames could be divided from the nebula spectra before frame alignment to correct for pixel response. However, this proved very unsatisfactory because of the vastly greater baseline intensity of the lamp spectra. It is necessary to normalize the the lamp spectra by a correcting integer before division. A *Macro* was written to vary the normalizing factor inside a "Do loop", and choose that number which resulted in the flattest nebula continuum.

It was however still possible that detector response variations were affecting the data, even after these procedures. It was deemed necessary to check for this by visual inspection of frames undergoing different degrees of processing. It was hoped that features that were reduced in intensity (but not eliminated) by these procedures could be detected in this way. However, none were found.

CHAPTER 7

THE RESULTS

After the data suffer the indignity of computer manipulation, the frames must be inspected and conclusions must be drawn. The purpose of this chapter is to discuss the spectral data and present the final conclusions, and includes lists of newly identified spectral features.

7.1 SPECTRAL LINE SEARCHES

After computer processing, the frames were individually searched for possible emission features, and all bumps that occurred on several frames were included in a preliminary list of possible lines. The line candidates were then sorted from spurious features and sky emission lines before inclusion in the lists of new spectral features.

The 7100Å frames present a special problem in line identification, as small breaks in the telluric absorption spectrum appear as bumps in the continuum of the planetary nebula. These could easily be mistaken for emission features. Furthermore, it could not be easily ascertained whether or not the candidate emission lines were the result of detector response variations despite the previously discussed correction procedures.

It was felt that two independent line searches should be carried out in order to be sure that all emission features were extraterrestrial in origin. The first search was done on the raw data that were unprocessed by RETICENT. The lines found on the raw nebula frames were compared to sky exposures, and any emission features common to both were removed from the list of possible nebula lines.

The problems of detector response variation and telluric absorption were solved in a similar manner. The lines discovered on undivided nebula frames were compared to lamp exposures (taken by Pritchet) and the comparison star frames. Any candidate emission line could not have a similar appearing counterpart on the non-emission spectra.

The detector response problem was also addressed by comparing nebula frames taken before and after the spectrograph grating was rotated. If a candidate spectral feature remained at the same pixel position after the grating was rotated, it would be removed from the emission line list. No false spectral features were found in this manner.

The nebula exposures were again searched after the data were sky subtracted and divided by the stellar frames. The loss of signal to noise in the subtraction procedure was overcome by frame coaddition. All the features in the final

line list were detectable on both the processed and unprocessed frames.

In order to be included in the line lists, each line has to have a scale height greater than 3σ on at least some of the frames. It was also required that the intensities of the candidate lines systematically increase when frames are coadded.

It is strongly felt that none of the faint emission features discovered in the nebula's spectrum is of terrestrial origin or is an artifact of the RETICON ™ detector. The final list of the newly discovered emission lines near $\lambda = 7100$ Å appears in Table 24.

The measured full width at half maximum of the new lines is ≈ 1.5 Å, which is similar to the width of the previously identified atomic transition lines. The exception to this is the line at $\lambda = 7253.7$ Å, with an FWHM of slightly less than 3 Å. There is no indication that this line is resolved into separate components.

TABLE 26

NEWLY DISCOVERED SPECTRAL FEATURES OF NGC 7027 NEAR 7100 Å

WAVELENGTH (Å)	ION	MULTIPLET	RELATIVE INTENSITY	IRRADIANCE (WATTS/M^2)
7032.4	Ne I	1	0.16	1.2×10^{-16}
7112.4	C II	20	0.07	5.3×10^{-17}
7115.1	C II	20	0.06	4.6×10^{-17}
7154.6	P		0.20	1.5×10^{-16}
7159.8			0.06	4.6×10^{-17}
7230.2	F III		0.25	1.9×10^{-16}
7244.0			0.09	6.9×10^{-17}
7253.7	Ar II		0.17	1.3×10^{-16}

The **ION** column contains the species responsible for emission if it has been identified, while the **MULTIPLET** column refers to multiplet number in C.E.Moore's *Revised Multiplet Table* (1945). Those lines without a **MULTIPLET** number were identified from Kurucz and Peytremann (1982). It should be noted that all line identifications are highly tentative. A second line of any of the identified multiplets is never observed, with the single exception of the pair of C II lines. The value of **RELATIVE INTENSITY** is determined by averaging the measured intensity ratios of the new line to that of [Ar III]'s 7170 Å line (see Appendix 3). All **RELATIVE INTENSITY** values are converted to a percentage scale with I(Hβ + Pi 8) = 100 by multiplication by the relative intensity of the 7170 Å line from Kaler *et al.* (1976, see Table 2). The error in the **RELATIVE INTENSITY** value is on the order of 20%, and all values are uncorrected for atmospheric absorption. The value of **IRRADIANCE** is determined from the Hβ irradiance calibration by Shaw and Kaler (1982).

7.2 Conclusions

It can easily be seen by comparing the lines listed in Table 26 with the H_3 features in Table 22 that there is no evidence of H_3 emission in NGC 7027. We therefore dispute the tentative identification of the 5624 Å emission feature as H_3 emission.

The irradiance of the faintest lines that were recovered is $\approx 5 \times 10^{-17}$ W/m^2, giving them a radiance of $\approx 8 \times 10^{-9}$ W m^{-2} sr^{-1} assuming that the nebula's a angular size is 6×10^9 sr (Atherton *et al.*, 1979). The brightest line in the spectrum of H_3 in this region is the 7156.74 Å blend of Q and R branch transitions, and so it found that the radiance of this blend must be $\leq 8 \times 10^{-9}$ W m^{-2} sr^{-1}.

King and Morokuma (1979) have calculated that the theoretical value of the transition moment of the 7100 Å transition is 3.36×10^{-29} C m. We also find from the system's Hönl-London formulae that the 7156.74 Å blend obtains 14 % of the radiant energy of this transition. We can then determine that the column density of H_3 in the upper state of this transition is ≤ 300 m^{-2}, which is a much higher limit than that found from chemical arguments in Chapter 3.

The reader will recall that it was found in Chapter 3 that H_2^+ is largely prevented from forming H_3 by rapid dissociative recombination with ambient electrons in the partially ionized

transition zone. In the cold molecular envelope electrons are very rare, and most H_3^+ is destroyed by ion-molecule reactions, and consequently does not recombine to form H_3. The total column density of all H_3 molecules is found to be twelve orders of magnitude less than the minimum required in the upper state of the 7100 Å transition in order to have detected that transitions most intense feature.

It is however found that the published chemical models discussed in Chapter 3 have problems, as shown by the strength of ultraviolet H_2^+ absorption in various planetary nebulae. However the discrepancy between observation and theory might be resolved if the models are less idealized. Specifically, it is found that the largest problem with current chemical models for the transition zone is the lack of dust in the model nebula. It is therefore suggested that chemical equilibrium models be written that include the effects of dust grains. These models should be run many times with different grain-size distributions, since there is some evidence of grains of extremely small size ($\approx$5 Å) in addition to grains of typical interstellar diameters ($\approx 10^3$ Å). The different predicted abundances of H_2^+ could then be compared to the H_2^+ column densities observed in other nebula.

A worthwhile project for the future would be a detailed model of NGC 7027's infrared H_2 emission. This model should account for the transition zone H_2 as well as the molecular

envelope H_2. The transition zone H_2 would be excited by UV radiation and residual energy from gas-phase formation reactions, while the molecular envelope H_2 must be excited by shocks through an *inhomogeneous* medium. The results of these models can then be compared to the observed intensity of the infrared bands, as well as their intensity ratios.

Another theoretical study that has yet to be carried out is a *time dependent* chemical model of planetary nebula. It was shown that a time independent approach is adequate for both the cold molecular envelope and the hot transition zone, but no mention of a *hot molecular envelope* was made. It is possible that significant H_3 may form in the ME after it is heated by the passage of the shock front. The postshock density of H_3 cannot be estimated since the chemical models of shocked interstellar gas that have been written to date have not included H_3 as one of the molecules. Nor have they incorporated the high ionization rates produced by a nearby hard UV source.

Recent observations of other planetary nebulae have produced intriguing results that deserve the attention of the theoreticians. Storey *et al.* (1987) have shown a correlation with H_2 emission strength and morphological type in a sample of 37 PN's (including NGC 7027). They determined the intensity ratio of the 2.12 μm H_2 line and atomic hydrogen's Brackett γ line (at 2.16 μm) for each nebula. It was found that the ratio

tends to be higher in those nebulae with a pronounced equatorial toroid and extended polar lobes. It is proposed that a strong stellar wind interacts with previously ejected material that is distributed in an equatorial disk. We can incorporate Storey *et al.*'s findings into a model of NGC 7027's H_2 emission by allowing for a latitudinally varying density distribution of the preshock gas, in addition to a random clumpiness.

Concerning future observational projects, there is a plethora of H_3 emission features that have yet to be searched for with our new spectrophotometric techniques. Most notably, the 6025 Å band contains sharper lines than do the 7100 Å and the 5600 Å bands, and so deserves close scrutiny.

The infrared signature of H_3 and H_3^+ may be present in NGC 7027. The molecule H_2D^+ has a strong dipole moment and may also be detectable at millimeter wavelengths. Because of atmospheric interference and the relatively low quantum efficiency of long wavelength detectors, these observations are however inherently more difficult to make than optical observations. Fortunately, the sensitivity of infrared and submillimeter equipment is continuously improving. Future observations of molecules in planetary nebulae may someday provide valuable information of the chemical reactions and isotopic abundances of these chemically evolved objects.

* * * *

REFERENCES

Agmon,N. (1982) *J.Chem.Phys.* **76**,17.

Agmon,N. (1982) *J.Chem.Phys.* **76**,1309.

Aller,L.H., Bowen,I.S.,Minkowski,R. (1955) *Ap.J.* **122**,62.

Atherton,P.D.,Hicks,T.R.,Reay,N.K.,Robinson,N.K., Worswick,S.P., Phillips,J.P. (1979) *Ap.J.* **232**,786.

Barrow,G.M. (1962) *Introduction to Molecular Spectroscopy.* New York: McGraw-Hill Book Company.

Beckwith,B.,Neugebauer,G.,Becklin,E.E.,Mathews,K. (1980) *A.J.* **85**,886.

Bhattacharyya,G.K.,Johnson,R.A. (1977) *Statistical Methods and Concepts.* New York: John Wiley and Sons.

Black,J.H. (1978) *Ap.J.* **222**,125.

Black,J.H. (1982) *Planetary Nebulae,I.A.U.Symposium No.103.* Page 91. Flower,ed. Dordrechet:D.Reidel.

Black,J.H.,Dalgarno,A. (1976) *Ap.J.* **203**,132.

Borkman,R.F.,Cobb,M. (1981) *J.Chem.Phys.* **74**,2920.

Broadfoot,A.L.,Kendall,K.R. (1968) *J.Geophys.Res.* **85**,886.

Capriotti,E.R.,Daub,C.T. (1960) *Ap.J.* **132**,677.

Carney,G.D.,Porter,R.N. (1974) *J.Chem.Phys.* **60**,4251.

Clutton-Brock,M. (1984) Lecture notes, *Fluid Mechanics in Astronomy.*

Child,M.S. (1963) *J.Mol.Spec.* **10**,357.

Child,M.S.,Longuet-Higgins,H.C. (1961) *Phil.Trans.Roy.Soc* **254A**,259.

Child,M.S.,Strauss,H.L. (1965) *J.Chem.Phys.* **42**,2283.

Collins,G.W.II, Daub,C.T.,O'Dell,C.R. (1961) *Ap.J.* **133**,471.

Condal,A.,Fahlman,G.G.,Walker,G.A.H.,Glaspey,J.W. (1981) *P.A.S.P.* **93**,191.

Curtis,H.D. (1917) *Publ.Lick Obs.* **13**,55.

Dabrowski,I.,Herzberg,G. (1977) *Trans.N.Y.Acad.Sci.* **38**,14.

Dabrowski,I.,Herzberg,G. (1980) *Can.J.Phys.* **58**,1238.

Dalgarno,A.,Lepp.S. (1987) *Astrochemistry, I.A.U.Symposium No.120*. Page 109. Vardya and Tarafdar,editors. Dordrechet: D.Reidel.

Dowling,J.M. (1961) *J.Mol.Spec.* **6**,550.

Duley,W.W.,Williams,D.A. (1984) *Interstellar Chemistry*. Academic Press.

Dunn,G.H. (1968) *Phys.Rev.* **172**,1.

Dykstra,C.E.,Swope,W.C. (1979) *J.Chem.Phys.* **70**,1.

Eaker,C.W.,Allard,L.R. (1981) *J.Chem.Phys.* **74**,1821.

Feibelman,W.A.,Bogess,A.,McCracken,C.W.,Hobbs,R.W. (1981) *A.J.* **86**,881.

Garcia,R.G.,Rossi,A.G.,Russek,A. (1979) *J.Chem.Phys.* **70**,5463.

Garing,J.S.,Neilsen,H.H.,Rao,K.N. (1959) *J.Mol.Spec.* **3**,496.

Gee,G.,Emerson,J.P.,Ade,P.A.R.,Robson,E.I.,Nolt,I.G. (1982) *M.N.R.A.S.* **208**,517.

Gurzadyan,G. (1969) *Planetary Nebulae (English Edition)*. Page 10. Gordon and Breach.

Hartquist,T.W.,Oppenheimer,M.,Dalgarno,A. (1980) *Ap.J.* **236**,182.

Heap,S.R.,Stecher,T.P. (1980) *The Universe at Ultraviolet Wavelengths*: NASA CP-2171.

Hendersen,R.S. (1955) *Phys.Rev.* **100**,723.

Herbst,E.,Klemperer,W. (1973) *Ap.J.* **185**,505.

Herzberg,G. (1945) *Infrared and Raman Spectra*. New York: D.Van Nostrand Company.

Herzberg,G. (1966) *Electronic Spectra of Polyatomic Molecules*. New York: D.Van Nostrand Company.

Herzberg,G.,Hougen,J.T.,Watson,J.K.G. (1982) *Can.J.Phys.* **60**,1261.

Herzberg,G.,Lew,H.,Sloan,J.J.,Watson,J.K.G. (1981) *Can.J.Phys.* **59**,428.

Herzberg,G.,Watson,J.K.G. (1980) *Can.J.Phys.* **58**,1250.

Hougen,J.T. (1962) *J.Chem.Phys.* **37**,1433.

Hutchins,J.B. (1976) *Ap.J.* **205**,103.

Iben,I. (1981) *Ap.J.* **246**,278.

Johnsen,R.,Biondi,M.A. (1974) *Icarus* **23**,139.

Jones,E.G.,Wu,R.L.C.,Hughes,B.M.,Tiernan,T.O.,Hopper,D.G. (1980) *J.Chem.Phys.* **73**,5631.

Jura,M. (1984) *Ap.J.* **286**,630.

Kaler,J.B.,Aller,L.H.,Czyzak,S.J.,Epps,H.W. (1976) *Ap.J.Suppl.* **31**,163.

King,H.F.,Morokuma,K. (1979) *J.Chem.Phys.* **71**,3213.

Kirby,K.,Guberman,S.,Dalgarno,A. (1979) *J.Chem.Phys.* **70**,4635.

Knapp,G.R.,Phillips,T.G.,Leighton,R.B.,Lo,K.Y.,Wannier,P.G., Wooten,H.A.,Huggins,P.J. (1982) *Ap.J.* **252**,616.

Kurucz,R.L.Peytremann,E. (1982) *A Table of Semi-Empirical gf Values Part 3: 599.4004 nm to 9997.2746 nm*. Smithsonian Astrophysical Observatory Special Report #362.

Kwan,J. (1977) *Ap.J.* **216**,713.

Kwok,S. (1980) *Ap.J.* **236**,592.

Kwok,S. (1982) *Ap.J.* **258**,280.

Kwok,S.,Purton,C.R.,FitzGerald,P.M. (1978) *Ap.J.Lett.* **219**,L125.

Leger,A.,Puget,J.L. (1984) *Astr.Astph.Lett.* **137**,L5.

Leu,M.,Biondi,M.A,Johnsen,R. (1973) *Phys.Rev.* **A8**,413.

Liller,W.,Aller,L.H. (1954) *Ap.J.* **120**,48.

Liller,W. (1955) *Ap.J.* **122**,240.

Longuet-Higgins,H.C.,Opik,U.,Pryce,H.L., (1955) *Ap.J.* **122**,240.

Masson,C.R.,Cheung,K.W.,Berge,G.L.,Claussen,M.J.,Heiligman,G. M.,Leighton,R.B.,Lo,K.Y.,Moffet,A.T.,Phillips,T.G., Sargent,A.I.,Scott,S.L.,Woody,D.P. (1985) *Ap.J.* **292**,464.

Miller,J.S.,Mathews,W.G. (1972) *Ap.J.* **172**,593.

Minkowski,R.,Aller,L.H. (1956) *Ap.J.* **117**,93.

Mitchell,G.F.,Ginsburg,J.L.,Kuntz,P.J. (1978) *Ap.J.Suppl.* **38**,39.

Moore,C.E. (1945) *Revised Multiplet Table*, Contr.Princeton Univ.Obs.,No.20.

Moseley,H. (1980) *Ap.J.* **238**,892.

Mufson,S.L.,Lyon,J.,Marionni,P.A. (1975) *Ap.J.Lett.* **201**,L85.

Oka,T. (1980) *Phys.Rev.Lett.* **45**,531.

Pottasch,S.R.,Goss,W.M.,Arnal,E.M.,Gauthier,R. (1982) *Astr.Astph.* **106**,229.

Pottasch,S.R.,Wesselius,P.R.,Wu,C.C.,Fieten,H.,van Duinen,R.J. (1978) *Astr.Astph.* **62**,95.

Pritchet,C.J.,Grillmair,C.J. (1984) *Pub.Ast.Soc.Pac.* **96**,349.

Pritchet,C.J.,Mochnacki,S.,Yang,S. (1982) *P.A.S.P.* **94**,733.

Russell,R.W.,Soifer,B.T.,Willner,S.P. (1977) *Ap.J.Lett.* **217**,L149.

Scrimger,J.N.,Lowe,R.P.,Moorhead,J.M.,Wehlau,W.H. (1978) *P.A.S.P.* **90**,257.

Sellgren,K.,Werner,M.W.,Dinerstein,H.L. (1983) *Ap.J.* **271**,L13.

Sellgren,K. (1984) *Ap.J.* **277**,623.

Shaw,R.A.,Kaler,J.B. (1982) *Ap.J.* **261**,510.

Siegbahn,P.,Liu,B. (1978) *J.Chem.Phys.* **68**,1457.

Smith,D.,Adams,N.G. (1984) *Ap.J.Lett.* **284**,L13.

Smith,H.A.,Larson,H.P.,Fink,U. (1981) *Ap.J.* **244**,835.

Spitzer,L. (1978) *Physical Processes in the Interstellar Medium.* New York:John Wiley and Sons.

Storey,J.W.V.,Webster.B.L.,Payne,P.,Dopita,M.A. (1987) *Astrochemistry, I.A.U.Symposium No.120.* Page 339. Vardya and Tarafdar,editors. Dordrechet: D.Reidel.

Telesco,C.M.,Harper,D.A. (1977) *Ap.J.* **211**,475.

Tokunaga,A.T.,Young,E.T. (1980) *Ap.J.Lett.* **237**,L93.

Thronson,H.A. (1983) *Ap.J.* **264**,599.

Treffers,R.R.,Fink,U.,Larson,H.P.,Gauthier,T.N.III, (1976) *Ap.J.Lett.* **230**,L175.

Truhlar,D.G.,Horowitz,C.J. (1978) *J.Chem.Phys.* **68**,2466.

Walker,G.A.H,Johnson,R.,Yang,S. (1987) Preprint.

Watson,J.K.G (1987) Personal Communication.

Watson,W.D. (1973) *Ap.J.Lett.* **183**,L17.

Weidmann,V.,Koester,D. (1983) *Astr.Astph.* **121**,77.

Wickramasinghe,N.C. (1967) *Interstellar Grains: The International Astrophysics Series Volume 9.* Page 112. Chapman and Hall Ltd.: London.

Williams,D.A. (1987) *Astrochemistry, I.A.U.Symposium No.120.* Page 531. Vardya and Tarafdar,editors. Dordrechet: D.Reidel.

Wilson,O.C. (1950) *Ap.J.* **111**,163.

Zuckerman,B. (1978) *Planetary Nebulae: Observations and Theory, I.A.U.Symposium No.76.* Page 305. Terzian,ed. Dordrecht: D.Reidel.

Zuckerman,B. (1982) *Planetary Nebulae,I.A.U.Symposium No.103.* Post paper discussion, page 101. Flower, ed. Dordrecht: D.Reidel.

APPENDIX 1

THE OBSERVING RECORDS

1.1 AUGUST, 1984

Date: 7/8 Aug 84 Observatory: DAO Telescope: 1.83m Page:1
Program: NGC7027 Observer:Pr
Spectrograph: 21121ER Slit/I.S.: Slit Remarks: N.B.clock
Grating:blaze:7500 l/mm:1200 width: 0.008 is set
order: 1 tilt:66.91° decker: narrow to PDT
image tube: No order filter:Yes

Tape:_____ Detector:1872 Reticon Computer: Nova 1200
gain: High prog: _____

File#	Rec#	Object	Exposure (seconds)	Seeing (")	Time of start	# of records	Signal
14	1-3	Ne-Cd Arc	3			3	
	4-6	Vega	20	3	21:59	3	~1000
	7	NGC 7027	600	2	22:59	1	
	8	NGC 7027	3600		23:05	1	
	9	Sky	1800		00:10	1	
	10	Vega	20		01:00	1	
	11	Ne-Cd Arc	3			1	
	12	NGC 7027	3600	3	01:14	1	
	13	garbage				1	
	14	Sky	1200		02:16	1	
	15-16	NGC 7027	3600		02:41	2	
	17	Sky	900		04:43	1	

Page: 2

Date: 8/9 Aug 84 Observatory: DAO Telescope: 1.83m
Program: NGC7027 Observer: Pr
Spectrograph: 21121ER Slit/I.S.: Slit Remarks: N.B. clock is set to PDT
Grating: blaze: 7500 l/mm: 1200 width: 0.008
order: 1 tilt: 66.91° decker: narrow
image tube: No order filter: Yes

Tape: _____ Detector: 1872 Reticon Computer: Nova 1200
gain: High prog: _____

File#	Rec#	Object	Exposure (seconds)	Seeing (")	Time of start	# of records	Signal
15	1-4	Vega	10	1		4	3000
	5	ν Cygni	200	1	21:50	1	1092
	6	Ne-Cd Arc	3			1	
	7	NGC 7027	3600	1		1	
	8	Sky	900			1	
	9	NGC 7027	3600		23:29	1	
	10	Sky	900		00:31	1	
	11	Ne-Cd Arc	3		00:52	1	
	12	Vega	10	2	01:01	1	1800
	13	ν Cygni	200	1	01:10	1	1952
	14	garbage					
	15	NGC 7027	3600	1.5	01:19	1	
	16	Sky	900		02:21	1	
	17-18	NGC 7027	3600		02:38	2	

Page: 3

Date: 9/10 Aug 84 Observatory: DAO Telescope: 1.83m
Program: NGC7027 Observer: Pr
Spectrograph: 21121ER Slit/I.S.: Slit Remarks: N.B. clock is set to PDT
Grating: blaze: 7500 1/mm: 1200 width: 0.008
order: 1 tilt: 66.91° decker: narrow
image tube: No order filter: Yes

Tape: _____ Detector: 1872 Reticon Computer: Nova 1200
gain: High prog: _____

File#	Rec#	Object	Exposure (seconds)	Seeing (")	Time of start	# of records	Signal
16	1-10	Lamp	2			10	1950
	11	Ne-Cd Arc	3			1	
	12	Vega	5		21:30	1	~2000
	13	ν Cygni	200	1.5	21:45	1	
	14	Ne-Cd Arc	3			1	
	15	NGC 7027	5400		21:56	1	
	16	Sky	900		23:27	1	
	17	NGC 7027	5400		23:44	1	
	18	Sky	900		01:36	1	
	19	NGC 7027	5400		01:56	1	
New grating rotation, $\theta = 74.05^{\circ}$. Check for Fe coronal lines!							
	20	NGC 7027	3600		03:31	1	

Page: 4

Date: 10/11 Aug 84 Observatory: DAO Telescope: 1.83m
Program: NGC7027 Observer: Pr
Spectrograph: 21121ER Slit/I.S.: Slit Remarks: N.B. clock
Grating: blaze: 7500 l/mm: 1200 width: 0.008 is set
order: 1 tilt: 66.91° decker: narrow to PDT
image tube: No order filter: Yes

Tape: _____ Detector: 1872 Reticon Computer: Nova 1200
gain: High prog: _____

File#	Rec#	Object	Exposure (seconds)	Seeing (")	Time of start	# of records	Signal
17	1	Vega	10		21:52	1	2692
	2	NGC 7027	5400		22:11	1	
	3	Sky	900		23:41	1	
	4	NGC 7027	5400		00:01	1	
	5	Sky	900		01:34	1	
	6	NGC 7027	5400		01:51	1	
	7	Sky	900		03:24	1	

1.2 AUGUST, 1986

Date: Sat/Sun Aug 16/17 1986

Spectrograph: 21121ER, Direct Reticon, 5970(7-51)order filter

Observer: Gu + Gy

Star	Record #	Time (PST) start	Time (PST) end	H.A. start	Seeing "	Exp counts
NGC 7027	3340^{C} 3341* 3342^{C}	00:01	01:02	00:23E	2	950
Vega	3343^{C} 3344*	01:22	+10"	04:14W	2	1000
Vega	3345^{C} 3346*	01:23	+20"	04:16W		2000
Vega	3347^{C} 3348*	01:26	+10"	04:17W		950
NGC 7027	3349^{C} 3350* 3351^{C}	01:42	3:00	02:06W	1.5	100
ν Cygni	3352^{C} 3353*	03:34	03:42	3:45W		
ν Cygni	3354* 3355^{C}	03:43	03:48	3:54W		
NGC 7027	3356*	04:00	04:20	4:22W		376

Date: Sun/Mon Aug 17/18 1986

Spectrograph: 21121ER, Direct Reticon, 5970(7-51)order filter

Observer: Gu + Gy

Star	Record #	Time (PST) start	Time (PST) end	H.A. start	Seeing "	Exp counts
Vega	3357C 3358* 3360C	20:16	+10"	00:44E	2	
Vega	3358* 3362C	20:18	+20"	00:45E		
NGC 7027	3363C 3364*	20:32	21:32	03:00E		1000
NGC 7027	3365C 3366* 3367C	21:37	22:39	01:56E		1000
ν Cygni	3368C 3369*	22:46	22:51	00:40E		
ν Cygni	3370* 3371C	22:52	23:02	00:32E		
NGC 7027	3372C 3373* 3374C	23:05	00:44	00:27E	1.5	1500
NGC 7027	3375* 3376C	00:45	01:56	01:11W	1.5	1000
ν Cygni	3377C 3378*	02:05	02:10	02:41W		
ν Cygni	3379* 3380C	02:10	02:20	02:46W		
NGC 7027	3381C 3382* 3383C	02:27	03:42	02:53W		1000
ν Cygni	3384C 3385* 3386C	03:51	04:01	04:27W	1	

Date: Mon/Tues Aug 18/19 1986

Spectrograph: 21121ER, Direct Reticon, 5970(7-51)order filter

Observer: Gu + Gy

Star	Record #	Time (PST) start	end	H.A. start	Seeing "	Exp counts
Vega	3387C 3388* 3389C	20:38	+10"	00:17E	2	
Vega	3390C 3391* 3392C	20:40	+20"	00:15E		
Vega	3393C 3394* 3395C	20:48	+30"	00:12E		
Vega	3396C 3397* 3398C	20:52	+40"	00:09E		
NGC 7027	3399C 3400* 3401C	21:07	22:32	02:23E	1.5	1200
Sky	3402*	22:36	23:38	00:54E		100
NGC 7027	3403C 3404* 3405C	23:42	00:48	00:10W		1000
ν Cygni	3406C 3407* 3408C	01:00	01:05	01:18W		
ν Cygni	3409* 3410C	01:10	01:20	01:28W		
ν Cygni	3411* 3412C	01:24	01:44	01:42W		
NGC 7027	3413C 3414* 3415C	01:56	03:18	02:25W		1000
ν Cygni	3416C 3417* 3418C	03:34	03:39	03:53W		
ν Cygni	3419* 3420C	03:43	03:54	04:01W		

Date: Tues/Wed Aug 19/20 1986

Spectrograph: 21121ER, Direct Reticon, 5970(7-51)order filter

Observer: Gu + Gy + TBL

Star	Record #	Time (PST) start	Time (PST) end	H.A. start	Seeing "	Exp counts
Vega	3421C 3422* 3423C	20:07	+20"	00:50E	3	
Vega	3424* 3425C	20:11	+40"	00:46E		
Vega	3426* 3427C	20:14	20:15	00:43E		
Nova Cyg	3428C 3429* 3430C	20:27	20:55	01:49E		1500
Nova Cyg	3431* 3432C	20:58	21:45	01:16E	2	3000
NGC 7027	3433C 3434* 3435C	21:57	23:04	01:30E		1000
NGC 7027	3436C 3437* 3438C	23:11	00:14	00:15E		1000
Sky	3439C 3440* 3441C	00:20	01:23	00:53W		123
ν Cygni	3442C 3443* 3444C	01:35	01:40	01:57W	1.5	
ν Cygni	3445* 3446C	01:44	01:54	02:06W		
NGC 7027	3447C 3448* 3449C	02:06	02:38	02:398E		1300

Date: Wed/Thur Aug 20/21 1986

Spectrograph: 21121ER, Direct Reticon, 5970(7-51)order filter

Observer: Gu + Gy

Star	Record #	Time (PST) start	Time (PST) end	H.A. start	Seeing "	Exp counts
Vega	3453^{C} 3454* 3455^{C}	20:16	+10"	00:37E	2	
Vega	3456* 3457^{C}	20:20	+20"	00:32E		
Vega	3458* 3459^{C}	20:25	+20"	00:28E		
Vega	3460* 3461^{C}	20:28	+30"	00:24E		
Vega	3462* 3463^{C}	20:32	+30"	00:19E		
NGC 7027	3464^{C} 3465* 3466^{C}	20:40	22:52	02:44E		2000
Sky	3467^{C} 3468* 3469^{C}	22:56	23:26	00:26E		80
ν Cygni	3470^{C} 3471* 3472^{C}	23:42	23:52	00:07W		
ν Cygni	3473* 3474^{C}	23:56	00:16	00:22W		
Nova Cyg	3475^{C} 3476* 3477^{C}	00:31	02:36	02:20W	1	4000
NGC 7027	3478^{C} 3479* 3480^{C}	02:42	03:55	04:40E		1000

Date: Thur/Fri Aug 21/22 1986

Spectrograph: 21121ER, Direct Reticon, 5970(7-51)order filter

Observer: Gu + Gy + TBL

Star	Record #	Time (PST) start	Time (PST) end	H.A. start	Seeing "	Exp counts
Vega	3481^{C} 3482* 3483^{C}	21:28	+20"	00:33W	2	
Vega	3484* 3485^{C}	20:20	+30"	00:32W		
Vega	3486* 3487^{C}	20:25	+40"	00:28W		
Vega	3488* 3489^{C}	20:28	20:29	00:24W		
NGC 7027	3490^{C} 3491* 3492^{C}	22:26	23:46	00:58E		1500
Sky	3493^{C} 3494* 3495^{C}	23:53	01:23	00:34W		219
NGC 7027	3496^{C} 3497* 3498^{C}	01:30	03:07	02:11W		1500
ν Cygni	3499^{C} 3500* 3501^{C}	03:26	03:36	03:56W	1	
ν Cygni	3502* 3503^{C}	03:39	03:44	04:09W		

APPENDIX 2

GLOSSARY OF SELECTED RETICENT COMMANDS [1]

Add

Add P1,P2,P3 [-,-,P1]
Word-by-word addition of frames P1 and P2. Result is stored in frame P3.

Data

Data Var1
N1,N2,N3,.../
Reads in up to 100 numbers in free format ending in CRNTL/Z (interactive use) or "/" (non-interactive use), and puts them in an array with name Var1. Up to 50 arrays are allowed. NOTE: Array Var1 will be created if it does not already exist.

Disp

Disp P1,Arr1,Arr2,P4 [0,-,-,5]
Dispersion polynomial is calculated using the spectrum in frame P1. Approximate line positions must be provided in the array Arr1. Wavelengths should be placed in Arr2. This command calls the command *Posn* to calculate exact positions of extrema within *NSearch* pixels of specified approximate positions.

Div

Div P1,P2,P3,P4 [-,-,P1,10000]
Word-by-word division of frame P1 by P2. The result is stored in frame P3. Division by zero produces a result of zero. Real quotient is multiplied by factor P4 before converting to 16-bit integer.

FiltDef

Filter P1,P2,...,P16 [32,64,-,-,...]
Define a filter for use with the *Filter* command. Parameters P3 and P4,P5 and P6, *etc.* are starting and ending frequencies (as a fraction of Nyquist) of "notches" in the Fourier domain (up to 7 notches are allowed).

---

[1] Condensed from the RETICENT "on line" documentation.

Filter

Filter P1,P2 [0,P1]

Frame P1 is filtered using the filter that was defined and calculated with the *FiltDef* command. The result is stored in frame P2.

Macro

Macro MacroName,Var2,...,Var16

The *Macro* "MacroName" is defined by the ensuing commands and terminated by the command *End MacroName*. Arguments are represented by parameters Var2 - Var16.

MultI

Multi P1,P2,P3 [-,-,P1]

Multiplication of each word of frame P1 by constant P2. The result is stored in P3.

NSearch

NSearch P1 [3]

Disp and *Posn* use an array of approximate spectral line positions as input for calculating accurate line positions. Each approximate position is searched over a range +/- P1. *NSearch* thus defines a tolerance to which approximate line positions must be specified.

Posn

Posn P1,Arr1,Var1 [0, -, -]

This command computes the positions of absorption or emission features in frame P1. The feature whose positions will be computed are within *NSearch* pixels of positions stored in "Arr1". If no third parameter is present, then the positions are stored for future reference. If a variable is present as the third parameter, then the positions for each feature are compared with positions which have previously been stored. A mean shift is calculated, displayed, and stored in variable "Var1".

Smooth

Smooth P1,P2,P3 [0,-,-]

A P2 point running mean of frame P1 is calculated and stored in frame P3.

N.B. 1) If P2 is even, then the spectrum ends up shifted left (*i.e.* to smaller pixel numbers) by 0.5 pixels.
2) The first and last P2/2 points are set to zero.

Shift

Shift P1,P2,P3 [0,-,P1]

Frame P1 is shifted by P2 pixels. (P2>0 means shift right). The result is stored in P3.

N.B. 1) *Shift* as used by the shift command is opposite in sign to the output in the third parameter of the *Posn* command.

2) If the shift to be applied is <0.001 pixels, no action is taken.

3) A non-integral shift is performed using the Fourier shift theorem.

Stretch

Stretch P1,P2,P3,P4 [0,-,P1,-]

A spectrum in frame P1 (for which dispersion coefficient set P2 is valid) is stretched so that its wavelength scale matches that of the current dispersion coefficient set. The result is stored in frame P3. This is a means of putting spectra on a common wavelength scale.

Sub

Sub P1,P2,P3 [-,-,P1]

Word-by-word subtraction of frames P1 and P2. Result is stored in frame P3.

Tek

Tek P1,Var2,Var3,Var4 [0,-,-,-]

Frame P1 is plotted on the Tektronix™ (or equivalent) using the IPPS package. After the plot a number of interactive commands are available (hit *M* or *V* to list subcommands). Data can be appended (the *+* subcommand) or deleted (the - subcommand) from the arrays with names corresponding to the argument Var2 (cursor X position),Var3 (cursor Y position),and Var4 (user entered identification number) using the Tektronix™ cursor mode.

Subcommand D

The *D* subcommand integrates (sums) all intensity values between two X-cursor positions and subtracts the continuum level (which is defined as the current Y position).

Subcommand O

The *O* subcommand (letter "oh") prompts the user for a frame number to overplot (without erasing) on current plot. The X and Y scales remain unchanged.

APPENDIX 3

MEASURED INTENSITIES OF NEWLY DISCOVERED EMISSION LINES

The intensity ratios of each newly discovered line to the $\lambda = 7170$ Å [Ar III] line are plotted for each of ten frames. The ratios are plotted against the measured intensity of the 7170 Å line, which is a rough measure of the ten frames' signal to noise ratio. Each frame is the coadded sum of all exposures taken during a single night. The integration dates and total exposure times of each frame are included in Table 28. It is required that there be no significant negative correlation between the measured line intensity ratio and the frame SN ratio.

FIGURE 19

THE LINE INTENSITY RATIO I(7032 Å)/I(7170 Å)

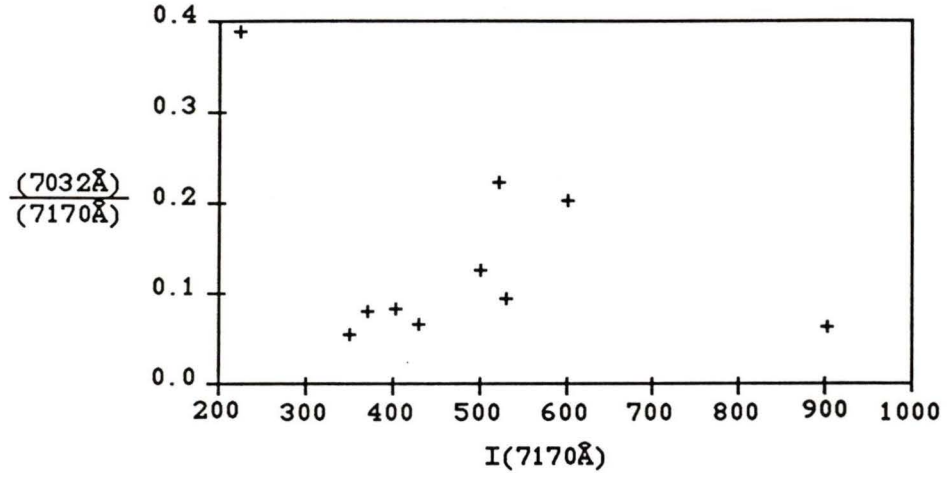

The mean intensity ratio of the 7032 Å line is $I(\lambda 7032)/I(\lambda 7170) = 0.14$, with a standard error of 0.03. The first and last points are however obviously spurious, and ignoring these values results in the adopted mean of 0.116 and standard error 0.02 for the reduced sample.

FIGURE 20

THE LINE INTENSITY RATIO I(7112 Å)/I(7170 Å)

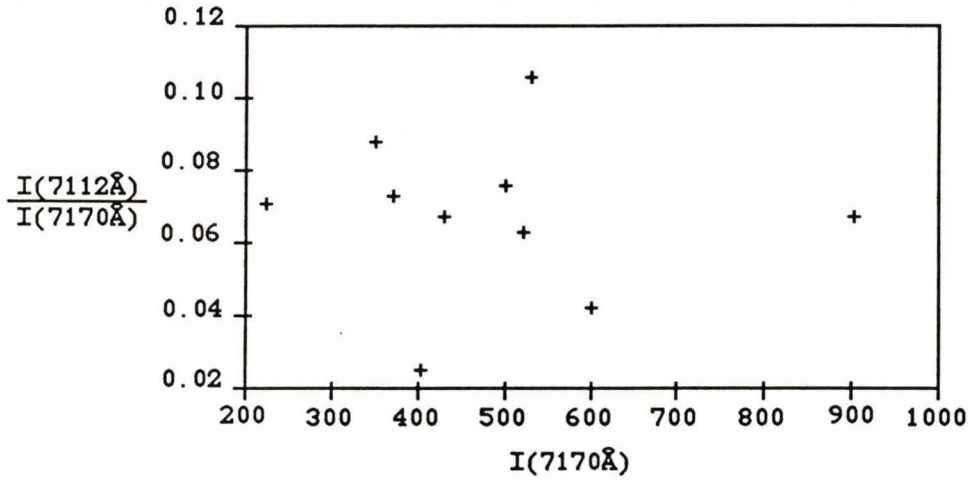

The mean intensity ratio of the 7112 Å line is I(λ7112)/I(λ7170) = 0.068, with a standard error of 0.007.

FIGURE 21

THE LINE INTENSITY RATIO I(7115 Å)/I(7170 Å)

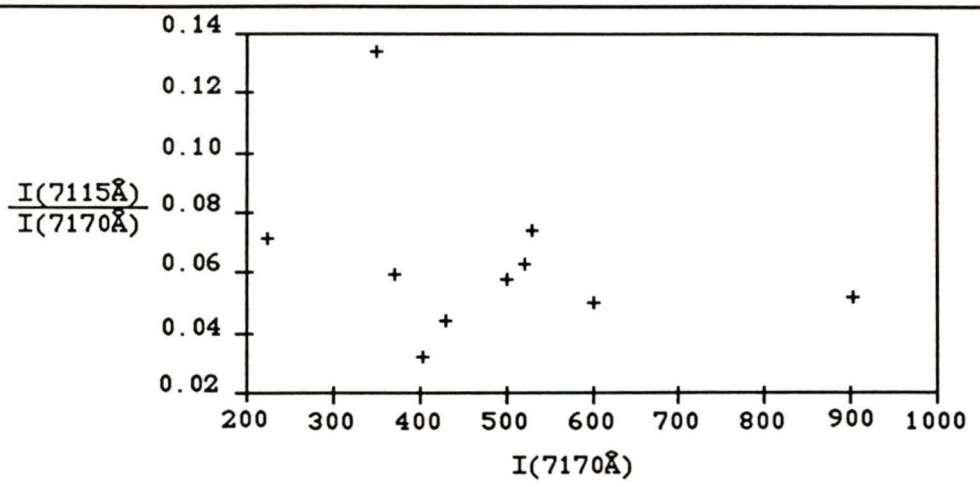

The mean intensity ratio of the 7115 Å line is I(λ7115)/I(λ7170) = 0.064, with a standard error of 0.009.

FIGURE 22

THE LINE INTENSITY RATIO I(7155 Å)/I(7170 Å)

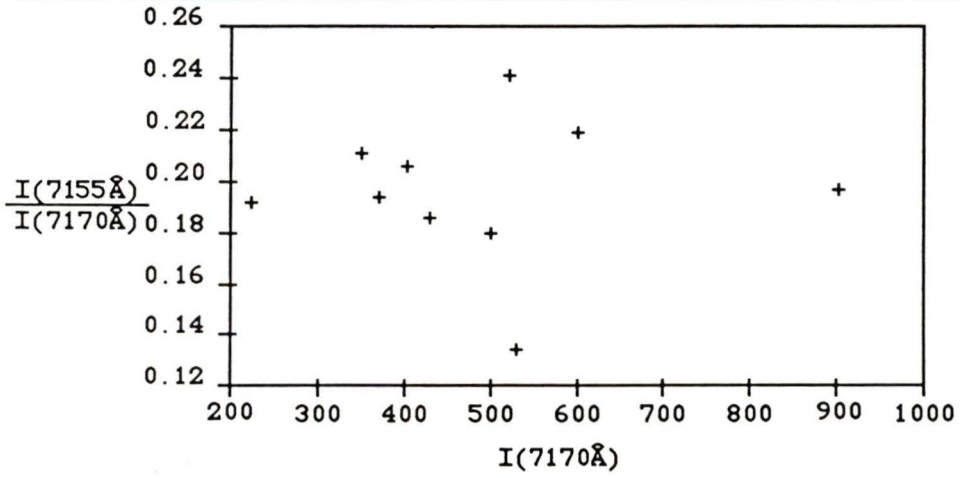

The mean intensity ratio of the 7155 Å line is I(λ7155)/I(λ7170) = 0.20, with a standard error of 0.009.

FIGURE 23

THE LINE INTENSITY RATIO I(7160 Å)/I(7170 Å)

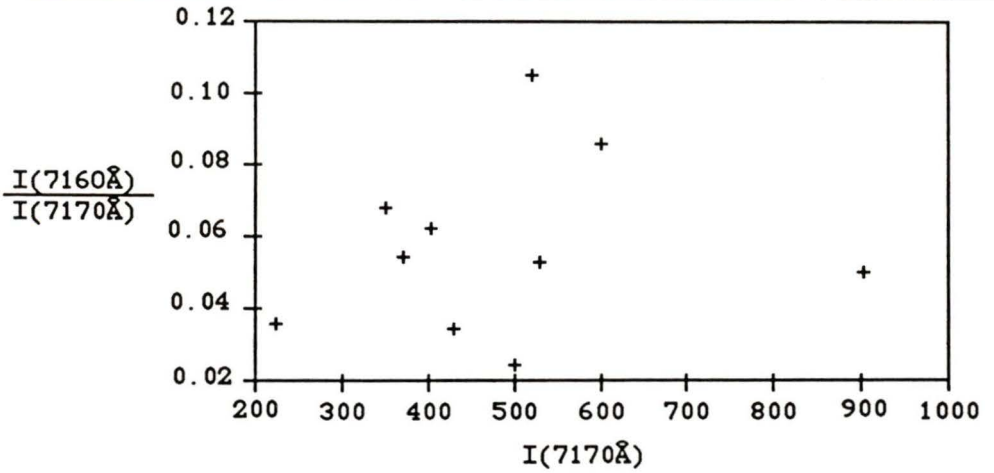

The mean intensity ratio of the 7160 Å line is $I(\lambda 7160)/I(\lambda 7170) = 0.057$, with a standard error of 0.008.

FIGURE 24

THE LINE INTENSITY RATIO I(7230 Å)/I(7170 Å)

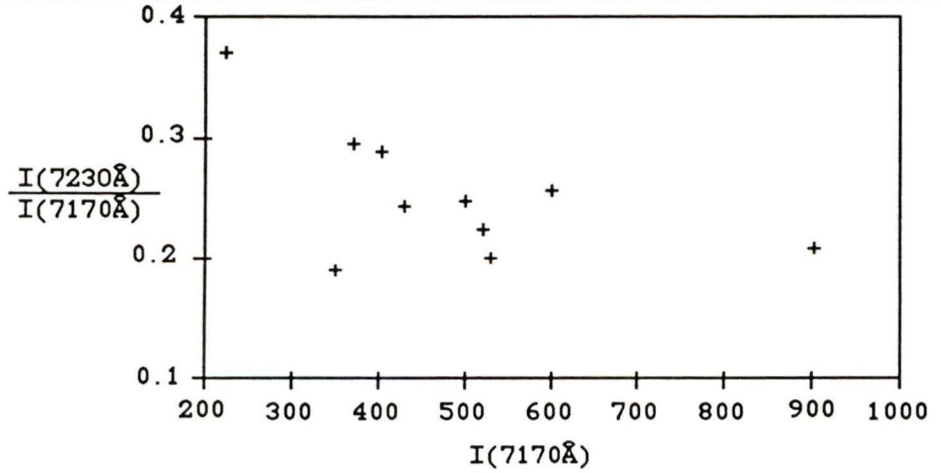

The mean intensity ratio of the 7230 Å line is $I(\lambda 7230)/I(\lambda 7170) = 0.25$, with a standard error of 0.02.

FIGURE 25

THE LINE INTENSITY RATIO I(7254 Å)/I(7170 Å)

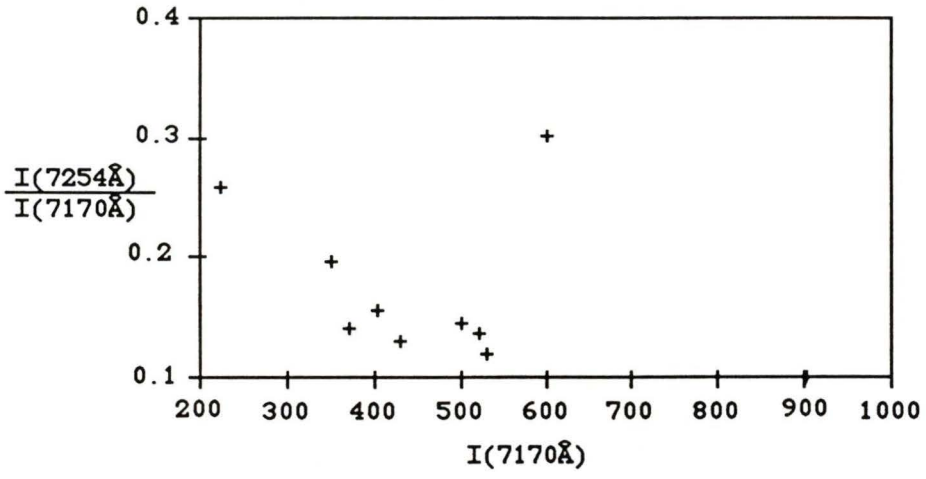

The mean intensity ratio of the 7254 Å line is $I(\lambda 7254)/I(\lambda 7170) = 0.17$, with a standard error of 0.02.

TABLE 27

THE MEASURED LINE 7170 Å INTENSITY AND INTEGRATION DATE OF EACH COADDED TEST FRAME

Frame #	Measured 7170 Å Line Intensity	Date of Integration D/M/Y
1	224	7-8/08/84
2	351	10-11/08/84
3	371	16-17/08/86
4	403	21-22/08 /86
5	431	20-21/08/86
6	500	18-19/08/86
7	522	8-9/08/84
8	530	19-20/08/86
9	602	9-10/08/84
10	902	17-18/08/86

VITA

Surname: Gussie **Given Names:** Grant Trevor

Place of Birth: Beausejour,MB **Date of Birth:** Oct.25,1963

Educational Institutions Attended, with Dates of Entering and Leaving:

University of Manitoba, Winnipeg 1981 to 1985

University of Victoria, BC 1985 to 1987

Degrees, Diplomas, Etc., Awarded, with Dates and Names of Institutions:

B.Sc. (Major) 1985 University of Manitoba

Honours and Awards:

Chown Centennial Scholarship, 1981

Saint John's College Alumni Science Award, 1982

University of Manitoba Gold Medal, 1985

N.S.E.R.C Post Graduate Scholarship, 1985/87

Publications:

PARTIAL COPYRIGHT LICENSE

I hereby grant the right to lend my thesis or dissertation (the title of which is shown below) to users of the University of Victoria Library, and to make single copies only for such users or in response to a request of any other university, or similar institution, on its behalf or for one of its users. I further agree that permission for extensive copying of this thesis for scholarly purposes may be granted by me or a member of the University designated by me. It is understood that copying or publication of this thesis for financial gain shall not be allowed without my written permission.

Title of Thesis:

A Search for H_3 Molecules in the

Planetary Nebula NGC 7027

Author:

[redacted]

Grant Gussie

August 6/1987